NIST-GCR-96-691

MIXING AND RADIATION PROPERTIES OF BUOYANT LUMINOUS FLAME ENVIRONMENTS

Z. Dai, S.K. Krishnan, R. Sangras,
J.S. Wu, and G.M. Faeth

FILE COPY
DO NOT TAKE

United States Department of Commerce
Technology Administration
National Institute of Standards and Technology

NIST-GCR-96-691

MIXING AND RADIATION PROPERTIES OF BUOYANT LUMINOUS FLAME ENVIRONMENTS

Z. Dai, S.K. Krishnan, R. Sangras,
J.S. Wu, and G.M. Faeth

Department of Aerospace Engineering
The University of Michigan
Ann Arbor, MI 48109-2118

October 1995
Issued June 1996

U.S. Department of Commerce
Michael Kantor, *Secretary*
Technology Administration
Mary L. Good, *Under Secretary for Technology*
National Institute of Standards and Technology
Arati Prabhakar, *Director*

Notice

This report was prepared for the Building and Fire Research Laboratory of the National Institute of Standards and Technology under grant number 60NANB4D1696. The statement and conclusions contained in this report are those of the authors and do not necessarily reflect the views of the National Institute of Standards and Technology or the Building and Fire Research Laboratory.

Report No. GDL/GMF-95-02

MIXING AND RADIATION PROPERTIES OF BUOYANT LUMINOUS FLAME ENVIRONMENTS

Z. Dai, S.K. Krishnan, R. Sangras, J.S. Wu and G.M. Faeth
Department of Aerospace Engineering
The University of Michigan
Ann Arbor, Michigan 48109-2118

Prepared for:

U.S. Department of Commerce
National Institute of Standards and Technology
(formerly National Bureau of Standards)
Laboratory for Building and Fire Research
Washington, D.C. 20234

Grant No. 60NANB4D1696
K. C. Smyth and H. R. Baum, NIST Scientific Officers

October 1995

Abstract

An investigation of the radiation and mixing properties of buoyant turbulent diffusion flames is described. The study was divided into two phases: (1) the optical and radiative properties of soot, which must be understood in order to develop nonintrusive methods for measuring soot properties and to estimate the continuum radiation properties of soot in flame environments, and (2) the structure and mixing properties of buoyant turbulent plumes, which must be understood in order to resolve effects of turbulence/radiation interactions and to benchmark computationally tractable models of buoyant turbulent flows.

Consideration of the optical and radiative properties of soot involved evaluation of the Rayleigh-Debye-Gans (RDG) scattering approximation for soot aggregates and the use of this theory to measure the refractive indices in the visible (350-800nm) of soot emitted from buoyant turbulent diffusion flames in the long residence time regime where emitted soot properties became independent of position in the flame and flame residence time. Measured soot optical properties were in reasonably good agreement with RDG predictions, even through optical size parameters for individual primary soot particles reached values as large as 0.42 over the test range. Soot refractive indices were measured for acetyline, propylene, ethylene and propane flames burning in air. It was found that soot refractive indices did not vary significantly with fuel type, compared with experimental uncertainties, in spite of significant variations of soot composition and morphological properties over the test range. Present soot refractive indices also are in fair agreement with early measurements of Dalzell and Sarofim (1969) even though these results have been criticized in the past. Furthermore, soot refractive indices did not exhibit a resonance condition in the near uv, supporting the recent observations of Vaglieco et al. (1990). In addition, dimensionless extinction coefficients were relatively independent of fuel type and wavelength over the test range, yielding a value of 5.1 with a standard deviation of 0.5; this value is significantly lower than values in the range 8.1-9.4 recently reported by Dobbins et al. (1994) and Choi et al. (1995) for reasons that still must be explained. Finally, soot fractal dimensions were reasonably robust with a mean value of 1.77 and a standard deviation of 0.04 which is in good agreement with recent measurments by Köylü and Faeth (1994a) for the same soot.

Consideration of the structure and mixing properties of buoyant turbulent plumes involved evaluation of potential effects of coflow on earlier measurements, and evaluation of various modeling approximations - emphasizing self-preserving round buoyant turbulent plumes. The measurements showed that effects of coflow were negligible so that earlier measurements provided mean and turbulent quantities in the self-preserving region. Evaluation of modeling concepts using the new measurements indicated problems of countergradient diffusion and variable model constants for simple theories, with little improvement of predictions using more advanced Reynolds stress models. Hopefully, the availability of present measurements of mean and fluctuating quantities in the self-preserving region of round buoyant turbulent plume will provide an opportunity to develop and evaluate improved methods for treating the complex buoyant turbulent flows found in fire environments.

Acknowledgments

This research was supported by the United States Department of Commerce, National Institute of Standards and Technology (formerly National Bureau of Standards), Grant No. 60NANB4D1696, with K.C. Smyth and H.R. Baum of the Laboratory for Building and Fire Research serving as Scientific Officers. The authors wish to acknowledge collaboration with T.L. Farias and M.G. Carvalho of IST, Lisbon, Portugal, for the ICP computations of simulated soot aggregates; this collaboration was sponsored, in part, by AGARD contract No. 573011D; and useful discussions with Ü. Ö. Köylü now of Yale University, New Haven, Connecticut.

Table of Contents

	Page
Abstract	iii
Acknowledgments	iv
List of Tables	vi
List of Figures	vii
Nomenclature:Soot Optical Properties	ix
Nomenclature:Buoyant Turbulent Plumes	xii
1. Introduction	1
2. Optical and Radiative Properties of Soot	2
2.1 Introduction	2
2.2 Experimental Methods	6
2.3 Theoretical Methods	12
2.4 Experimental Conditions	14
2.5 Soot Scattering Properties	16
2.6 Soot Fractal Properties	21
2.7 Soot Optical Properties	27
2.8 Conclusions	30
3. Buoyant Turbulent Plumes	32
3.1 Introduction	32
3.2 Experimental Methods	35
3.3 Self-Preserving Scaling	35
3.4 Experimental Results	38
3.5 Modeling Implications	46
3.6 Conclusions	55
References	65

List of Tables

Table	Titles	Page
1.	Light sources used for measurements of scattering from soot	11
2.	Summary of test conditions for round buoyant turbulent diffusion flames in the long residual time regime	15
3.	Summary of the structure and physical properties of soot from the overfire region of round buoyant turbulent diffusion flames in the long residence time regime	15
4.	Summary of measurements of scattering from soot within the overfire region of round buoyant turbulent diffusion flames in the long residence time regime	17
5.	Values of depolarization ratios at 514.5 mm for soot within the overfire region of round buoyant turbulent diffusion flames in the long residence time regime	19
6.	Values of ρ_{sa} at 514.5 nm for soot within the overfire region of round buoyant turbulent diffusion flames in the long residence time regime	19
7.	Summary of the fractal properties of soot from the overfire region of round buoyant turbulent diffusion flames in the long residence time region	19
8.	Values of the fractual properties of soot within the overfire region of round buoyant turbulent diffusion flames in the long residence time regime	19
9.	Summary of the optical properties of soot from the overfire region of round buoyant turbulent diffusion flames in the long residence time regime	28
10.	Buoyant turbulent plume test conditions	37
11.	Summary of self-preserving turbulent plume constants	45

List of Figures

Figure	Caption	Page
1.	TEM photograph of a typical overfire soot aggregate from a buoyant turbulent ethylene/air diffusion flame in the long residence time regime. Note that the TEM length label is 100 nm long.	3
2.	Sketch of the buoyant turbulent diffusion flame apparatus.	7
3.	Sketch of the radiation extinction and scattering instrument	10
4.	Volumetric extinction and scattering cross sections as a function of wavelength for overfire soot from buoyant turbulent fuel/air diffusion flames in the long residence time regime	20
5.	Measured and predicted volumetric vv cross sections at 632.8 nm as functions of the modulus of the scattering vector for overfire soot from buoyant turbulent fuel/air diffusion flames in the long residence time regime	22
6.	Measured and predicted angular scattering patterns at 632.8 nm of overfire soot from buoyant turbulent propane/air diffusion flames in the long residence time regime	23
7.	Measured and predicted angular scattering patterns at 351.2 nm of overfire soot from buoyant turbulent propane/air diffusion flames in the long residence time regime	24
8.	Measured and predicted angular scattering patterns at 632.8 nm of overfire soot from buoyant turbulent acetylene/air diffusion flames in the long residence time regime	25
9.	Measured and predicted angular scattering patterns at 351.2 nm of overfire soot from buoyant turbulent acetylene/air diffusion flames in the long residence time regime	26
10.	Measured refractive indices of soot in the ultra-violent and visible portions of the spectrum	29
11.	Measured dimensionless extinction coefficients of soot in the visible and near infrared portions of the spectrum.	31
12.	Sketch of round buoyant turbulent plume test apparatus	36
13.	Radial profiles of mean mixture fractions in round buoyant turbulent plumes	39
14.	Radial profiles of mean streamwise velocities in round buoyant turbulent plumes	41
15.	Radial profiles of r.m.s. mixture fraction fluctuations in round buoyant turbulent plumes	42

16. Radial profiles of r.m.s. velocity fluctuations in round buoyant turbulent plumes..... 43

17. Radial profiles of mean mixture fractions and streamwise velocities in round buoyant turbulent plumes at various coflow rates..... 47

18. Radial profiles of r.m.s. mixture fraction and streamwise velocity fluctuations for round self-preserving buoyant turbulent plumes at various coflow rates 48

19. Measured and predicted mean streamwise velocity and mixture fraction distributions..... 50

20. Measured and predicted turbulence Prandtl/Schmidt numbers..... 51

21. Distributions of the mechanical/scalar time scale ratios, C_{μ} and C_{g2} 52

22. Radial profiles of turbulent mass fluxes in round buoyant turbulent plumes..... 53

23. Measured and predicted third velocity moments in round buoyant turbulent plumes..... 56

24. Measured and predicted third velocity moments in round buoyant turbulent plumes..... 57

25. Measured and predicted combined third velocity moments in round buoyant turbulent plumes 58

26. Measured and predicted combined third velocity moments in round buoyant turbulent plumes 59

27. Radial distributions of fourth moments of velocity fluctuations in round buoyant turbulent plumes 60

28. Radial distributions of fourth moments of velocity/mixture fraction fluctuations involving first moments of mixture fraction fluctuations in round buoyant turbulent plumes..... 61

29. Radial distributions of fourth moments of velocity/mixture fraction fluctuations involving higher moments of mixture fraction fluctuations in round buoyant turbulent plumes..... 62

Nomenclature: Soot Optical Properties

C	=	optical cross section
d	=	burner diameter
d_p	=	primary particle diameter
D_f	=	mass fractal dimension, Eq. (1)
D_{30}	=	volume averaged soot aggregate diameter
$E(m)$	=	refractive index function = $\mathrm{Im}((m^2-1)/(m^2+2))$
f_v	=	soot volume fraction
$g(\lambda,R_g,D_f)$	=	aggregate total scattering factor
$F(m)$	=	refractive index function $=\lvert(m^2-1)/(m^2+2)\rvert^2$
i	=	$(-1)^{1/2}$
I	=	light intensity
k	=	wave number = $2\pi/\lambda$
k_e	=	dimensionless extinction coefficient
k_{eR}	=	k_e at the Rayleigh scattering limit, Eq. (22)
k_f	=	fractal prefactor, Eq. (1)
L	=	light path length, mean flame length
m	=	soot refractive index = $n+i\kappa$
n	=	real part of soot refractive index
n_p	=	mean number of primary particles per unit volume
N	=	number of primary particles per aggregate
N_c	=	critical aggregate size for power-law regime, Eq. (11)
$p(N)$	=	probability density function of N.
q	=	modulus of scattering vector=$2k\sin(\theta/2)$
Q	=	volumetric optical cross section
Re	=	Reynolds number of burner = $u_0 d/n_0$

R_g = radius of gyration of an aggregate

t_r = characteristic flame residence time

t_s = characteristic flame residence time at laminar smoke point

T_s = gas temperature at measurement condition

u = streamwise gas velocity

x_p = primary particle size parameter=$\pi d_p/\lambda$

θ = angle of scattering from forward direction

κ = imaginary part of refractive index of soot

λ = wavelength of radiation

ν = kinematic viscosity

ρ = gas density

ρ_s = density of soot

ρ_{sa} = ratio of scattering to absorption cross sections

ρ_v = depolarization ratio, Eq. (23)

Subscripts

a = absorption

c = centerline value

d = differential

e = extinction

h = horizontal polarization

ij = incident (i) and scattered (j) polarization directions

s = total scattering

v = vertical polarization

Superscripts

^{o}	=	burner or light source exit condition
^{a}	=	aggregate property
p	=	primary particle property
$(\bar{})$	=	mean value over a polydisperse aggregate population

Nomenclature: Buoyant Turbulent Plumes

B_o	=	source buoyancy flux, Eq. (27)
C_μ	=	turbulence modeling constant, Eq. (27)
d	=	source diameter
E_o	=	plume entrainment constant, Eq. (36)
$E_f(n), E_u(n)$	=	temporal power spectral densities of f and u
f	=	mixture fraction
$F(r/(x-x_o))$	=	scaled radial distribution of $\bar{f}$ in self-preserving region, Eq. (33)
Fr_o	=	source Froude number, $(4/\pi)^{1/4} \ell_M/d$
g	=	acceleration of gravity, scalar variance
k	=	turbulence kinetic energy
k_f, k_u	=	plume width coefficients, based on $\bar{f}$ and $\bar{u}$, Eq. (35)
ℓ_c	=	characteristic plume radius
ℓ_f, ℓ_u	=	characteristic plume radii based on $\bar{f}$ and $\bar{u}$, Eq. (35)
ℓ_M	=	Morton length scale, Eq. (25)
M_o	=	source specific momentum flux, Eq. (26)
n	=	frequency
PDF (f)	=	probability density function of mixture fraction
Q	=	plume volume flux
r	=	radial distance
Re_c	=	characteristic plume Reynolds number, $\bar{u}_c \ell_c/\nu_\infty$
Re_o	=	source Reynolds number, $u_o d/\nu_o$
u	=	streamwise distance
$U(r/(x-x_o))$	=	scaled radial distribution of $\bar{u}$ in self-preserving region, Eq. (34)
v	=	radial velocity
w	=	tangential velocity

x	=	streamwise distance
δ_{ij}	=	Kronecker delta function, =1, i=j; =0, i≠j
ε	=	rate of dissipation of turbulence kinetic energy
ε_{ij}	=	rate of dissipation of velocity correlation $\overline{u_i' u_j'}$
η	=	dimensionless radial distance, Eq. (16)
ν	=	kinematic viscosity
ν_T	=	effective turbulence kinematic viscosity
ρ	=	density
σ_T	=	effective turbulence Prandtl/Schmidt number
τ_f, τ_u	=	temporal integral scale of f′ and u′

Subscripts

c	=	centerline value
o	=	initial value or virtual origin location
∞	=	ambient value

Superscripts

$(\bar{})$	=	time-averaged mean value
$(\bar{})'$	=	root-mean-squared fluctuating value

1. Introduction

An investigation is described that is relevent to two aspects of unwanted fires: (1) effects of fuel type and flame condition on the optical and radiative properties of soot in flame environments, and (2) the structure and mixing properties of buoyant turbulent flows typical of fire environments. The findings of the research have applications to modeling unwanted fires; to controlling the emission of radiant energy, toxic materials and soot from fires; to developing materials test codes for fire properties; and to developing fire detectors.

The first phase of the research is addressing the optical and radiative properties of soot in flame environments. The motivation for this investigation is that earlier results demonstrated a strong correlation between carbon monoxide and soot emissions from turbulent diffusion flames (Köylü et al., 1991, 1992; Köylü and Faeth, 1991a, b), while continuum radiation from soot is the main radiative effect in practical fires (Köylü and Faeth, 1993a). Understanding the optical properties of soot is crucial for a better understanding of both of these problems: soot concentrations and structure generally are measured using nonintrusive laser-based methods that require knowledge about soot optical properties in order to correctly interpret the measurements, while soot optical properties are a controlling factor in the continuum radiation properties of flames. Past work showed that soot morphology could be approximated by mass fractal aggregates of spherical primary particles, where the primary particles were nearly monodisperse while the aggregates exhibited broad distributions of the number of primary particles per aggregate, in agreement with earlier work (Köylü and Faeth, 1992, 1993a). Then the use of the Rayleigh-Debye-Gans (RDG) scattering approximation, while approximating soot aggregates as polydisperse mass fractal objects, was shown to be acceptable for soot within diffusion flames based on evaluation of the approximate RDG predictions by both measurements and more exact predictions (Köylü and Faeth, 1993a,b,1994a,b; Farias et al., 1993, 1995a, b, c). Subsequently, soot structure properties needed for RDG predictions of soot optical properties were studied, considering relationships between actual and projected soot images, and the mass fractal dimensions and prefactors of soot in flames (Köylü et al., 1995; Dai et al., 1994b). These results also showed that the main limitation preventing reliable nonintrusive measurements of soot properties in flames, as well as reliable estimates of the continuum radiation properties of soot in flames, was inadequate information about the refractive indices of soot. Thus, the objective of this phase of the investigation is to experimentally determine effects of fuel type and flame condition on soot refractive indices for wavelengths ranging from the near ultra-violet to the infra-red (350-5000 nm) which covers the wavelength range relevent to practical soot optical property and radiation applications.

The second phase of the research is addressing the properties of buoyant turbulent flows that are a central feature of the environment of unwanted fires and are needed in order to understand turbulence/radiation interactions. In particular, stochastic simulation techniques have been developed to estimate effects of turbulence/radiation interactions in flames, based on laminar flamelet concepts and a knowledge of mixture fraction statistics, see Kounalakis et al. (1991) and references cited therein. In spite of extensive past studies, however, available information about the turbulence properties of buoyant turbulent flows was too limited to allow use of the stochastic simulation methology to estimate effects of turbulence/radiation interactions. Furthermore, the first phase of the present investigation revealed that past work had not completed measurements sufficiently far from the source to observe fully-developed (self-preserving) buoyant turbulent plume behavior (Dai et al., 1993, 1994a,b,c, 1995a,b; Köylü et al. 1992, 1993). This finding is problematical because self-preserving conditions are important for developing models of buoyant turbulent flows that are needed to address problems of practical fire environments. Thus, the objective of this phase of the investigation is to experimentally determine the mean and turbulent properties of self-preserving buoyant turbulent plumes, and to use these results to evaluate models of plume structure and turbulence properties.

The studies of soot optical properties and buoyant turbulent plumes are described, in turn, in the following. The present description is brief; therefore, other reports and publications resulting from the investigation should be studied for more details, e.g., Dai (1995), Dai and Faeth (1995), Dai et al. (1993, 1994a,b,c, 1995a,b), Faeth (1994, 1995), Faeth and Köylü (1995), Farias et al. (1993, 1995a,b,c), Köylü (1992), Köylü and Faeth (1991a, 1991b, 1992, 1993a,b, 1994a,b,, 1995) and Köylü et al. (1991, 1992, 1993, 1995). The description of each phase of the research is sufficiently complete, however, so that it can be read independently.

2. Optical and Radiative Properties of Soot

2.1 Introduction

Practical hydrocarbon-fueled flames contain and emit soot, which affects their radiation, structure, toxic substance emission and pollutant emission properties. These effects have motivated considerable interest in the structure and optical properties of soot, in order to develop nonintrusive methods for measuring soot properties and to estimate the continuum radiation properties of soot in flame environments. Motivated by these observations, this phase of the investigation seeks a better understanding of soot optical and radiation properties in flame environments. Earlier work on this phase of the investigation addressed the morphological properties of soot and the applicability of the Rayleigh-Debye-Gans (RDG) scattering approximation to treat the optical properties of soot over the visible and infra-red wavelength ranges; current work on this phase of the investigation is addressing the refractive index properties of soot.

Earlier work concerning the structure and optical properties of soot only will be discussed briefly, more details can be found in the reviews by Charalampopoulos (1992), Faeth (1995), Faeth and Köylü (1995), Faeth et al. (1987, 1989, 1990), Jullien and Botet (1987), Köylü and Faeth (1993a), Tien and Lee (1982) and Viskanta and Mengüc (1987). In addition, earlier work in this laboratory dealing with these properties is described by Dai et al. (1994b), Faeth and Köylü (1995), Faeth et al. (1987, 1989, 1990), Farias et al. (1995a,b,c),, Köylü and Faeth (1992, 1993a,b, 1994a,b, 1995), and Köylü et al. (1992, 1993, 1995). In the following, the structure and optical properties of soot will be discussed in turn.

Numerous earlier studies have shown that soot consists of small spherical primary particles, having nearly constant diameters at a particular flame condition, collected into open structured aggregates that have broad distributions of the number of primary particles (Dalzell et al., 1970; Dobbins and Megaridis, 1987, 1991; Dobbins et al., 1993; Erickson et al., 1964; Jullien and Botet, 1987; Martin and Hurd, 1987; Megaridis and Dobbins, 1990; Samson et al., 1987; Wersborg et al., 1972). A typical example of soot aggregate structure can be seen from the transmission election microscope (TEM) image illustrated in Fig. 1. In particular, distributions of primary particle diameters have standard deviations of 15-25% of the mean primary particle diameter while soot aggregates exhibit log-normal size distribution functions with aggregate sizes in the range 30-1800 primary particles. It also is generally agreed that flame-generated soot aggregates exhibit mass fractal-like behavior with a Hausdorf or fractal dimension, $D_f < 2$, even when the number of primary particles in an aggregate is small, which implies (Jullien and Botet, 1987):

$$N = k_f(R_g/d_p)^{D_f} \qquad (1)$$

Earlier work has established that the fractal properties of soot aggregates in flame environments are relatively durable, yielding current best estimates of $D_f = 1.82$ with an

Figure1. TEM photograph of a typical overfire soot aggregate from a buoyant turbulent ethylene/air diffusion flame in the long residence time regime. Note that the TEM length label is 100 nm long.

uncertainty (95% confidence) of 0.08 and $k_f = 8.5$ with an uncertainty (95% confidence) of 0.5 (Köylü et al., 1995).

Measurements have shown that flame-generated soot ranges from small aggregates (dimensions on the order of 10 nm) near the start of soot formation, to large aggregates (dimensions on the order of 1 μm) emitted from large buoyant turbulent diffusion flames (Köylü and Faeth, 1992, 1993a,b, 1994a,b). Thus, even though primary particle diameters are less than 60nm, which implies Rayleigh scattering from individual primary particles for wavelengths of practical interest, use of traditional approximate scattering theories has not been very effective (Köylü and Faeth, 1994a,b). These difficulties were established by direct measurements of soot scattering properties during early work (Erickson et al., 1964; Dalzell et al., 1970; Wersborg et al., 1972); for example, strong forward scattering was observed which is not representative of Rayleigh scattering behavior, while use of the Mie scattering approximation for an equivalent sphere still did not provide an adequate fit of the scattering measurements. The former behavior follows because the larger soot aggregates in the size distribution dominate scattering properties and are too large to be approximated as Rayleigh scattering objects (Köylü and Faeth, 1993a); the latter behavior follows because $D_f<2$ which implies that aggregate structure is too open to be represented by a compact object such as an equivalent Mie scattering sphere (Berry and Percival, 1986). The limitations of the Rayleigh and Mie scattering theories prompted subsequent development of optical theories of soot aggregates based on the Rayleigh-Debye-Gans (RDG) approximation for mass fractal objects consisting of constant diameter spherical primary particles that just touch one another, and satisfy the Rayleigh scattering approximation as individual particles, with polydisperse aggregate size distributions (Jullien and Botet, 1987; Köylü and Faeth, 1993a, 1994a; Martin and Hurd, 1987; Dobbins and Megaridis, 1991). The resulting RDG theory, which will be denoted RDG-PFA theory in the following, was questioned, however, because the relatively large refractive indices of soot raised concerns about the validity of the RDG scattering approximation (Köylü and Faeth, 1993a).

In view of concerns about the RDG scattering approximation for soot aggregates, earlier work in this laboratory sought an experimental and computational evaluation of RDG-PFA theory (Köylü and Faeth, 1993a, 1994a,b; Farias et al., 1995a,b,c). The experimental evaluation involved comparing RDG-PFA scattering predictions, based on measured soot structure properties from thermophoretic sampling and TEM analysis, with *in situ* measurements of scattering for the same aggregate population. This study considered both large soot aggregates in the fuel-lean (overfire) region of buoyant turbulent diffusion flames in the long residence time regime, where soot properties become independent of position in the overfire region and residence time, see Sivathanu and Faeth (1990) and Köylü and Faeth (1992), which emphasized the large-angle (power-law) regime (Köylü and Faeth (1994b), and small soot aggregates in the fuel-rich (underfire) region of laminar diffusion flames, which emphasized the small angle (Guinier) regime (Köylü and Faeth, 1994b). The predictions and measurements agreed within experimental uncertainties for the power-law regime, where soot aggregate properties that dominate aggregate scattering properties could be found accurately from structure measurements. The evaluation was less than definitive in the Guinier regime, however, due to difficulties of accurately measuring both scattering properties at small angles and the higher moments of the aggregate size distribution functions (e.g., $\overline{N^2}$) that dominate scattering properties at small angles (Köylü and Faeth, 1994a,b). This limitation of the experimental evaluation of RDG-PFA theory was a concern because multiple scattering effects that could compromise the use of RDG-PFA theory are most significant in the Guinier regime (Nelson, 1989a,b).

Farias et al. (1995a,b) undertook a subsequent computational evaluation of RDG-PFA theory in order to obtain more definitive results in the Guinier regime. This evaluation was initially based on computations using the ICP formulation of Iskander et al. (1989) which provides a more exact treatment of the Guinier regime than RDG-PFA theory by

including effects of multiple and self-induced scattering. Notably, Ku and Shim (1992) review several theories of aggregate optical properties that are more accurate than the RDG approximation, concluding that the ICP formulation was superior to the popular Jones and Purcel-Pennypacker solutions. Subsequently, Lou and Charalampopoulos (1994, 1995) find improved results from the ICP approach using the Goedecke-O'Brian (GO) solution which provides a more exact treatment of the optical theorem (energy conservation); however, differences between ICP and GO predictions are negligible compared to computational uncertainties (roughly 10%) for conditions of present interest (Farias et al., 1995b). In addition, problems of adequately defining the size distribution functions of polydisperse aggregates during experiments were avoided by using numerical simulations to generate aggregates having prescribed sizes and fractal properties. This computational evaluation was carried out for $x_p \leq 0.4$ and $N \leq 512$ for mass fractal objects having fractal and refractive index properties typical of soot (notably, this range of x_p also is typical of soot in the visible portion of the spectrum that is used for soot laser diagnostics). Evaluation of the ICP algorithm using Mie scattering predictions indicated satisfactory performance in the Guinier regime for conditions of interest, with progressive build-up of errors as x_p, the refractive index and the scattering angle increased into the power-law regime. Finally, the ICP and RDG-PFA predictions agreed within computational uncertainties, roughly 10%, within the Guinier regime. Thus, taken together, the combined experimental and computational evaluations suggest that the RDG-PFA theory is satisfactory for $x_p \leq 0.4$ for refracitve indices typical of soot, which covers the range of conditions normally encountered for flame-generated soot.

Given successful evaluation of the RDG-PFA theory for the optical properties of soot, there is potential for developing methods for solving the inverse problem so that soot structure properties can be found nonintrusively from scattering measurements and for treating continuum radiation from soot in flame environments. Unfortunately, this potential has not been realized due to large uncertainties concerning soot refractive indices in the critical visible and infrared wavelength regimes (Chang and Charlampopoulis, 1990; Choi et al., 1994, 1995; Dobbins et al., 1993; Köylü and Faeth, 1993a; Sorensen et al., 1992a,b). Conventional wisdom is that soot refractive indices are relatively independent of fuel type, temperature and residence time in the flame. Nevertheless, some recent work finds variations of soot refractive indices with residence time in flame environments, and potentially large effects of fuel type, see Chang and Charalampopoulos (1990) and references cited therin. Thus, in spite of recent measurements by Choi et al. (1994, 1995), Köylü and Faeth (1994a) and Dobbins et al. (1993), which tend to support the classical soot refractive index measurements of Dalzell and Sarofim (1969), widespread criticism of these measurements has not yet been resolved (Tien and Lee, 1982, 1983). These difficulties are a substantial impediment to progress toward developing methods for predicting the continuum radiation properties of flames; in fact, potential errors caused by uncertainties concerning soot refractive indices are far larger than differences between the Rayleigh and RDG-PFA scattering theories for typical soot aggregates (Köylü and Faeth 1994a,b).

In view of these considerations, this phase of the investigation seeks to advance our understanding of soot refractive indices in flame environments by completing an experimental study of the effects of fuel type and flame conditions on soot refractive indices in the visible and infrared wavelength ranges. This work has involved *in-situ* measurements of soot scattering properties which are subsequently interpreted using RDG-PFA theory to find soot refractive indices and other soot optical properties. Thus far, measurements have been limited to soot in the overfire region of large gas-fueled buoyant turbulent diffusion flames in the long residence time regime, when soot properties became universal for a particular fuel type burning in air (Köylü and Faeth, 1992).

The discussion begins with consideration of experimental and theoretical methods. Results are then presented, considering soot scattering properties, refractive indices and dimensionless extinction coefficients, in turn.

2.2 Experimental Methods

Apparatus. A sketch of the test apparatus appears in Fig. 2. The arrangement is similar to earlier work considering overfire soot in the long residence time regime of buoyant turbulent diffusion flames (Köylü and Faeth, 1992, 1994a; Sivathanu and Faeth, 1990). The components of the apparatus include a burner, a soot collection system and an exhaust system.

The 50 mm diameter water-cooled burner used by Sivathanu and Faeth (1990) provided the flame source. The present measurements were limited to gaseous hydrocarbons—acetylene, propylene, ethylene and propane—burning in still air. A bed of metal beads was used to disperse the fuel gas. The fuels are injected vertically upward from the burner with the flames stabilizing naturally at the burner exit. Burner operation yielded strongly buoyant, pool-like turbulent flames in the long residence time regime where soot properties are independent of both position in the overfire region and characteristic flame residence time (Sivathanu and Faeth, 1990).

Soot properties were measured by collecting the combustion products in a sampling hood and duct that were heated to prevent thermophoretic deposition of soot on their surfaces. The exhaust duct had a diameter of 152 mm, with the measuring station at the exit of the duct. This duct discharged into the main hood of the apparatus. Measurements showed that mixing within the heated duct was sufficient to yield uniform soot and gas species concentrations across the duct exit, see Köylü and Faeth (1994a). Note that since the soot structure, and the generation of soot per kg of fuel carbon burned, are independent of position in the overfire region for operation within the long residence time regime (Sivathanu and Faeth, 1990; Köylü and Faeth, 1992), collection in this manner does not affect soot structure properties.

The burner and soot collection system were located within a large outer enclosure (2400 x 2400 x 3600 mm high). The enclosure had a metal hood at the top and an adjustable exhaust system to collect and remove combustion products. The side walls of the enclosure were plastic strips which minimized effects of room disturbances.

Instrumentation. Several measurements were made in order to determine soot scattering properties, soot refractive indices and the dimensionless extinction coefficients of soot, including: soot structure, soot density, temperature distributions along the optical path, a gravimetric determination of soot volume fraction and finally, extinction and scattering measurements at the wavelengths of interest. These measurements will be discussed, in turn, in the following.

The structure of the soot being studied had already been characterized by thermophoretic sampling and TEM measurements (Köylü and Faeth, 1992). Nevertheless, these measurements were repeated to insure that the soot structure was known thoroughly (particularly d_p which must be known accurately in order to determine soot refractive indices). Procedures for sampling and analyzing the structure of soot, however, were similar to Köylü and Faeth (1992). The sampling surfaces were the carbon-supported copper grids used to hold TEM specimens (3 mm diameter, 200 mesh copper grids supported by a 20 nm thick elemental carbon film, SPI Supplies, Philadelphia, part no. 3520C). The grids were aligned in the vertical direction, parallel to the mean flow direction at the axis. The grids were mounted on a 1x4x15 mm metal strip using double-backed

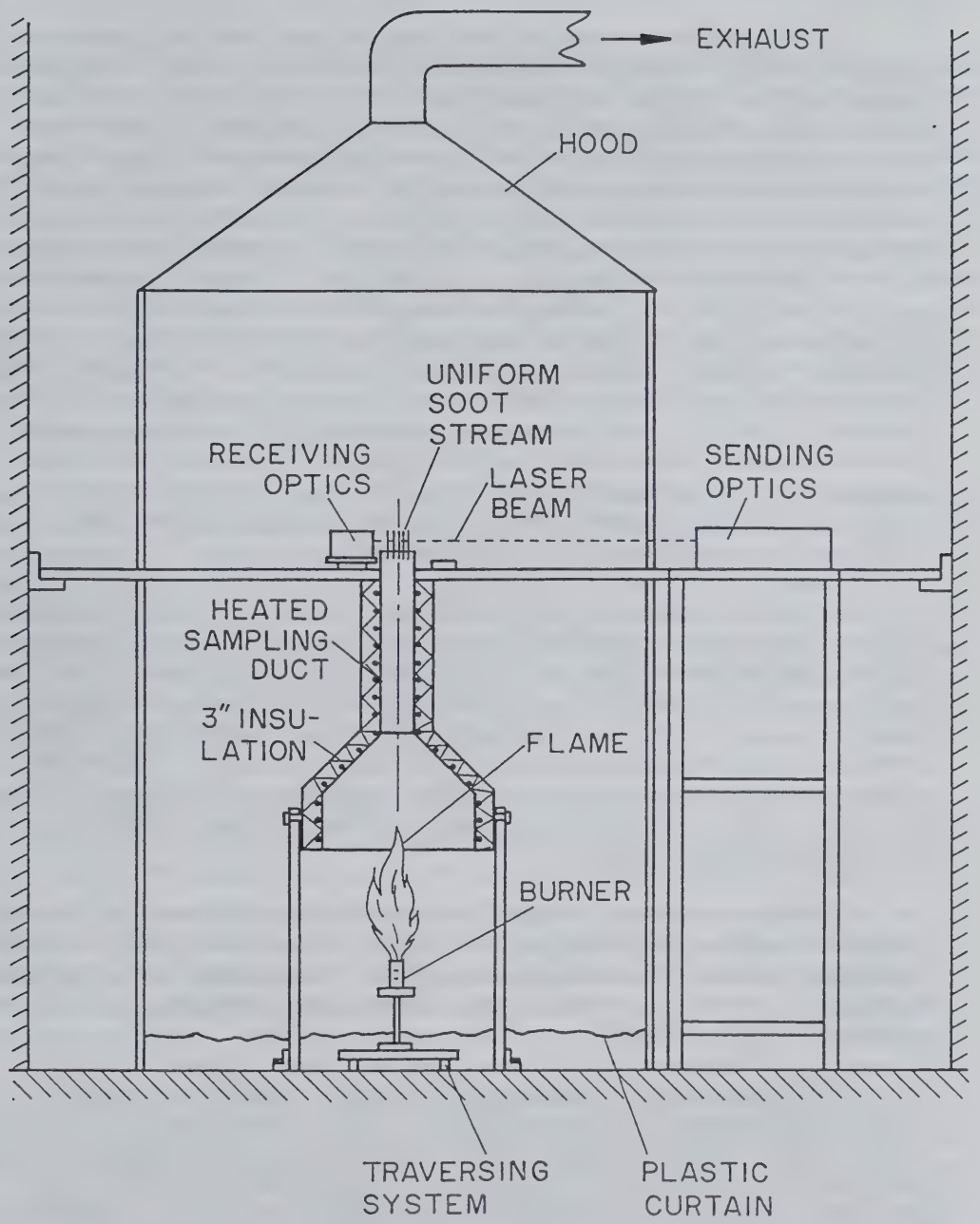

Figure 2. Sketch of the buoyant turbulent diffusion flame apparatus.

adhesive which was mounted in turn on a retractable probe. The probe was stored outside the duct in a soot-free region, with roughly a 100 mm stroke to reach the flame axis. A double-acting pneumatic cylinder rapidly drove the probe to the sampling position and returned it when sampling was complete. Sampling times were measured using a pair of light-interrupting sensors. Sampling times were controlled so that soot aggregates covered no more than 10% of the surface of the TEM grid in order to avoid overlapping aggregates on the grid.

The principles of thermophoretic sampling are discussed elsewhere (Dobbins and Megaridis, 1987; Köylü and Faeth, 1992; Rosner et al., 1991). For present conditions, primary particle diameters are smaller than the mean free path so that the thermophoretic velocities of individual particles are the same. In addition, Rosner et al. (1991) have shown that the thermophoretic velocities of aggregates are the same as individual primary particles, even when the aggregates are larger than mean free path lengths. Thus, there is no intrinsic bias with respect to aggregate size for the thermophoretic sampling technique. The samples were observed using a JEOL 2000 FX analytical electron microscope system with a 1 nm edge-to edge resolution. Latex spheres having a diameter of 91 nm (with a standard deviation of 5.8 nm) were used to calibrate the TEM measurements. Magnifications used for present measurements were in the range 600-200,000. The proceedure involved selecting aggregates randomly at low magnification, and then increasing the magnification to analyze them. Images were processed using the IMAGE computer algorithm to find primary particle diameters. A sample of roughly 400 primary particles, selected from more than 50 aggregates, was used to measure d_p, to obtain uncertainties of the average value of d_p less than 2%. Similar to the observations of Köylü and Faeth (1992), the standard diviations of the d_p were relatively small, corresponding to 17-21% of the mean value of d_p over all the fuels.

Soot density was found by collecting samples of soot at the measuring location. The sampling system consisted of a water-cooled plate so that soot deposited on the cooled surfaces due to thermophoresis. The soot was periodically scraped from the plate surface until a sample of roughly 500 mg was obtained. The samples were then compressed into pellets to facilitate density measurements by helium pycnometry. These measurements were carried out by Micrometrics Inc., Norcross, GA using a 1000 mm^3cell. The precision of the density measurements was excellant, involving uncertanities (95% confidence) less than 0.4%. The composition of the soot had been obtained earlier by Köylü (1992) and these results were not repeated.

Temperatures were measured along the optical path using a thermocouple probe. Temperatures of the mixture at the exit of duct were relatively low, 380-450 K, and were uniform across the duct exit as discussed earlier. Thus, conduction and radiation errors of these measurement were small, and experimental uncertainties (95% confidence) are estimated to be less than 10K.

The next step in measuring soot refrative indices using the present *in situ* method involved gravimetric determinations of the soot volume fractions in the region where extinction and scattering measurements were made. The approach used to make these measurements was similar to Dobbins et al. (1993) and Choi et al. (1994, 1995). This involved a sampling train consisting of a sampling probe, a filter assembly, a flowmeter and a vacuum pump. The present flow is uniform over a 150 mm diameter cross section; therefore, it was not necessary to employ a small probe for good spatial resolution. Thus, a 13 mm inside diameter water cooled sampling probe, aligned in the flow direction, was used. This probe was connected to a modified Gelman filter holder (Product 2220, in-line, 47mm) which in turn was connected through a flowmeter and valve to a vacuum pump. The flowmeter had a manometer at its inlet and was calibrated over the required range of inlet pressures using a wet test meter. A Gelman filter (Part no. 66143, 0.2 nm, TF200, 47mm, PTFE membrane filter) was used in the filter holder to collect soot for a timed

period while a second filter was used to mechanically collect any soot in the sampling line and the filter assembly. The mass of sampled soot was found by weighing the filters before and after sampling using an electronic balance. Then given the density of the soot, the mass of soot collected and the volume of gas sampled during the sampling period, the gravimetric soot volume fraction can be calculated in a straight-forward manner. Times of sampling were adjusted for these measurements in order to achieve experimental uncertainties (95% confidence) less than 6%.

The final results required for the *in situ* measurement of soot refractive indices are extinction and scattering measurements at the wavelengths of interest. The test arrangement for these measurements was identical to Köylü and Faeth (1994a). A sketch of the arrangement appears in Fig. 3 (on this figure, PR denotes polarization rotator, C denotes chopper, BS denotes beam splitter, L denotes lens, S denotes slit, P denotes polarization analyzer, F denotes narrow-band optical filter, NDF denotes neutral density filter, A denotes aperture, PMT denotes photomultiplier tube and D denotes photodetector). Although the figure indicates a laser as the source of illumination, various sources were used to cover the wavelength range as summarized in Table 1. The incident light beam was passed through a polarization rotator and a mechanical chopper (operating at 1250 Hz) before being focused at the centerline of the exhaust duct using a 1000 mm focal length lens. The collecting optics were mounted on a turntable surrounding the exhaust duct so that scattering angles, θ=5-160 deg, could be considered.

The collecting optics consisted of an 85 mm focal length lens, a dichroic sheet polarizer, a line filter (1nm bandwidth for the lasers, and 10nm bandwidth for the lamp), and a photomultiplier. The lens aperture defined a solid collection angle of 0.7 msr. Neutral density filters were used in the optical path to control the dynamic range of detection. The experimental area as well as the receiving optics were covered with black cloth to reduce optical noise from the room lighting and the flame. The test room also was windowless and provided dark-room conditions. The detector output passed through a lock-in amplifier and was stored on a computer sampling at 500Hz for 10s and averaging five sampling periods to achieve repeatability within 10%.

Except as noted, the angular light scattering system was calibrated by measuring Rayleigh scattering from propane gas. After correction for the reciprocal sin θ effect due to the geometry of the measuring volume, the vv and hh differential cross sections were within 5% of Rayleigh scattering predictions for θ of 20-160 deg. Absolute volumetric differential scattering cross sections of soot were found from ratios of the detector signal for soot and propane, after accounting for signal attenuation in the optical path, based on the propane and n-butane optical properties of Dyer (1979) and Rudder and Bach (1968). Total volumetric diffential scattering cross sections were found by integrating the volumetric diffential scattering cross sections over the whole spherical surface. This required extrapolation of the measurements to reach $\theta = 0$ and 180^0, however, uncertainties caused by the extrapolations were small due to the relatively small solid angles involved. The overall experimental uncertainties (95% confidence) of the angular and the total light scattering measurements were comparable and were estimated to be less than 20%, dominated by finite sampling times, the finite aperture of the detector and the angular uncertainty of the collecting optics.

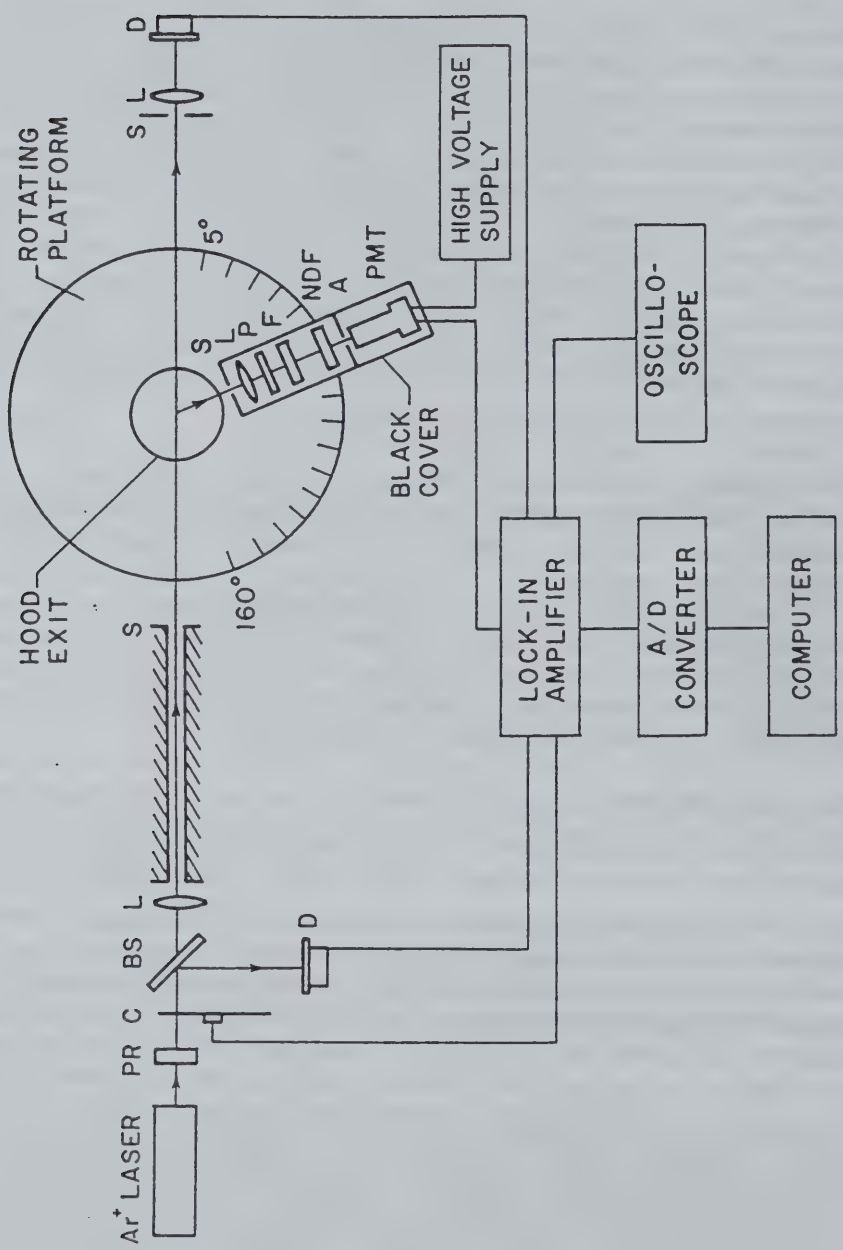

Figure 3. Sketch of the radiation extinction and scattering instrument.

Table 1 Light Sources for the Soot Scattering Measurements

Wave length (nm)	Light Source	Manufacturer and Model	Power
351.2	Argon-Ion Laser	Coherent Innova 90-4	100 mW
405.0	Mercury Lamp	Oriel 6333	100 W
488.0	Argon-Ion Laser	Coherent-Innova 90-4	1300 mW
514.5	Argon-Ion Laser	Coherent-Innova 90-4	1700 mW
632.8	He-Ne Laser	Jodon, Model HNIOGIR	28 mW
800.0	Diode Laser	SDL-2360-P3	700 mW

2.3 Theoretical Methods

RDG-PFA Theory. Analysis of the optical measurements to find soot refractive indices was based on RDG-PFA theory, see Köylü and Faeth (1994a) for a complete description of this formulation. The major assumptions of RDG-PFA theory are as follows: individual primary particles satisfy the Rayleigh scattering approximation, soot aggregates satisfy the Rayleigh-Debye-Gans (RDG) scattering approximation, spherical primary particles having constant diameters, primary particles just touch one another, uniform refractive indices, aggregates are mass fractal-like objects and aggregate sizes (represented by the number of primary particles in an aggregate, N) satisfy a log-normal size distribution function. As discussed earlier, all these approximations are reasonable for soot, based on the experimental and computational studies of Köylü and Faeth (1994a,b), Köylü et al. (1995) and Farias et al. (1995a,b,c).

Under the present approximations, individual (non-aggregated) primary particles satisfy the following Rayleigh scattering relationships (Bohren and Huffman, 1983; Kerker, 1969):

$$C_a^p = 4\pi x_p^3 E(m)/k^2 \tag{2}$$

$$C_s^p = 8\pi x_p^6 F(m)/(3k^2) \tag{3}$$

$$C_{vv}^p = x_p^6 F(m)/k^2 \tag{4}$$

where $C_{hv}^p = C_{vh}^p \approx 0$, $C_{hh}^p = C_{vv}^p \cos^2\theta$ and $C_e^p = C_a^p + C_s^p$. The cross sections of Eqs. (2)-(4) will be used in the following to normalize aggregate cross sections. The treatment of aggregate scattering properties begins with the scattering cross sections found for individual fractal aggregates under the RDG approximation:

$$C_{vv}^a(\theta) = C_{hh}^a(\theta)/\cos^2\theta = N^2 C_{vv}^p f(qRg) \tag{5}$$

where the form factor, $f(qR_g)$, is expressed as follows in the small-angle (Guinier) and large-angle (power-law) regimes, respectively (Freltoft et al., 1986; Jullien and Botet, 1987; Lin et al., 1989; Martin and Hurd, 1987):

$$f(qR_g) = \exp(-(qR_g)^2/3), \text{ Guinier regime; } = (qR_g)^{-D_f}, \text{ power-law regime} \tag{6}$$

These two asymptotic expressions are matched at the condition $(qR_g)^2 = 3D_f/2$, following Dobbins and Megaridis (1991), in order to define $f(qR_g)$ over the complete range of scattering angles. Within the present approximations, $C_{hv}^a = C_{vh}^a = 0$, so that the total scattering cross section becomes:

$$C_s^a = N^2 C_s^p g(\lambda, R_g, D_f) \tag{7}$$

where $g(\lambda, R_g, D_f)$ takes on different forms depending on whether the power-law regime is reached for $q \leq 180$ deg or not; see Köylü and Faeth (1994a) for these expressions. Finally, under these approximations, the absorption and extinction cross sections become:

$$C_a^a = NC_a^p \tag{8}$$

$$C_e^a = C_a^a + C_s^a \tag{9}$$

Given the properties of individual aggregates from Eqs. (2)-(9) we now turn to polydisperse aggregate populations. The mean optical cross sections of populations of

randomly oriented polydisperse aggregate populations (polydisperse aggregates) are found by integrating over all aggregate sizes, as follows:

$$\overline{C}^{a}_{j} = \int_{N=1}^{\infty} C^{a}_{j}(N)p(N)dN; \quad j=pp,s,a \tag{10}$$

where p(N) is the measured (log-normal) aggregate size distribution function. In general, Eqs. (10) must be integrated numerically when scattering extends over both the Guinier and power-law regimes. However, simple closed-form expressions are possible when all the aggregates are either in the Guinier regime ($p(N) << 1$ for $N \geq N_c$) or the power-law regime ($p(N) << 1$ for $N \geq N_c$), where

$$N_c = k_f(3D_f/(2q^2d_p^2))^{D_f/2} \tag{11}$$

When these conditions are satisfied, the vv differential scattering cross sections become (Köylü and Faeth (1993a):

Guinier regime:

$$\overline{Q}^{a}_{vv}(\theta)/Q^{p}_{vv} = \overline{C}^{a}_{vv}(\theta)/(\overline{N}C^{p}_{vv}) = (\overline{N}^2/\overline{N})\exp(-q^2\overline{R}^2_g/3) \tag{12}$$

Power-law regime:

$$\overline{Q}^{a}_{vv}(\theta)/Q^{p}_{vv} = k_f(qd_p)^{-D_f} = (\overline{N}^2/\overline{N})(q\overline{R}_g)^{-D_f} \tag{13}$$

Expressions for $\overline{R}_g$ at the Guinier and power-law regime limits can be found in Köylü and Faeth (1994a). Volumetric cross sections have been introduced in Eqs. (12) and (13) because these quantities are measured directly. In order to obtain Eqs. (12) and (13), the following relationships between volumetric optical cross sections and optical cross sections have been used:

$$\overline{Q}^{a}_{j} = n_a\overline{C}^{a}_{j} = n_p\overline{C}^{a}_{j}/\overline{N} \tag{14}$$

$$Q^{p}_{j} = n_pC^{p}_{p} = n_a\overline{N}C^{p}_{p} \tag{15}$$

Based on Eqs. (14) and (15), it can be seen that the ratios of volumetric cross sections given by Eqs. (12) and (13) represent the amplification of scattering effects by aggregates, compared to scattering from the same number of individual (unaggregated) primary particles. Under the same approximations, the absorption cross section in both regimes becomes:

$$\overline{Q}^{a}_{a}/Q^{p}_{a} = \overline{C}^{a}_{a}/(\overline{N}C^{p}_{a})=1 \tag{16}$$

Similarly, the extinction cross section in both regimes becomes:

$$\overline{Q}^{a}_{e}/Q^{p}_{e} = \overline{C}^{a}_{e}/(\overline{N}C^{p}_{a})=1+\rho_{sa} \tag{17}$$

where $\rho_{sa} = \overline{Q}^{a}_{s}/\overline{Q}^{a}_{a} = \overline{C}^{a}_{s}/\overline{C}^{a}_{a}$ is the ratio of the total scattering to absorption cross sections.

Refractive Indices. Evaluation of refractive indices is based on RDG-PFA theory as summarized by Eqs. (2)-(17). The first step in these calculations involved the determination of the mean number of primary particles per unit volume at the test condition from the gravimetric measurements of soot volume fraction, f_v, and the TEM measurement of d_p, as follows:

$$n_p = f_v/(\pi d_p^3/6) \quad (18)$$

The measurements of the volumetric optical cross sections, noting that $\overline{Q}_a^a = \overline{Q}_e^a - \overline{Q}_s^a$, then yield the refractive index functions, E(m) and F(m), as follows:

$$E(m) = k^2 \overline{Q}_a^a/(4\pi x_p^3 n_p) \quad (19)$$

$$F(m) = k^2(qd_p)^D f\, \overline{Q}_{vv}^a(\theta)/(k_f x_p^6 n_p) \quad (20)$$

where it is required that θ is large enough so that $\overline{Q}_{vv}^a(\theta)$ in Eq. (20) is properly within the power-law regime. This requirement was established by plotting $\overline{Q}_{vv}^a(\theta)/\overline{Q}_{vv}^p(\theta)$ as a function of qd_p to see that the proper power law behavior was achieved according to Eq. (13), as discussed later. Finally, E(m) and F(m) provide two nonlinear algebraic equations which are solved for the real and imaginary parts of the refractive indices of soot, n and κ.

Dimensionless Extinction Coefficients. The dimensionless extinction coefficient, k_e, is a useful optical property due to the simple relationship between extinction ratios and soot volume fractions along an optical path when optical properties are uniform and when k_e is known (Choi et al., 1994, 1995). As a result, this parameter was determined for present test conditions. The basic relationship used to find k_e was as follows (Choi et al., 1994, 1995):

$$k_e = -\lambda \ln(I/I_o)/(Lf_v(1+\rho_{sa})) \quad (21)$$

where I/I_o is the ratio of transmitted and incident light intensities over an optical path length, L, when optical properties are uniform.

Evaluation of k_e was based on Eq. (21), using the gravimetrically determined values of f_v. In keeping with general usage, where the simplest possible relationships between extinction measurements and soot volume fractions is sought, present evaluations of k_e were made using the approximation that $\rho_{sa} = 0$, even though ρ_{sa} was measured for present conditions and generally was not zero. Thus, values of the dimensionless extinction ratio reported here are actually based on the Rayleigh scattering approximation ($\rho_{sa} = 0$), or more precisely:

$$k_{eR} = k_e(1+\rho_{sa}) \quad (22)$$

Noting that $0.23 \leq \rho_{sa} \leq 0.46$ for present test conditions, as discussed later, k_{eR} is roughly 25-50 percent larger than k_e for present test conditions.

2.4 Experimental Conditions

Measurements were made using turbulent acetylene, propylene, ethylene and propane diffusion flames burning in still air. As noted earlier, characteristic flame residence times were sufficiently long so that the flames were in the long residnece time regime where soot properties are independent of position within the fuel-lean region and the residence time, as described by Sivathanu and Faeth (1990) and Köylü and Faeth (1992).

The properties of the test flames, as well as soot volume fractions based on the present gravimetric determinations, are summarized in Table 2. The test flames are ordered in terms of decreasing propensity to soot, as indicated by progressively increasing characteristic flame residence times at the laminar smoke point, t_s. The test flames had chemical energy release rates of 5140-7400 W, mean flame lengths of 440-500 mm and characteristic flame residence times roughly an order of magnitude longer than the

Table 2. Summary of test conditions for round buoyant turbulent diffusion flames in the long residence time regime.[a]

Fuel	Acetylene	Propylene	Ethylene	Propane
ρ_o(kg/m^3)	1.08	1.70	1.16	1.77
t_s(ms)	14	16	41	48
Re[b]	290	430	320	490
Q_f(W)	6160	6580	5140	7400
L(mm)	440	450	500	450
t_r(ms)	339	474	282	278
f_v(ppm)[c]	0.476	0.268	0.0446	0.0278
n_p(M part/mm^3)[d]	8.76	6.84	2.60	1.97
T_s(K)[e]	380	420	420	450

[a]Vertical fuel injection in still air at normal temperature and pressure using a 50 mm diameter burner. Flame length and residence times found from measurements and correlations of Sivathanu and Faeth (1990).

[b]$Re = u_o d/\nu_o$ based on average velocity at the burner exit conditions.
[c]Based on gravimetric measurements of soot volume fractions at the test location.
[d]Based on gravimetric measurements of soot volume fractions and TEM measurements of primary particle diameters, at the test location.
[e]At the test location.

Table 3. Summary of the structure and physical properties of soot from the overfire region of round buoyant turbulent diffusion flames in the long residence time regime.[a]

Fuel	Acetylene	Propylene	Ethylene	Propane
ρ_o(kg/m^3)	1870	1850	1930	1900
d_p(nm)	47	41	32	31
$\overline{N}$	417	400	467	364
D_{30}(nm)	350	301	247	214
Composition (% by mass):[b]				
C	96.3 (0.30)	95.2 (0.60)	---	85.3 (1.9)
H	0.48 (0.12)	0.47 (0.13)	---	0.59 (0.08)
O	1.2	2.2	---	---
N	0.38 (0.06)	0.27(0.14)	---	0.30 (0.10)
Atomic Ratios:				
C/H	16.8	17.0	---	12.1
C/O	107	57.6	---	---
C/N	295	411	---	332

[a]Measured by Köylü and Faeth (1994a) except for the present helium pycnometry measurements of ρ_s and confirmation of d_p values.
[b]Numbers in parnetheses indicate standard deviation.

corresponding laminar smoke point residence times, placing the flames in the long residence time regime (Sivathanu and Faeth, 1990; Köylü and Faeth, 1992). The exhaust plume flow has been diluted significantly by mixing in the fuel-lean overfire region before the measurement location is reached, e.g., soot volume fractions are in the range 0.0278-0.476 ppm and primary particle concentrations are in the range 1.97-8.76 M part/m^3. The substantial degree of dilution of the exhaust plume also is evident from the relatively low gas temperatures at the measurement location, 380-450 K.

The structure and physical properties of the soot aggregates at the measurement location are summarized in Table 3 for the four flames. Properties given in the table include soot density, ρ_s, primary particle diameters, d_p, the average number of primary particles per aggregate, $\overline{N}$, the volume averaged soot aggregate diameter D_{30}, the composition of soot (C,H,O and N in % by mass) and the C/H, C/O and C/N atomic ratios. Properties given in the table are from Köylü and Faeth (1992) and Köylü and Faeth (1994a) for the same flames, except for the present helium pycnometry measurements of soot density and confirmation of primary particle diameters. Notably, present measurements of d_p agreed with the earlier results of Köylü (1992) and Köylü and Faeth (1994a) within experimental uncertainites. Present determinations of soot densities yielded values in the range 1850-1930 kg/m^3, which is typical of earlier measurements in the literature (Jullien and Botet, 1987; Köylü and Faeth 1993a). Values of primary particle diameters are in the range 31-47nm, tending to increase with increasing propensity to soot; these values are relatively large due to the rather long soot growth periods available for buoyant turbulent diffusion flames in the long residence time regime. These long residnece times are also reflected by rather large aggregate sizes, with average numbers of primary particles per aggregate in the range 364-467 and volume-averaged soot aggregate diameters in the range 214-350 nm—both tending to increase with increasing propensity to soot. Finally, C/H, C/O and C/N atomic ratios are in the ranges 12.1-16.8, 57.6-107 and 295-332; these results suggest somewhat higher carbon concentrations for soot when there are higher carbon concentrations in the fuel; however, more data are needed to reliably establish this trend.

Typical aggregate dimensions for the present test conditions were on the order of 1000 nm, which is somewhat larger than the visible wavelength range (350-800 nm) considered during present experiments. Thus, present measurements emphasized aggregates in the power-law regime as required by the algorithm used to find soot refractive indices discussed in Section 2.3. Scattering measurements to establish this behavior will be discussed next.

2.5 Soot Scattering Properties

The main features of the present scattering measurements for overfire soot aggregates are summarized in Table 4. The values of x_p are found directly from the measurements of d_p summarized in Table 3. Present measurements involved $0.12 \leq x_p, \leq 0.42$ with the largest values of x_p comparable to the largest values of this parameter used thus far to evaluate RDG-PFA theory (Farias, 1985a,b,c).

Present measurements of depolarization ratio, ρ_v, are given to Table 4 at all wavelengths considered. This parameter is defined as follows:

$$\overline{C}^{\,a}_{hv} = \overline{C}^{\,a}_{vh} = \overline{C}^{\,a}_{hh}\,(90\text{deg}) = \overline{C}^{\,a}_{vv}\,(90\text{deg})\,\rho_v \qquad (23)$$

Table 4. Summary of measurements of scattering from soot within the overfire region of round buoyant turbulent diffusion flames in the long residence time regime.[a]

Fuel	Acetylene	Propylene	Ethylene	Propane
Wavelength = 351.2 nm:				
$x_{p,}$	0.42	0.37	0.29	0.28
ρ_v	0.070	0.065	0.056	0.044
ρ_{sa}	0.46	0.37	0.32	0.28
$\overline{Q}^{a}_{a}(m^{-1})$	3.477	2.782	0.487	0.0331
$\overline{Q}^{a}_{vv}(m^{-1}) \cong 130$ deg	0.04197	0.02540	0.00375	0.00256
Wavelength = 405.0 nm:				
$x_{p,}$	0.36	0.32	0.25	0.24
ρ_v	0.055	0.042	0.041	0.038
ρ_{sa}	0.43	0.42	0.33	0.25
$\overline{Q}^{a}_{a}(m^{-1})$	3.452	2.501	0.468	0.333
$\overline{Q}^{a}_{vv}(m^{-1}) \cong 150$ deg	0.05240	0.01570	0.00240	0.00141
Wavelength = 488.0 nm:				
$x_{p,}$	0.30	0.26	0.21	0.20
ρ_v	0.042	0.033	0.026	0.022
ρ_{sa}	0.43	0.42	0.32	0.24
$\overline{Q}^{a}_{a}(m^{-1})$	3.338	2.185	0.432	0.254
$\overline{Q}^{a}_{vv}(m^{-1}) \cong 160$ deg	0.04113	0.02360	0.00414	0.00207
Wavelength = 514.5 nm:				
$x_{p,}$	0.29	0.25	0.20	0.19
ρ_v	0.041	0.030	0.023	0.020
ρ_{sa}	0.42	0.40	0.31	0.23
$\overline{Q}^{a}_{a}(m^{-1})$	3.267	2.064	0.402	0.243
$\overline{Q}^{a}_{vv}(m^{-1}) \cong 160$ deg	0.03586	0.02085	0.00356	0.00201
Wavelength = 632.8 nm:				
$x_{p,}$	0.23	0.20	0.16	0.15
ρ_v	0.038	0.028	0.022	0.019
ρ_{sa}	0.41	0.42	0.33	0.24
$\overline{Q}^{a}_{a}(m^{-1})$	2.849	1.538	0.277	0.200
$\overline{Q}^{a}_{vv}(m^{-1}) \cong 140$ deg	0.02856	0.01612	0.00211	0.00135
Wavelength = 800.0 nm[b]:				
$x_{p,}$	0.18	0.16	0.13	0.12
ρ_v	0.032	---	---	---
ρ_{sa}	0.41	0.40	0.32	0.25
$\overline{Q}^{a}_{a}(m^{-1})$	2.402	1.304	0.204	0.137
$\overline{Q}^{a}_{vv}(m^{1}) \cong 140$ deg	0.0283	0.0166	0.00219	0.00117

[a]Physical properties of soot taken from Table 2.

[b]Results at this wavelength found by assuming that the dispersion of ρ_{sa} was negligible with $\overline{Q}^{a}_{s}$ obtained from the assumed values of ρ_{sa}.

Present measurements indicate that $0.019 \leq \rho_v \leq 0.070$, tending to increase with decreasing wavelength and increasing propensity to soot. These results are in reasonably good agreement with the earlier measurements of ρ_v at 514.5 nm for the same soot from Köylü and Faeth (1994a), see the comparison summarized in Table 5. These values also are roughly an order of magnitude larger than values found for Rayleigh scattering from gases, see Rudder and Bach (1968).

The ratios of scattering to absorption cross sections, ρ_{sa}, were measured at all wavelengths except 800 nm, where signal-to-noise ratios were too low to obtain satisfactory calibrations of absolute scattering levels based on Rayleigh scattering from propane. It was noticed, however, that ρ_{sa} varied rather slowly for each fuel over the available wavelength range of the measurements; namely, 351.2 to 632.8nm. Thus, in order to obtain an estimate of the refractive indices at $\lambda = 800$, it was assumed that the ρ_{sa} were the same as the other wavelengths for each fuel; therefore, values obtained from this estimate are given in the table at 800 nm. Values of ρ_{sa} are in the range 0.23-0.46, tending to increase with increasing propensity to soot, and to a lesser degree with decreasing wavelength. The values of ρ_{sa} are sufficiently large to indicate significant effects of aggregate scattering, e.g., interpretation of these measurements to find soot volume fractions assuming Rayleigh scattering (i.e.., ignoring the contribution of scattering to extinction) would result in overestimation of soot volume fractions by roughly 25-50%. Present measurements of ρ_{sa} also are in reasonably good agreement with the earlier measurements of Köylü and Faeth (1994a) for the same soot, see the comparison summarized in Table 6.

The values of $\overline{Q}_a^a$ and $\overline{Q}_{vv}^a$ used to determine refractive indices are also documented in Table 4; the behavior of these parameters will be discussed next.

Similar to Köylü and Faeth (1994a), it was possible to achieve a good fit between the measured and predicted scattering properites of the present overfire soot aggregates using RDG-PFA theory. The resulting predicted and measured values of $\overline{Q}_e^a$ and $\overline{Q}_s^a$ are plotted as a function of wavelength for the four fuels in Fig. 4. It should be noted, however, that the agreement between predictions and measurements seen in Fig. 4 does not represent a definitive evaluation of RDG-PFA predictions because it rests on fits of both the aggregate size distribution functions and the refractive indices to provide a good match between predicted and measured scattering properties. Several features of the volumetric extinction and scattering cross sections plotted in Fig. 4 are of interest. First of all, extinction coefficients are significantly greater than scattering coefficients, with values of $\overline{Q}_e^a/\overline{Q}_s^a$ in the range 3.3-5.4, tending to increase with decreasing tendency to soot. Another feature of the results of Fig. 4 is that $\overline{Q}_e^a$ tends to decrease relatively slowly with increasing wavelength over the visible portion of the spectrum, rather than exhibiting the $1/\lambda$ or greater variation that is inferred from Eqs. (2), (3), (7) and (16). This behavior follows because effects of scattering are not dominant while the reduction of absorption coefficient with increasing wavelength is largely compensated by an increase of the refractive indices of soot over the same wavelength range. This behavior suggests that the extinction properties of the present soot will not vary significantly in the visible wavelength range so that the dimensionless extinction coefficient might be a constant as suggested by Dobbins et al. (1993), Choi et al. (1994, 1995) and Zhou and Choi (1995); this possibility will be considered in more detail later.

Table 5. Values of depolarization ratios at 514.5 nm for soot within the overfire region of round buoyant turbulent diffusion flames in the long residence time regime.

Fuel	Acetylene	Propylene	Ethylene	Propane
Present Measurements	0.041	0.030	0.023	0.020
Köylü and Faeth (1994a)	0.041	0.033	0.028	0.022

Table 6. Values of ρ_{sa} at 514.5 nm for soot within the overfire region of round buoyant turbulent diffusion flames in the long residence time regime.

Fuel	Acetylene	Propylene	Ethylene	Propane
Present Measurements	0.042	0.040	0.031	0.023
Köylü and Faeth (1994a)	0.041	0.033	0.028	0.022

Table 7. Summary of the fractal dimensions of soot from the overfire region of round buoyant turbulent diffusion flames in the long residence time regime.[a]

Wavelength (nm)	Acetylene	Propylene	Ethylene	Propane
351.2	1.75	1.80	1.78	1.81
405.0	1.70	1.85	1.85	1.85
488.0	1.74	1.81	1.73	1.78
514.5	1.72	1.73	1.78	1.73
632.8	1.78	1.74	1.79	1.74
800.0	1.76	1.78	1.76	1.79

[a]Based on scattering measurements in the power-law regime.

Table 8. Values of the fractal dimensions of soot within the overfire region of round buoyant turbulent diffusion flames in the long residence time regime.[a]

Fuel	Acetylene	Propylene	Ethylene	Propane
Present Study	1.72	1.73	1.78	1.73
Köylü and Faeth (1994a)	1.85	1.84	1.83	1.77

[a]Based on scattering measurements at 514.5 nm in the power-law regime.

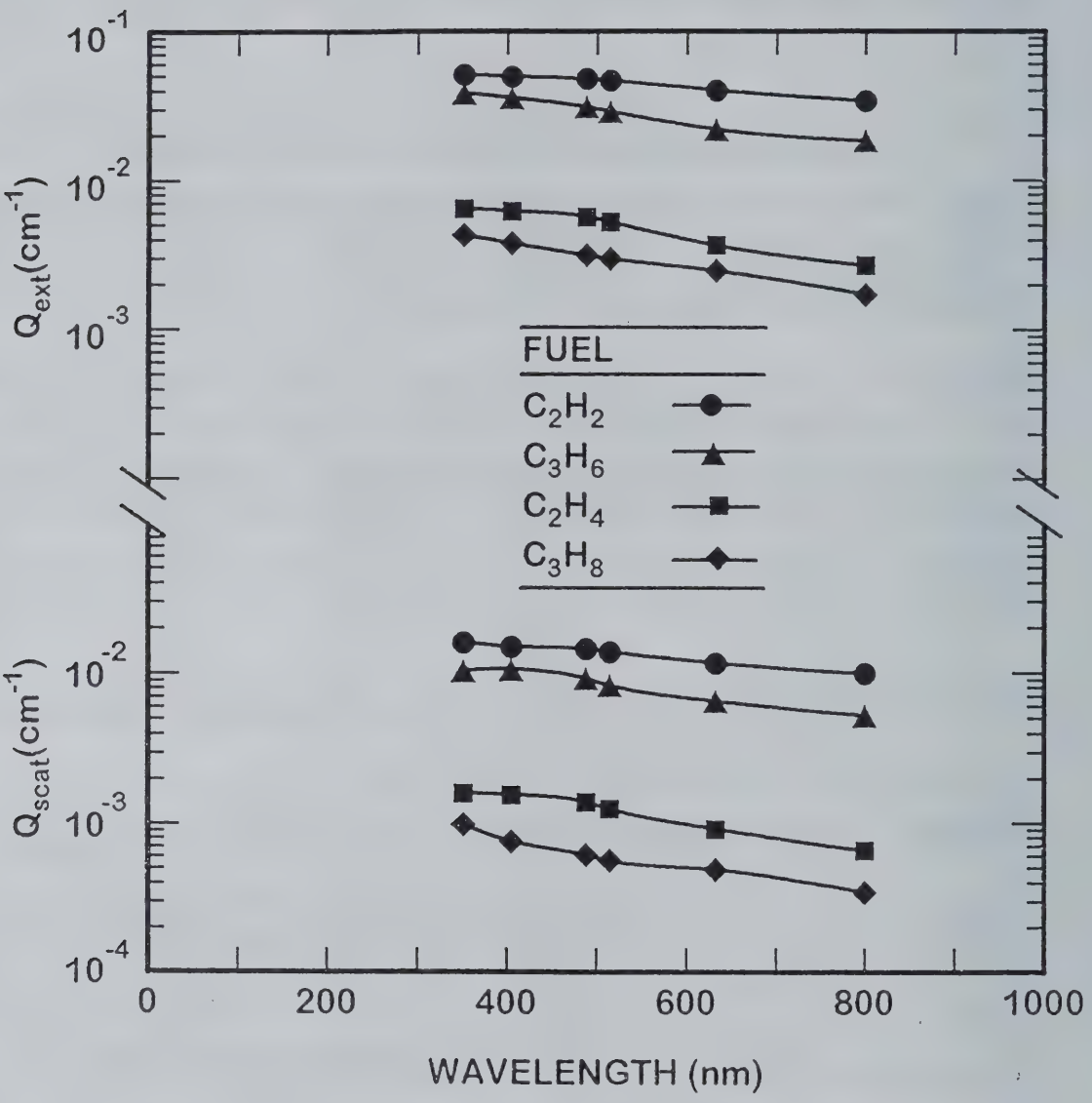

Figure 4. Volumetric extinction and scattering cross sections as a function of wavelength for overfire soot from buoyant turbulent fuel/air diffusion flames in the long residence time regime.

Measured and predicted values of $\overline{Q}^{a}_{vv}(qd_p)/\overline{Q}^{p}_{vv}$ are plotted as a function of qd_p in Fig. 5 for the four fuels. These results are for $\lambda = 632.8$ nm, but they are representative of behavior at other wavelengths, see Köylü and Faeth (1994a) for similar results at 514.5 nm. In addition to predictions over the entire accessible range of qd_p, extrapolations of large-angle (power-law) behavior from Eq. (13) also are shown on the plots for reference purposes. The substantial departure from Rayleigh scattering behavior (where $\overline{Q}^{a}_{vv}(qd_p)$ would be independent of qd_p) is evident, with forward scattering 100-1000 times larger than back scattering for the present large soot aggregates. The measurements are seen to provide an extended power-law regime where scattering properties are represented by Eq. (13), e.g., roughly $qd_p > 0.1$; however, access to the Guinier regime is limited due to the large size of the present soot aggregates and the practical difficulties of making accurate scattering measurements at small angles. As discussed by Köylü and Faeth (1994a), the scattering measurements in the power-law regime provide a convenient method for measuring the fractal dimension. These results will be considered in the next section.

Typical predicted and measured angular scattering patterns are illustrated in Figs. 6-9. The results shown include propane at 632.8 and 352.1 nm, Figs. 6 and 7, and acetylene at 632.8 and 352.1 nm, Figs. 8 and 9, which spans both the range of wavelengths where absolute scattering measurements were made, and effects of the sooting tendencies of the fuel, for the present experiments. Similar to past findings, RDG-PFA predictions provide an excellent correlation of the measurements over the present test range, which is promising in view of the relatively large values of x_p reached for these results. The results clearly exhibit very strong scattering at small values of θ, particularly for strongly sooting fuels, e.g., acetylene, at short wavelengths, see Fig. 9. The formulations of hh, vh and hv scattering were modified slightly, following Köylü and Faeth (1994a), in order to account for observed depolarization effects. This was done by using the depolarization ratios measured for soot aggregates, ρ_v, analogous to Rayleigh scattering theory, see Rudder and Bach (1968). Thus $\overline{C}^{a}_{hv}$ and $\overline{C}^{a}_{vh}$ were predicted from ρ_v and $\overline{C}^{a}_{vv}$ (90 deg) as given by Eq. (23), while predicted values of $\overline{C}^{a}_{hh}(\theta)$ were found as follows:

$$\overline{C}^{a}_{hh}(\theta) = \overline{C}^{a}_{vv}(\theta)[(1-\rho_v)\cos^2\theta + \rho_v] \qquad (24)$$

using the values of ρ_v summarized in Table 4. The resulting predictions of $\overline{C}^{a}_{hh}(\theta)$ are excellent, similar to predictions $\overline{C}^{a}_{vv}(\theta)$. The predicted and measured values of the vh and hv scattering components also are in good agreement with Rayleigh scattering ideas, except near the forward scattering direction where measured values increase and the vh and hv components are no longer equal. The measured behavior may be due to experimental difficulties because problems of alignment are severe in the forward scattering direction where scattering levels are very high; additional study of the hv and vh components in this region is clearly needed.

2.6 Soot Fractal Properties

Measurements in the power-law regime, typified by the results illustrated in Fig. 5, can be used to find the fractal dimension. For example, based on Eq. (13), the slope of $\overline{Q}^{a}_{vv}(qd_p)/Q^{p}_{vv}$ as a function of qd_p in the power-law regime gives D_f. The values of D_f measured in this manner have been summarized in Table 7. The variations of D_f for various fuel types and wavelengths are small compared to experimental uncertainties and yield a mean value of $D_f = 1.78$ with a standard deviation of 0.04. These values are in reasonably good agreement with the earlier measurements of D_f at 514.5 nm for this soot,

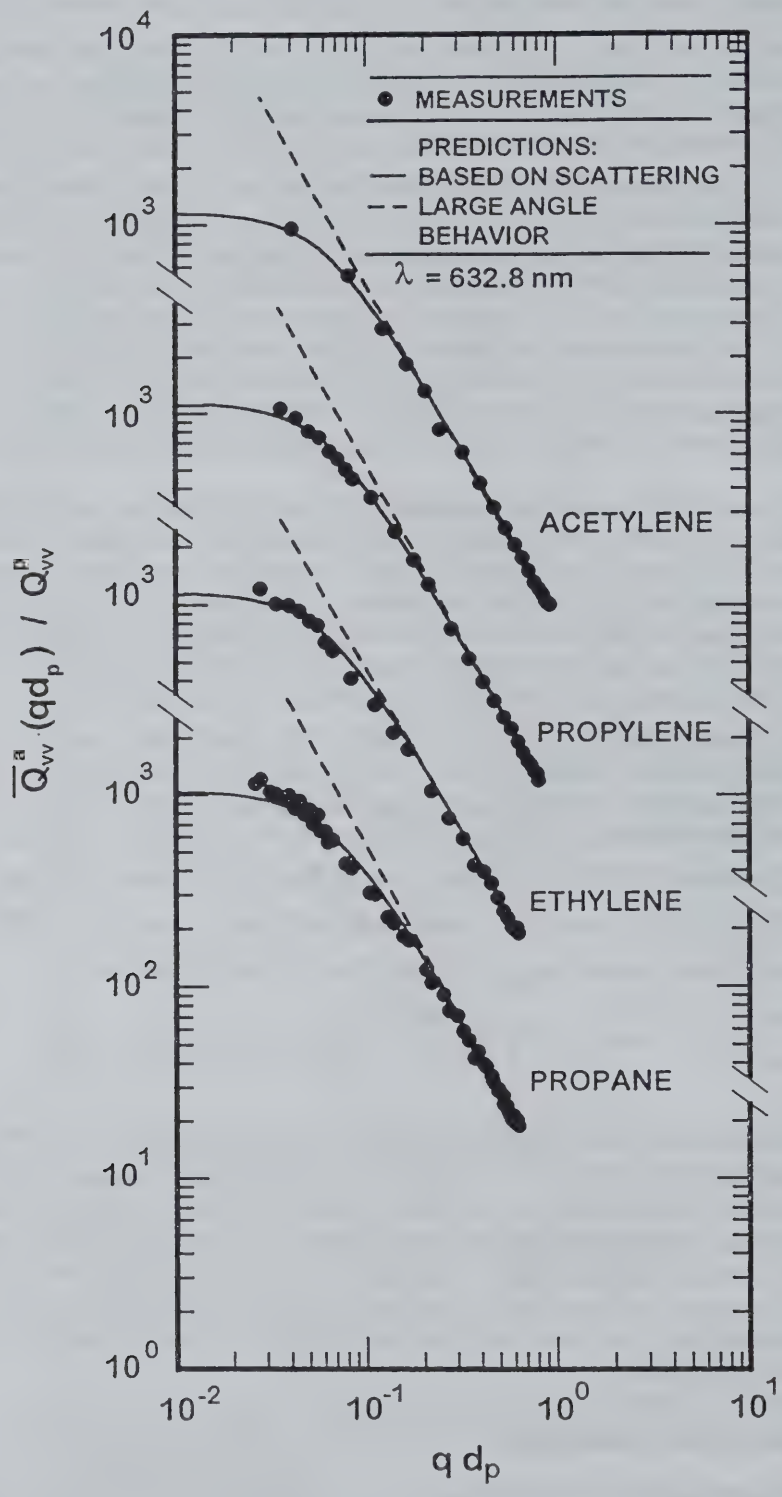

Figure 5. Measured and predicted volumetric vv cross sections at 632.8 nm as functions of the modulus of the scattering vector for overfire soot from buoyant turbulent fuel/air diffusion flames in the long residence time regime.

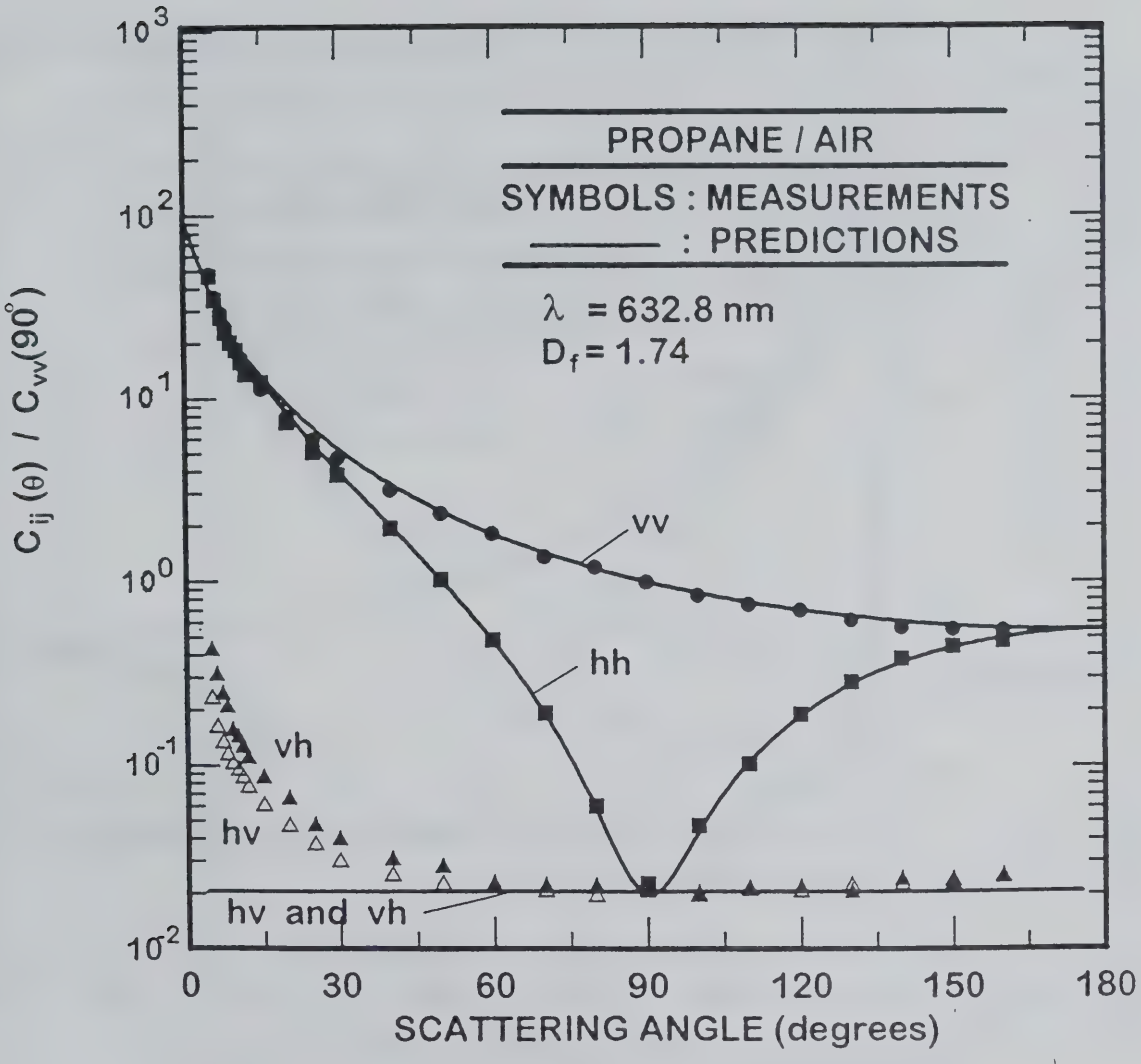

Figure 6. Measured and predicted angular scattering patterns at 632.8 nm of overfire soot from buoyant turbulent propane/air diffusion flames in the long residence time regime .

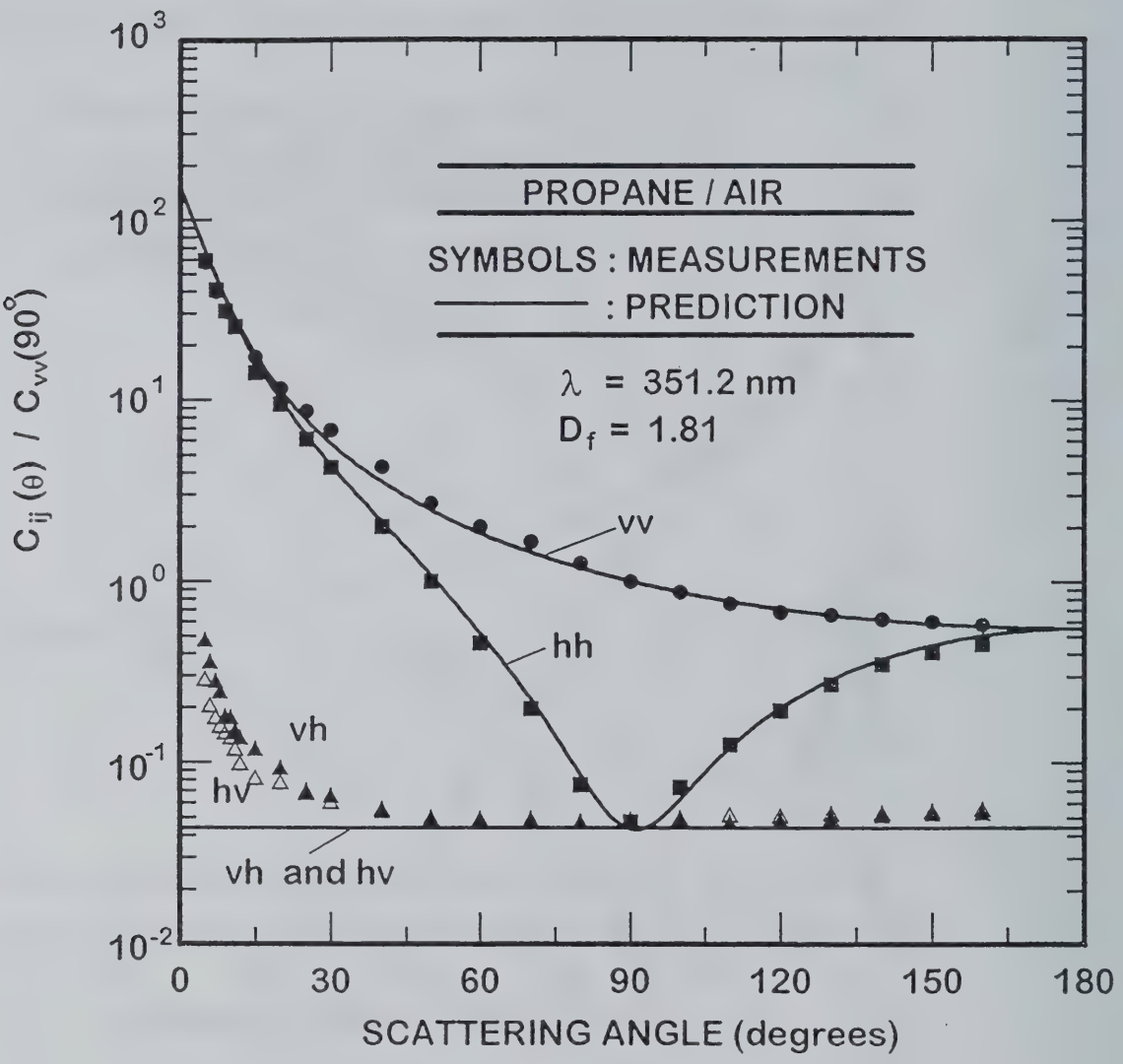

Figure 7. Measured and predicted angular scattering patterns at 351.2 nm of overfire soot from buoyant turbulent propane/air diffusion flames in the long residence time regime.

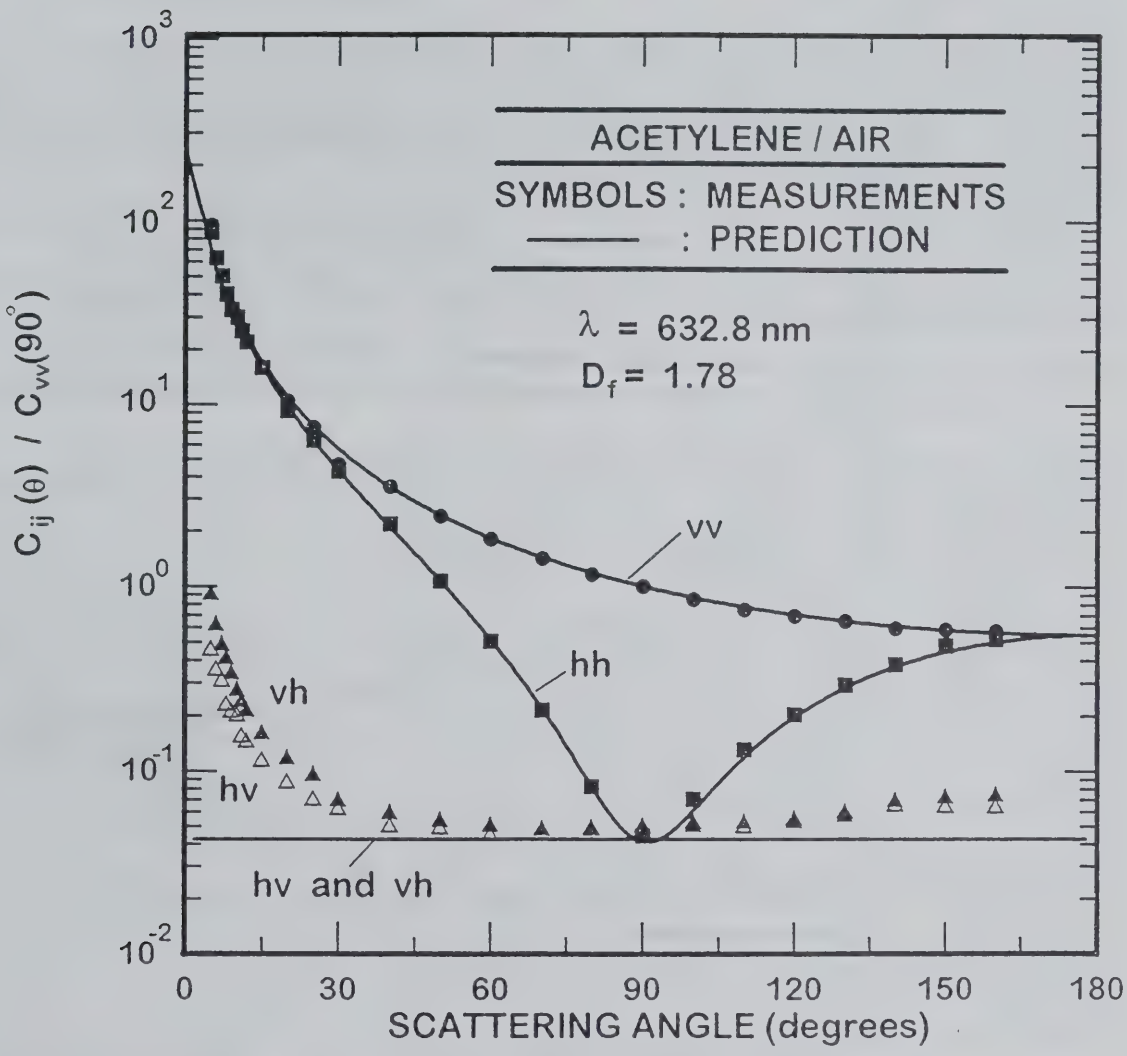

Figure 8. Measured and predicted angular scattering patterns at 632.8 nm of overfire soot from buoyant turbulent acetylene/air diffusion flames in the long residence time regime.

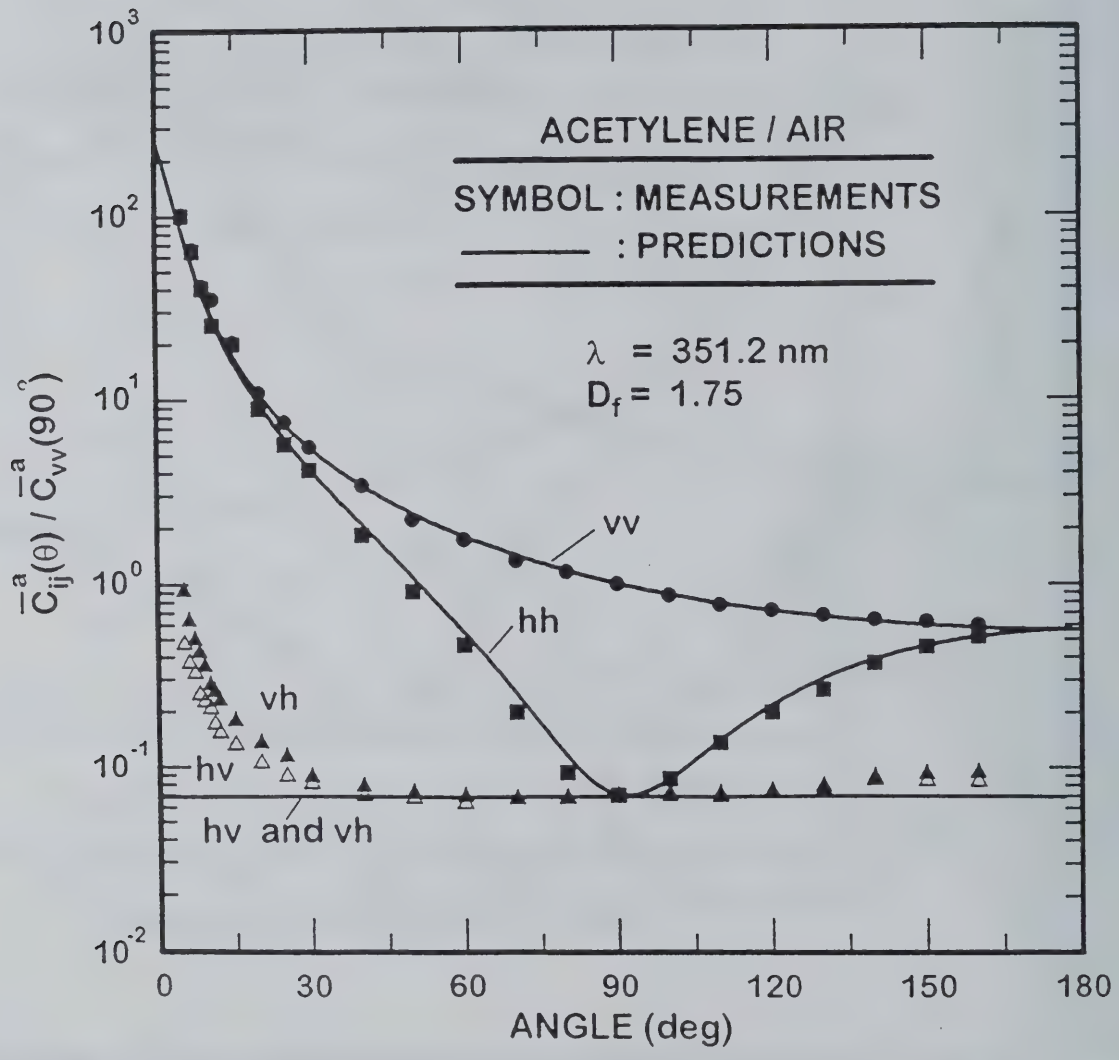

Figure 9. Measured and predicted angular scattering patterns at 351.2 nm of overfire soot from buoyant turbulent acetylene/air diffusion flames in the long residence time regime.

made in the same manner by Köylü and Faeth (1994a), that are summarized along with present results at this wavelength in Table 8, and yield a mean value of $D_f = 1.82$ and a standard deviation of 0.04. Given the scattering and fractal properties of the soot, consideration of soot optical properties can begin, as discussed next.

2.7 Soot Optical Properties

Results thus far have demonstrated good performance of the RDG-PFA scattering theory for present test conditions, robust soot fractal properties that are in good agreement with the earlier results of Köylü and Faeth (1994a) for the same soot, and strong evidence that present results at large angles ($qd_p>0.1$) are within the power-law regime. As a result, Eqs. (18)-(22) were used to compute soot optical properties from the present extinction and scattering measurements after adopting the fractal property $k_f = 8.5$ from Köylü et al. (1995). The results of these calculations are summarized in Table 9, where E(m), F(m), n, κ and k_{eR} are tabulated as functions of fuel type and wavelength. As mentioned earlier in connection with Table 4, these results were based on absolute scattering measurements except at $\lambda = 800$ nm where low signal-to-noise ratios required extrapolation of ρ_{sa} values from measurements at lower wavelengths in order to estimate soot optical properties.

The real and imaginary parts of the refractive indices of soot from the present measurements are plotted as a function of wavelength, with fuel type as a parameter, in Fig. 10. Several earlier measurements are illustrated on the plot as well, including: the classical *ex situ* reflectometry measurements for soot collected from the fuel-lean region of acetylene and propane/air diffusion flames, due to Dalzell and Sarofim (1969); the *in situ* measurements for soot in the overfire region of plexiglass/air diffusion flames, due to Lee and Tien (1981); the *in situ* measurements for soot in the overfire region of C_2H_2 and C_3H_8/air flames, due to Chang and Charalampopoulos (1990); and the *in situ* measurements for soot in the post-flame region of fuel-rich premixed ethylene/air flames due to Vaglieco et al. (1990). It should be noted that the *ex situ* measurements of Dalzell and Sarofim (1969) have been criticized by Lee and Tien (1980), who suggest potential sampling problems, and by Felske et al. (1984), who suggest potential problems of diffuse scattering due to surface roughness for the reflectometry measurements. On the other hand, the *in situ* measurements of Lee and Tien (1981), Batten (1985), Chang and Charalampopoulos (1990) and Vaglieco et al. (1990) all involve questionable models of the optical properties of soot, and for soot transport properties in cases where dynamic scattering measurements are used to infer soot aggregate size properties. In addition, Chang and Charalampopoulos (1990) observe variations of soot optical properties with increasing residence time in the post-flame region of premixed flames, attributed to an effect of aging, so that their results are indicated by limits.

Present experiments of soot refractive indices do not exhibit a strong variation with fuel type, compared to experimental uncertainties; this behavior agrees with past observations of soot refractive indices and optical properties in diffusive flames, see Köylü and Faeth (1995) and Dalzell and Sarofim (1969). Nevertheless, potential effects of age, seen in premixed flames, still must be resolved, along with effects of fuel type over a wider range of fuel properties than the present study. Another significant observation is that present measurements of soot refractive indices do not exhibit any effect of resonance in the near ultra-violet range of the spectrum, which agrees with the recent observations of Vaglieco et al. (1990). Finally, present measurements agree best with the findings of Dalzell and Sarofim (1995), similar to the findings of Köylü and Faeth (1995), in spite of past criticism of this methodology. While these findings are promising, adequately resolving efects of fuel type, wavelength, flame condition, residence time and the discrepancies among the various investigations clearly merits additional study. Thus, work

Table 9. Summary of the optical properties of soot from the overfire region of round buoyant turbulent diffusion flames in the long residence time regime.[a]

Fuel	Acetylene	Propylene	Ethylene	Propane
Wavelength = 351.2 nm:				
E(m)	0.14	0.20	0.20	0.22
F(m)	0.07	0.09	0.11	0.12
n	1.35	1.31	1.39	1.39
κ	0.25	0.36	0.36	0.41
k_{eR}	4.0	4.8	5.0	4.7
Wavelength = 405.0 nm:				
E(m)	0.16	0.21	0.23	0.22
F(m)	0.14	0.13	0.13	0.12
n	1.55	1.44	1.40	1.39
κ	0.34	0.40	0.43	0.41
k_{eR}	4.3	5.1	5.6	5.1
Wavelength = 488.0 nm:				
E(m)	0.18	0.23	0.25	0.22
F(m)	0.15	0.20	0.22	0.19
n	1.55	1.59	1.60	1.58
κ	0.39	0.50	0.55	0.48
k_{eR}	5.0	5.4	6.2	4.8
Wavelength = 514.5 nm:				
E(m)	0.19	0.26	0.25	0.24
F(m)	0.16	0.21	0.23	0.32
n	1.56	1.55	1.62	1.59
κ	0.40	0.55	0.56	0.53
k_{eR}	5.1	5.3	6.0	4.8
Wavelength = 632.8 nm:				
E(m)	0.21	0.21	0.21	0.24
F(m)	0.21	0.23	0.25	0.21
n	1.65	1.70	1.74	1.75
κ	0.48	0.50	0.53	0.60
k_{eR}	5.3	5.2	5.2	5.8
Wavelength = 800.0 nm:[b]				
E(m)	0.21	0.22	0.27	0.20
F(m)	0.30	0.40	0.40	0.34
n	1.46	1.24	1.36	1.35
κ	0.59	0.66	0.73	0.61
k_{eR}	5.8	5.2	4.8	4.4

[a]Physical, scattering and fractal properties of soot taken from Tables 2, 3, 4 and 7 while taking $k_f = 8.5$.

[b]Results at this wavelength were found by assuming that the dispersion of ρ_{sa} was negligible with Q_s^a found from the assumed values of ρ_{sa}.

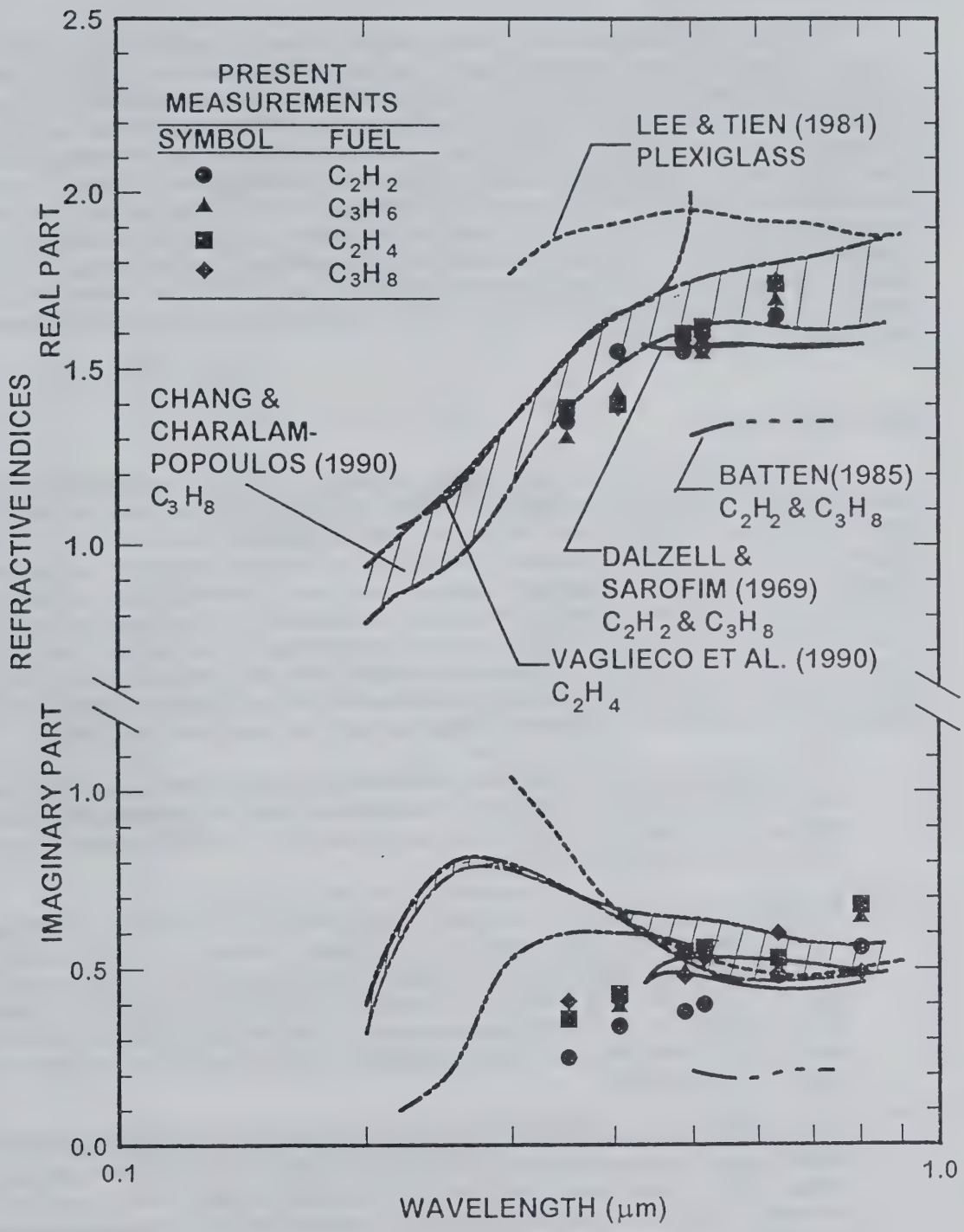

Figure 10. Measured refractive indices of soot in the ultra-violent and visible portions of the spectrum

along these lines is currently in progress, emphasizing effects of fuel type, flame conditions and experimental methods.

Present determinations of the dimensionless extinction coefficient, k_{eR}, are plotted in Fig. 11, along with earlier measurements for soot in the post-flame region of premixed fuel-rich acetylene/air flames, due to Choi et al. (1995); and for soot in the overfire region of crude-oil/air diffusion flames, due to Dobbins et al. (1994). Present values of k_{eR} are in the range 4.0-6.2 and really do not exhibit significant variations with wavelength and fuel type. This behavior comes about due to a fortuitous cancellation of effects of scattering, wavelength and refraction index variations. Averaging over all the present data yields an average value of $k_{eR} = 5.1$, with a standard deviation of 0.5; this correlation also is illustrated in the figure. The present mean value is significantly lower than $k_{eR} = 8.6$ with a standard deviaiton of 0.5 recently reported by Choi et al. (1995), and values of k_{eR} in the range 8.1-9.4 reported by Dobbins et al. (1994). Specific reasons for these differences are not known at the present time.

2.8 Conclusions

A study of the optical and fractal properties of soot, emphasizing improved understanding of soot refractive indices in flame environments, has been described. The study was limited to soot found within the overfire region of large buoyant turbulent diffusion flames in the long residence time regime, where soot properties are independent of position in the overfire region and residence time, for a particular fuel burning in air. The study involved measurements of extinction and scattering properties of soot in flames fueled with acetylene, propylene, ethylene and propane burning in still air, for the visible wavelength range (350-800 nm). The measurements were interpreted using a theory based on the Rayleigh-Debye-Gans scattering approximation for polydisperse fractal aggregates (denoted RDG-PFA theory). The major conclusions of the study are as follows:

1. The approximate RDG-PFA theory yielded predictions that agreed with present measurements within experimental uncertainties, even for primary particle optical diameters as large as 0.42 (for acetylene soot) which severely tests the approximations of RDG-PFA theory.

2. Soot refractive indices did not vary significantly with fuel type, compared to experimental uncertainties, in spite of significant variations of soot composition over the test range (e.g., atomic C/H ratios in the range 12-17, C/O ratios in the range 57-107 and C/N ratios in the range 295-411); this finding is promising because analysis of scattering measurements to find soot properites and estimates of soot radiation properties are vastly simplified when refractive indices do not vary with soot composition.

3. Present determinations of soot refractive indices are in fair agreement with the early reflectometry measurements of Dalzell and Sarofim (1969), even though these measurements have been criticized for potential errors from modified soot properties due to soot sample collection and preparation (ex situ measurements) and for effects of sample roughness on the reflectometry measurements to find refractive indices.

4. Results in the near uv wavelength range do not exhibit approach to the resonance condition that is observed for graphite; instead, refractive indices decline continuously as the uv is approached. This behavior is similar to past observations of Vaglieco et al. (1990) for amorphous carbon and soot and points to problems of

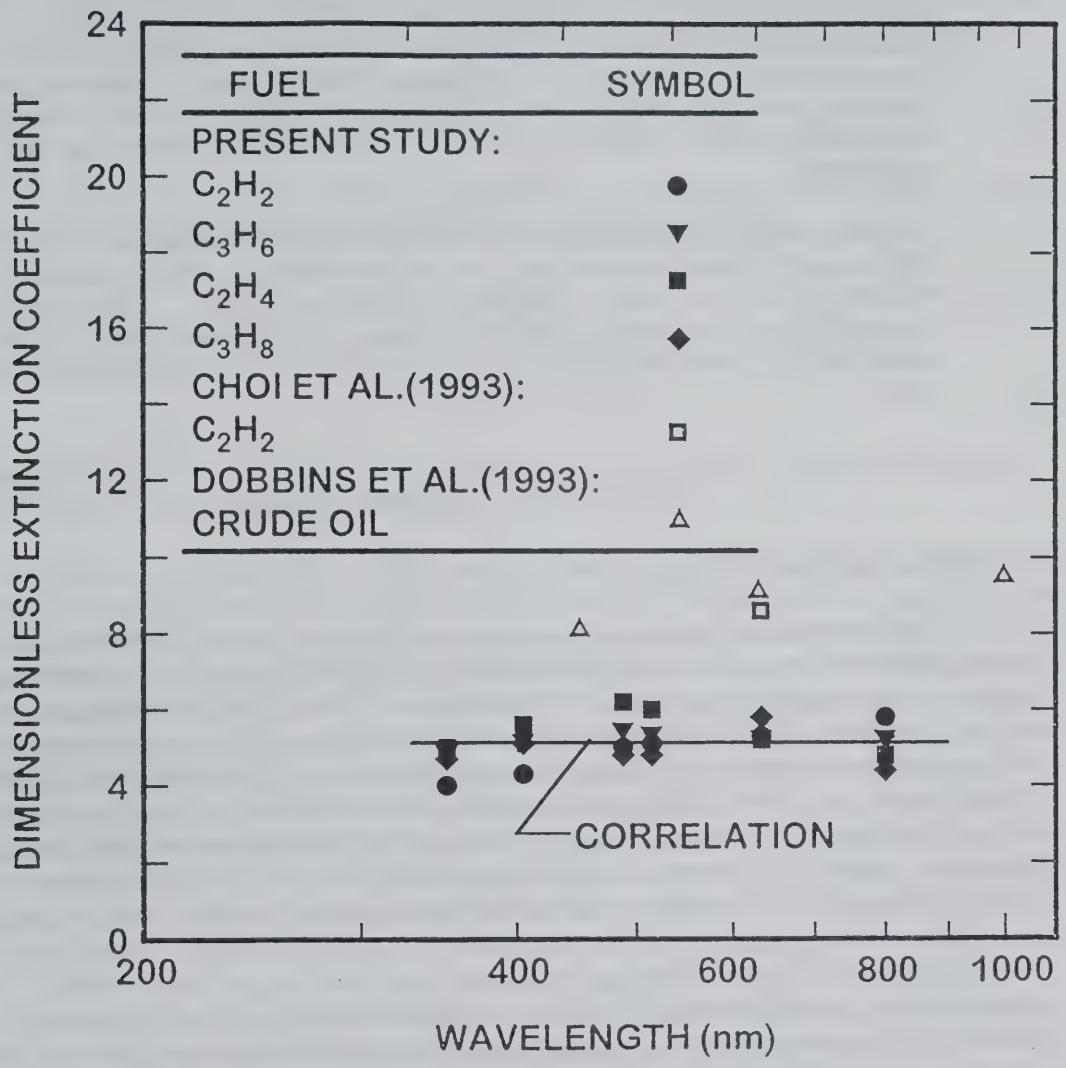

Figure 11. Measured dimensionless extinction coefficients of soot in the visible and near infrared portions of the spectrum.

past determinations of soot refractive indices which involve the use of dispersion relationships that assume resonance behavior in the near uv.

5. The dimensionless extinction coefficient of the present soot was relatively independent of fuel type and wavelength over the present test range, yielding an average value of 5.1 and a standard deviation of 0.5, this behavior is promising because it offers a robust measurement of soot volume fractions from extinction measurments in the visible. The present dimensionless extinction coefficients, however, are significantly lower than values in the range 8.1-9.4 recently reported by Dobbins et al. (1994) and Choi et al. (1995), for reasons that still must be explained.

6. Present optical determinations showed that fractal dimensions of soot were robust with respect to variations of fuel type and wavelength over the present test range, yielding $D_f = 1.78$ with a standard deviation of 0.04. These results are in reasonably good agreement with the findings of Köylü and Faeth (1994a) for the same soot at a wavelength of 514.5 nm e.g., $D_f = 1.82$ with a standard deviation of 0.04.

3. Buoyant Turbulent Plumes

3.1 Introduction

The structure and mixing properties of buoyant turbulent plumes in still and unstratified environments is an important fundamental problem that has attracted significant attention since the classical study of Rouse et al. (1952). However, recent work has highlighted the need for a better fundamental understanding of buoyant turbulent plumes in order to address effects of turbulence/radiation interactions (Faeth et al., 1987, 1989, 1990; Kounalakis et al., 1991), and to help develop and evaluate models of buoyant turbulent flows (Durao et al.,1989; Malin and Younis, 1990; Panchapakesan and Lumley, 1993; Pivovarov et al., 1992; Ramaprian and Chandrasekhara, 1985, 1989; Shabbir and Taulbee, 1990; Shih et al., 1987). Thus, the overall objective of this phase of the investigation is to complete new measurements of the properties of buoyant turbulent plumes and to exploit the information to improve both understanding and modeling of these flows. The fully-developed region (where effects of the source have been lost and the properties of the flow become self-preserving) is emphasized because these conditions simplify both theoretical considerations and the interpretation of measurements (Tennekes and Lumley, 1972), even though few practical plumes reach a self-preserving state.

Several reviews of turbulent plumes have appeared (Chen and Rodi, 1980; Kotsovinos, 1985; List, 1982; Papanicolaou and List, 1987, 1988); therefore, the following discussion of past studies will be brief. The earliest work emphasized the development of similarity relationships for flow properties within fully-developed (self-preserving) buoyant turbulent plumes (Rouse et al., 1952). Subsequently, many workers reported observations of properties at self-preserving conditions, however, these determinations generally were not in good agreement (Chen and Rodi, 1980; George et al., 1977; Kotsovinos, 1985; Mizushima et al., 1979; Ogino et al., 1980; Papanicolaou and List, 1987, 1988; Papantoniou and List, 1989; Peterson and Bayazitoglu, 1992; Shabbir and George, 1992; Zimin and Frik, 1977). Papanicolaou and List (1987, 1988) attribute these discrepancies mainly to problems of fully reaching self-preserving conditions, with conventional experimental uncertainties serving as a contributing factor.

Self-preserving round buoyant turbulent plumes are reached when streamwise distances from the plume source are large in comparison to both the source diameter, (as a measure of conditions where effects of source disturbances have been lost) and the Morton length scale (as a measure of conditions where effects of buoyancy are dominant). For round buoyant jet sources, the Morton length scale is defined as follows (List, 1982):

$$\ell_M = M_o^{3/4} / B_o^{1/2} \tag{25}$$

For round plumes that have uniform properties at the source, the source specific momentum and buoyancy fluxes can be found as follows (List 1982):

$$M_o = (\pi/4)d^2u_o^2 \tag{26}$$

$$B_o = (\pi/4)d^2u_o g|\rho_o-\rho_\infty|/\rho_\infty \tag{27}$$

where an absolute value of the density difference has been used in Eq. (27) in order to account for both rising and falling plumes.

Papantoniou and List (1987, 1988) suggest that buoyancy dominated conditions for mean and fluctuating quantities are reached when $(x-x_o)/\ell_M$ is greater than roughly 6 and 14, respectively, which has been satisfied by most past measurements seeking results at self-preserving conditions. However, except for some limited measurements by Papanicolaou and List (1989), which involved unusually large Schmidt numbers in liquids, existing measurements of plume structure have been limited to $6 \le (x-x_o)/d \le 62$, with most of the measurements limited to the lower end of this range. This range of streamwise distances is suspiciously small to achieve self-preserving conditions, based on findings for nonbuoyant round turbulent jets where values of $(x-x_o)/d$ greater than roughly 40 and 100 are required to achieve self-preserving profiles of mean and fluctuating properties, respectively (Hinze, 1985; Panchapakesan and Lumley, 1993; Tennekes and Lumley, 1972).

Other deficiencies of existing measurements of buoyant turbulent plumes involve information concerning higher order mixture-fraction and velocity statistics, including combined mixture-fraction/velocity statistics. In particular, higher order mixture-fraction and velocity statistics are needed to define turbulent diffusion of mixture-fraction and velocity fluctuations. Furthermore, combined mixture-fraction/velocity statistics are direct measures of scalar mixing and define turbulent diffusion of mixture fraction fluctuations. These properties also are important for mass-weighted(Favre)averages that appear in some models of turbulent flame environments (Bilger, 1976; Starner and Bilger, 1983). Papanicolaou and List (1988) provide some limited data on these properties, however, their results are questionable for several reasons: they did not achieve self-preserving conditions (as discussed later), they identified errors in their measurements that were not resolved, and they considered liquid plumes whose large Schmidt numbers are not representative of the scalar mixing properties of gaseous fire environments. Panchapakesan and Lumley (1993) also report measurements of higher order correlations for round buoyant turbulent jets but in this case buoyancy dominated conditions were not achieved.

The preceding discussion suggests that existing measurements of the structure of buoyant turbulent plumes are inadequate for a number of reasons: the results generally involve transitional plumes which introduces uncertainties due to source disturbances and source momentum; information about higher-order mixture-fraction, velocity and combined mixture-fraction/velocity statistics, needed to define turbulent transport fluxes and turbulent diffusion, is limited and faulted; and the most general existing results involve liquid plumes whose large Schmidt numbers are not representative of scalar mixing within gas flows in fire environments

In view of these difficulties, this phase of the investigation seeks to improve our understanding of buoyant turbulent flows by studying buoyant turbulent plumes in gases with the following specific objectives:

1. To complete measurements of mean and fluctuating mixture fraction, velocity and combined mixture-fraction/velocity statistics, emphasizing self-preserving conditions.

2. To exploit the new measurements in order to develop and evaluate theories of buoyant turbulent flow, considering classical similarity theories as well as more complex turbulence modeling procedures that are needed to treat turbulence/radiation, turbulence/buoyancy and other turbulence interactions in practical fire environments.

Work thus far has emphasized consideration of round buoyant turbulent plumes in the self-preserving portion of the flow. The initial phases of the study involved measurements of mixture fraction statistics (Dai et al., 1993, 1994a,b,c; Köylü et al., 1992, 1993), velocity statistics (Dai et al., 1994b, 1995a) and combined velocity/mixture fraction statistics (Dai et al., 1994b, 1995b) and interpretation of these measurements in terms of simple self-preserving theories. In addition, the availability of this data base allowed evaluation of the measurements by conservation checks and by interpretation of flow behavior using budgets of mean and turbulent quantities. Thus work during this report period emphasized two additional aspects of round, buoyant turbulent plumes in the self-preserving region, as follows:

1. Evaluation of effects of experimental conditions on measured results, particularly effects of confinement on self-preserving properties.

2. Exploitation of the measurements to evaluate various turbulence modeling procedures for round buoyant turbulent flows.

Initial reports of this work can be found in Dai (1995) and Dai and Faeth (1995)

The following discussion begins with descriptions of experimental methods and self-preserving scaling. The experimental results, emphasizing new measurements of effects of confinement on flow properties, and modeling implications, using past experimental results to evaluate a variety of turbulence modeling ideas, are then considered in turn.

3.2 Experimental Methods.

Figure 12 is a sketch of the experimental apparatus. The arrangement consists of a large outer enclosure (3000 x 3000 x 3400 mm high) containing the test plume within a smaller screened enclosure (1100 x 3200 mm high). The plumes involved source flows of gaseous carbon dioxide and sulfur hexafluoride in still air at atmospheric pressure and temperature, in order to provide a straightforward specification of the plume buoyancy flux. This yielded negatively buoyant, downward flowing plumes that were removed at the bottom of the enclosure using a blower and bypass system. The inner enclosure and the position of the source could be traversed to accommodate rigidly-mounted instrumentation.

Mixture fractions were measured using laser-induced iodine fluorescence (LIF), velocities were measured using laser-velocimetry (LV), and combined mixture-fraction/velocity statistics were measured using combined LIF/LV, similar to Lai et al. (1988) and Lai and Faeth (1987a,b). The LIF measurements involved seeding the source flow with iodine vapor which fluoresces naturally when excited by the 514.5 nm line of an argon-ion laser. The fluorescence signals were measured using two detectors which allowed measurements of two-point spatial correlations. Long-pass optical filters in front of the detectors blocked Rayleigh and Mie scattering at the laser line and allowed the yellow fluorescence signal to be detected even in the presence of LV scattering.

The LV measurements involved seeding the ambient air with oil drops (roughly 1μm nominal diameter) using several multiple jet spray generators. In this case, measurements were limited to the self-preserving region where maximum mixture fractions were less than 6% so the that effects of concentration bias (because only the ambient air was seeded) were negligible. A single-channel, dual-beam, frequency-shifted LV was used for the velocity measurements, based on the 514.5 nm line of an argon-ion laser, similar to the LIF measurements. Various orientations of the plane of the laser beams were used to find various velocity components and cross correlations, as described by Lai and Faeth (1987a,b).

Test conditions are summarized in Table 10 for the two plume sources. For $(x-x_o)/d \geq 87$, where self-preserving conditions were observed, the turbulence microscales were smaller than 350 μm. These dimensions are smaller than the LIF and LV measuring volumes so that the smallest scales of turbulence could not be resolved; nevertheless, experimental uncertainties were maintained less than 5 and 13% for mean and fluctuating quantities within the self-preserving region.

3.3 Self-Preserving Scaling

The general state relationship for density as a function of mixture fraction, assuming ideal gas behavior, is as follows for the present plume flows:

$$\rho = \rho_\infty / (1 - f(1 - \rho_\infty / \rho_o)) \tag{28}$$

Then, noting that $f << 1$ in the self-preserving region, Eq.(28) can be linearized as follows:

$$\rho = \rho_\infty + f\rho_\infty(1 - \rho_\infty / \rho_o),\ f << 1 \tag{29}$$

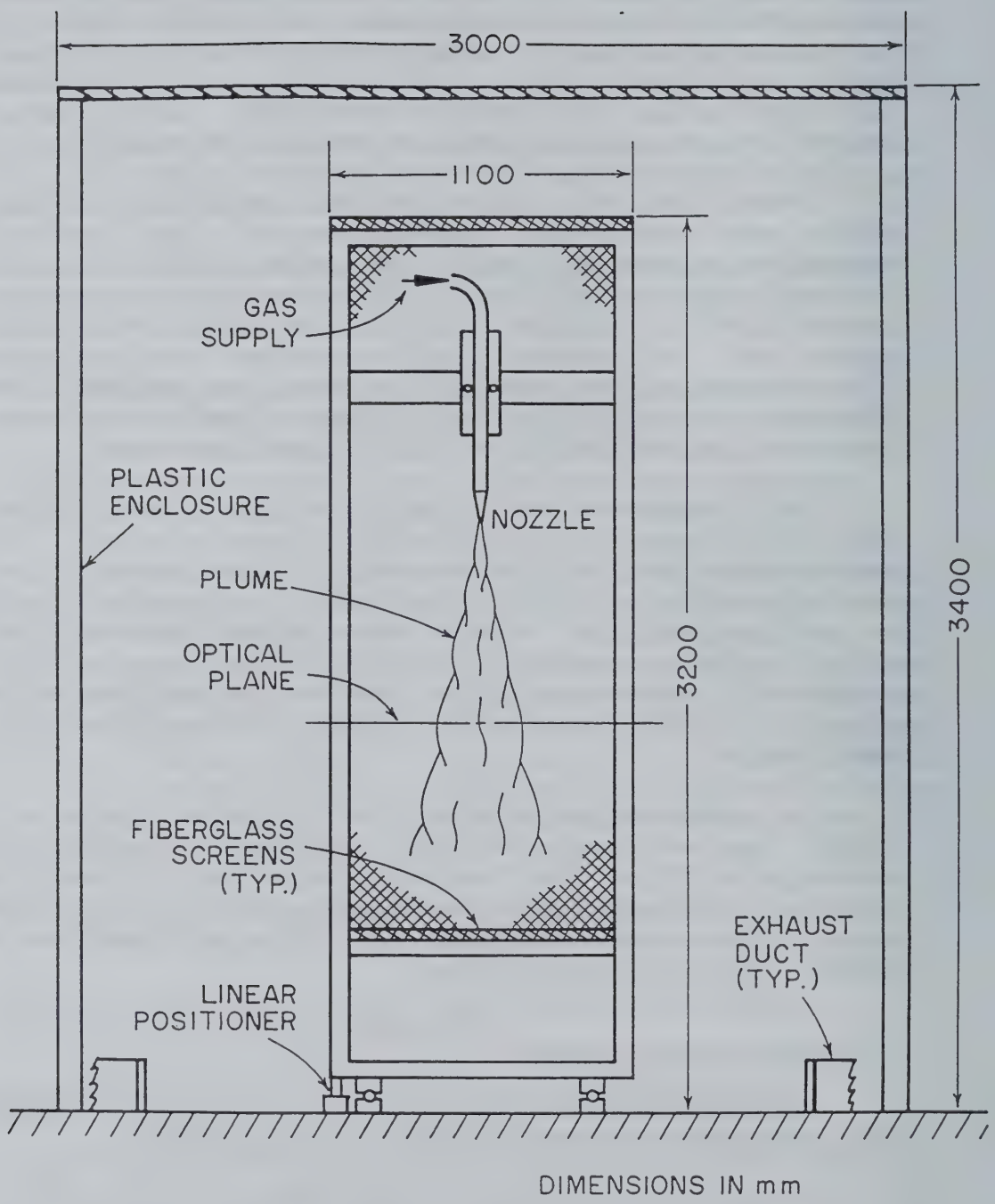

Figure 12. Sketch of round buoyant turbulent plume test apparatus.

Table 10. Buoyant Turbulent Plume Test Conditions[a]

Source Properties	Carbon Dioxide	Sulfur Hexafluoride
Density (kg/m^3)	1.75	5.87
Kinematic viscosity (mm^2/s)	8.5	2.6
Diameter (mm)	9.7	6.4
Average velocity (m/s)	1.74	1.89
Reynolds number, Re_0	2,000	4,600
Froude number, Fr_0	7.80	3.75
Morton length scale, ℓ_M/d	7.34	3.53
Virtual origin, x_0/d, based on f	12.7	0.0
Virtual origin, x_0/d, based on $\overline{u}$	0.0	0.0

[a]Flow directed vertically downward in still air with ambient pressure and temperature of 99± 0.5 kPa and 297 ± 0.5 K. Source length-to-diameter ratios of 50:1.

Under present assumptions, conservation principles and the state relationship for density imply that the buoyancy flux is conserved for buoyant turbulent plumes. Then mean streamwise velocities and mixture fractions for round buoyant turbulent plumes burning in air can be scaled as follows in the self-preserving region, where flow properties are independent of source properties like d and u_o (List, 1982):

$$f\, gB_o^{-2/3}(x-x_o)^{5/3}|d\ln\rho/df|_{f\to 0}=F(r/(x-xo)) \tag{30}$$

$$\bar{u}((x-x_o)/Bo)^{1/3}=U(r/(x-xo)) \tag{31}$$

For present conditions, it can be seen from Eq. (29) that:

$$|d\ln\rho/df|_{f\to 0} = |\rho o - \rho\infty|/\rho o \tag{32}$$

is a measure of the buoyancy potential with the extent of mixing. As before, an absolute value has been used in Eq. (32) to account for both rising and falling plumes. The x_o in Eqs. (30) and (31) are the virtual origins for $\bar{f}$ and $\bar{u}$, respectively, as noted in Table 10. The $F(r/(x-x_o))$ and $U(r/(x-x_o))$ are appropriately scaled radial profile functions of mean streamwise velocities and mixture fractions, which become universal functions in the self-preserving region far from the source where Eq. (29) applies. Equations (30) and (31) were used to extrapolate present measurements of mean mixture fractions and velocities along the axis to find the corresponding values of the virtual origins.

The functions $F(r/(x-x_o))$ and $U(r/(x-x_o))$ are typically approximated by Gaussian fits, as follows (Rouse et al., 1952; Papanicolaou and List, 1988; Mizushima et al., 1979; Ogino et al., 1980; Shabbir and George, 1992; George et al., 1977):

$$F(r/(x-x_o)) = F(0)\exp\{-k_f^2(r/(x-x_o))^2\} \tag{33}$$

$$U(r/(x-x_o)) = U(0)\exp\{-k_f^2(r/(x-x_o))^2\} \tag{34}$$

where

$$k_f = (x-x_o)/\ell_f, \qquad k_u = (x-x_o)/\ell_u \tag{35}$$

and ℓ_f and ℓ_u are characteristic plume radii when $\bar{f}/\bar{f}_c=\bar{u}/\bar{u}_c=e^{-1}$.

3.4 Experimental Results

Self-Preserving Behavior. All the present experimental results for round buoyant turbulent plumes in the self-preserving region can be found in Dai (1995), Dai and Faeth (1995) and Dai et al. (1994a,c, 1995a,b); therefore, only a portion of the findings will be considered here. In the following, results establishing self-preserving behavior will be considered first. This will be followed by experimental assessment of the effect of confinement on these results. Other measurements of flow properties will be discussed during consideration of modeling procedures in Section 3.5.

The development of transitional plumes toward self-preserving conditions can be seen from the radial profiles of mean mixture fractions illustrated in Fig. 13. In this case, the scaling parameters of Eq. (30) are used so that the ordinate is equal to $F(r/(x-x_o))$. The radial mean mixture fraction profiles exhibit progressive narrowing, with scaled values at the axis progressively increasing, as the streamwise distance increases. However, self-

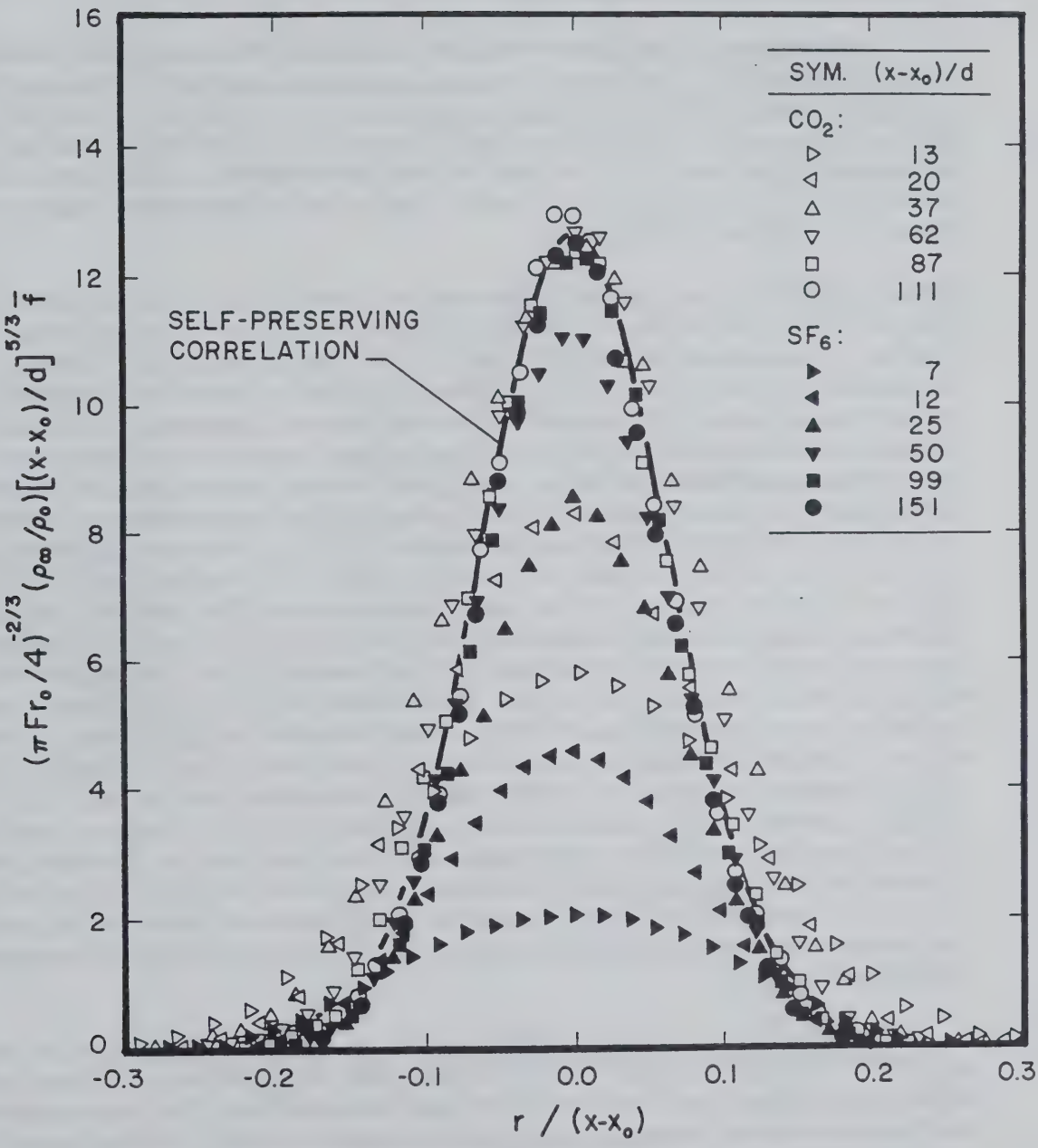

Figure 13. Radial profiles of mean mixture fractions in round buoyant turbulent plumes

preserving conditions are observed within experimental uncertainties for $12 \le (x-x_o)/\ell_M \le 43$ and $87 \le (x-x_o)/d \le 151$ (the upper end of these ranges represents the largest streamwise distance considered during present measurements). This regime corresponds to plume Reynolds numbers of 2500-4200 which are reasonably large for unconfined turbulent flows. The best fit of the present data within the self-preserving region yielded $F(0)=12.6$, $k_f^{\prime}=125$ and $\ell_f/(x-x_o)$ of roughly 0.09.

Measurements of velocities were limited to the self-preserving region; namely, $(x-x_o)/d \ge 87$ and $(x-x_o)/\ell_M \ge 12$. Profiles of mean streamwise velocities are illustrated in Fig. 14 which is plotted in terms of the scaling parameters of Eq. (31) so that the ordinate is equal to $U(r/(x-x_o))$. It is evident that $U(r/(x-x_o))$ is a universal function within experimental uncertainties over the range of the measurements, as anticipated for self-preserving flow. The best fit of present data in the self-preserving region yielded $U(0)=4.3$, $k_u^{\prime}=93$ and $\ell_u/(x-x_o)=0.10$.

Radial profiles of mixture fraction fluctuations are plotted in Fig. 15 for the two sources. Near the source, the profiles are broad and exhibit a dip near the axis, similar to the behavior of nonbuoyant jets (Becker et al., 1967; Panchapakesan and Lumley, 1993; Papanicolaou and List, 1987, 1988). However, both the width and the magnitude of the dip near the axis gradually decrease as streamwise distance is increased. Eventually, self-preserving behavior is obtained within the same range of streamwise distances where mean mixture fractions were self-preserving. Analogous to mean mixture fractions, most earlier measurements of r.m.s. mixture fraction fluctuations are representative of transitional plumes with broader profiles and smaller values of $(\overline{f}'/\overline{f})_c$. For example, Papanicolaou and List (1987, 1988), Shabbir and George (1992) and George et al. (1977) find $(\overline{f}'/\overline{f})_c=0.40$, rather than 0.45 for the present measurements. The other result in the self-preserving region, due to Papantoniou and List (1989), yields $(\overline{f}'/\overline{f})_c=0.64$; however, this large value probably is caused by the large Schmidt number of the liquid plumes that they studied, as noted earlier. The gradual disappearance of the dip in mixture fraction fluctuations is an interesting feature of the results illustrated in Fig. 15; this behavior is unique to buoyant flows and is due to effects of streamwise buoyant instability which causes turbulence production of mixture fraction fluctuations near the axis (Dai et al., 1994a). In particular, this production term is proportional to the streamwise gradient of mean mixture fraction which is a rather unique behavior for a flow that otherwise satisfies the boundary layer approximations. Furthermore, this gradient differs for round and plane plumes which should affect $\overline{f}$; thus, studies of plane plumes are needed to help establish this unique buoyancy/turbulence interaction as well as the proposed unusual non-boundary layer behavior.

Radial profiles of velocity fluctuations for the self-preserving region of the two sources are illustrated in Fig. 16. It is seen that the profiles are universal within experimental uncertainties over the range of conditions considered. The presence of the dip near the axis is similar to nonbuoyant jets and is expected because turbulence production is reduced near the axis due to symmetry (Panchapakesan and Lumley, 1993). Nevertheless, this behavior differs from mixture fraction fluctuations, illustrated in Fig. 15, and is another unusual feature of buoyant turbulent plumes. Finally, while the velocity fluctuations are nearly isotropic near the edge of the plumes, streamwise velocity fluctuations are roughly 25% larger than the cross stream velocity fluctuations near the axis.

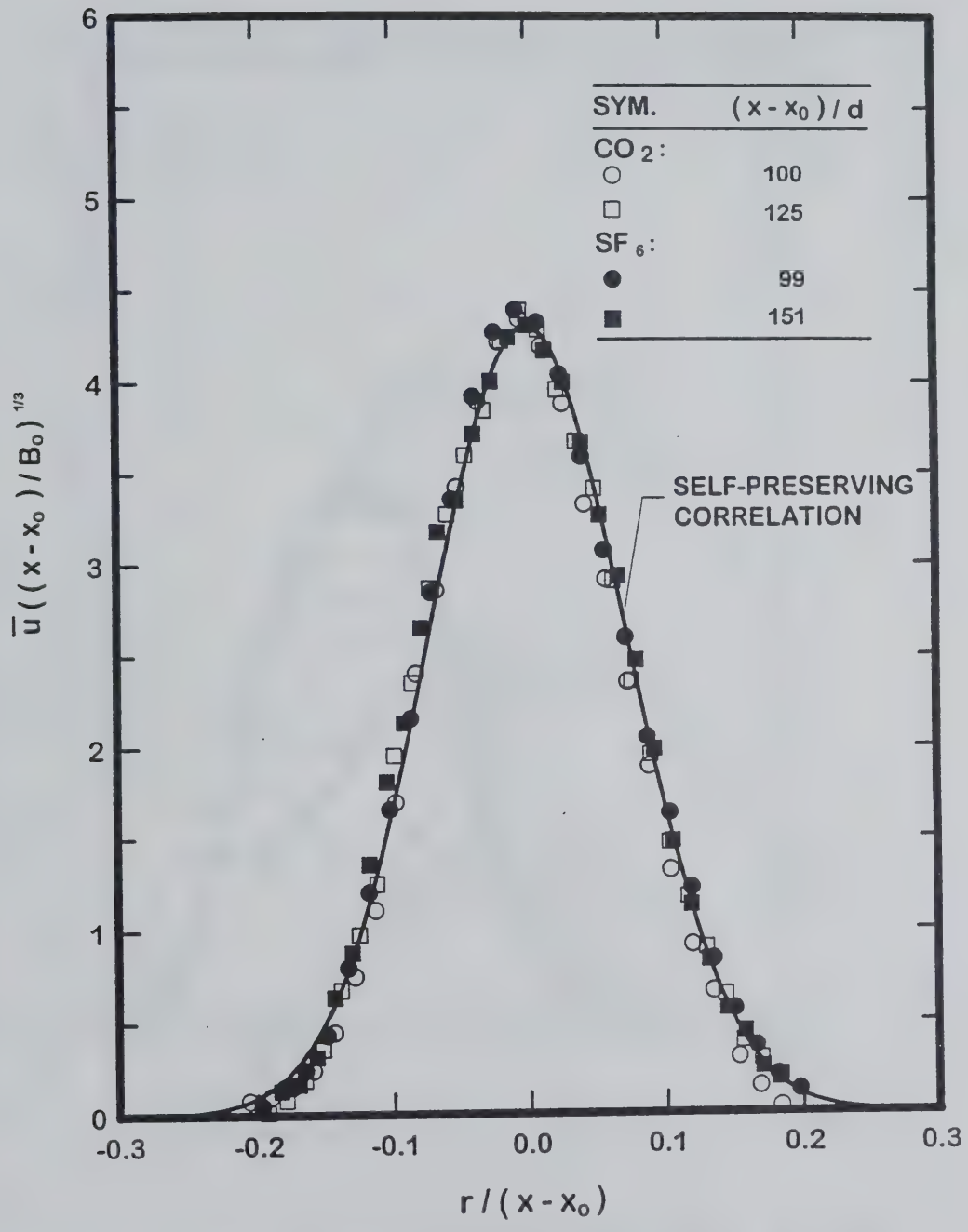

Figure 14. Radial profiles of mean streamwise velocities in round buoyant turbulent plumes.

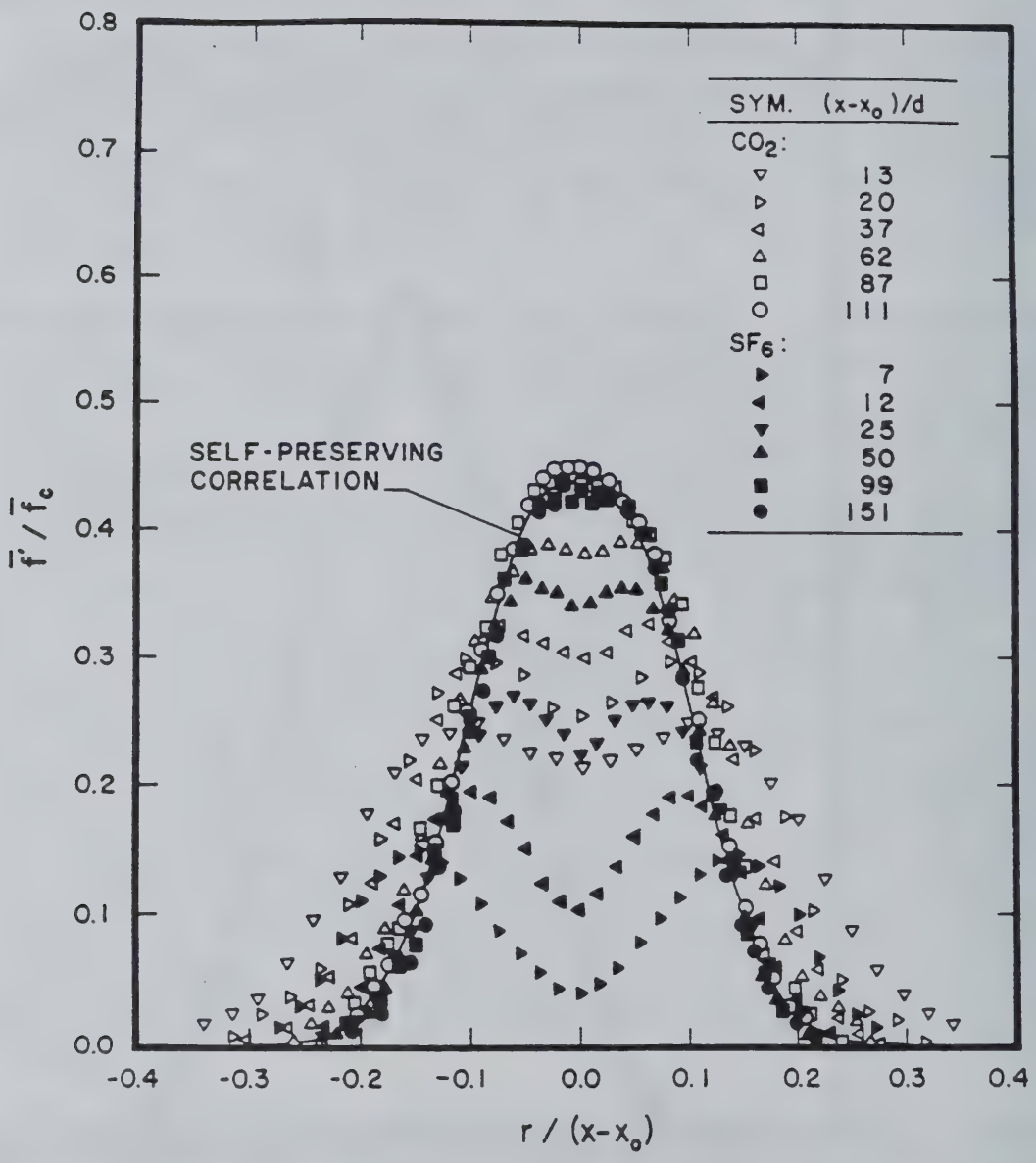

Figure 15. Radial profiles of r.m.s. mixture fraction fluctuations in round buoyant turbulent plumes.

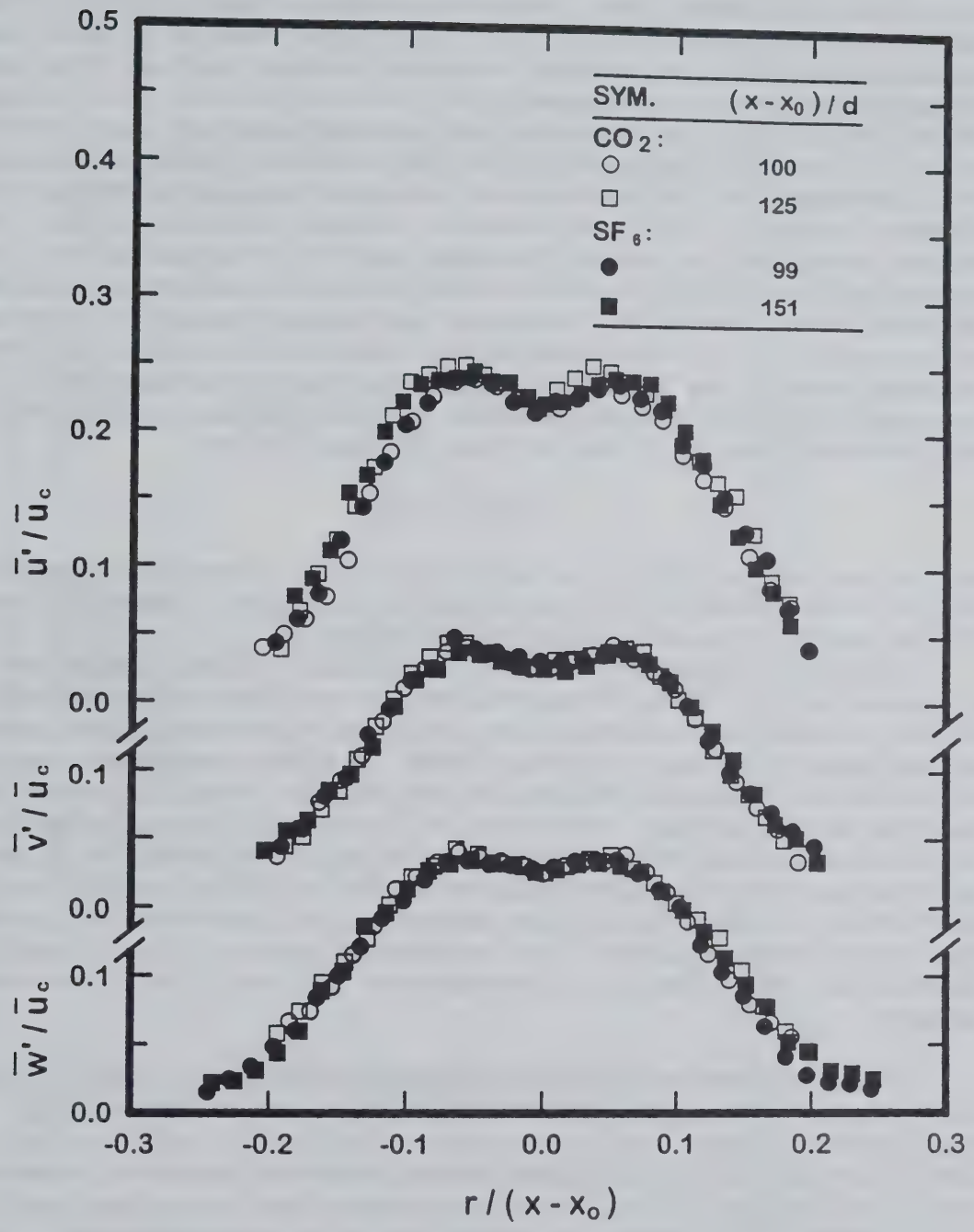

Figure 16. Radial profiles of r.m.s. velocity fluctuations in round buoyant turbulent plumes.

Present values of $(x-x_o)/d$ required to reach self-preserving conditions within round buoyant turbulent plumes are substantially larger than streamwise distances reached during most past measurements of the self-preserving properties of turbulent plumes. This behavior is quantified in Table 11. Aside from the present study, these results were obtained at values of $(x-x_o)/d$ that normally are not associated with self-preserving conditions for free turbulent flows. Similar to the tendency of transitional plumes to have broader profiles than self-preserving plumes in Fig. 13, the values of k_f^z and k_u^z tend to progressively increase as the maximum streamwise position is increased. This yields a corresponding reduction of the characteristic plume radius of 30 to 40%, and an increase of F(0) and U(0) of 30%, when approaching self-preserving conditions (ignoring the large value of F(0) found by Papanicolaou and List (1988) which they attribute to an instrument error). Discrepancies of this magnitude have a substantial impact on attempts to develop turbulence models for plumes and contribute to current controversies about proper modeling procedures. For example, Pivovarov et al. (1992) suggest that the standard constants used in k-ε turbulence models are inadequate based on past measurements within transitional plumes, however, their predictions using standard constants are in reasonably good agreement with the present measurements. Development effects also can be seen in fluctuating properties near the axis, with $(\overline{f}'/\overline{f})_c$ progressively increasing, and $(\overline{u}'/\overline{u})_c$ Progressively decreasing, as the self-preserving. The final item summarized in Table 11 is the entrainment constant, E_0, defined as follows (Dai et al., 1994b):

$$dQ/dx = E_0 \ell_u / \overline{u}_c \tag{36}$$

which implies that $E_0 = 5/(6k_u)$. E_0 is seen to progressively decrease as the distance from the source increases, until the self-preserving region is reached with a reduction of roughly 40% over the range of measurements summarized in Table 11.

Effects of Confinement. Due to concern about potential artifacts of their experiments, Dai et al. (1994a, 1995a,b) completed several checks of their measurements, including evaluating the measurements using the governing equations for mean quantities and establishing conservation of buoyancy fluxes. In addition, preliminary experiments indicated that the measurements were relatively independent of the rate of removal of plume gases from the test enclosure. Nevertheless, the observation of narrower self-preserving plumes than earlier results in the literature raised new concerns about effects of the removal rates of exhaust gases from the test enclosure because this flow places the plumes in a coflow which would tend to make them narrower than truly unconfined self-preserving round buoyant turbulent plumes. Thus, measurements were carried out to quantify the effects of plume exhaust rates on the distributions of $\overline{f}$, $\overline{u}$ and $\overline{f}'$ and $\overline{u}'$ that were just discussed.

The major parameters of the new measurements involved SF_6 plumes as follows: d=6.4 mm, u_o=1890 mm/s, ρ_o/ρ_∞=5.06,Fr_o=3.75, ℓ_M/d=3.53 and x_o/d=0.0. The measuring station farthest from the source was at $(x-x_o)/d$=151, while the edge of the plume is at roughly η=0.2, which yields plume diameters and streamwise distances less than 360 and 900 mm. This implies that the maximum plume cross-sectional area is less than 1.2 percent of the enclosure cross-sectional area, which is reasonably small. Exhaust volume flow rates were roughly half, equal to and twice the nominal flow rates used earlier, or 0.052, 0.090 and 0.22m^3/s, with highest flow rate approaching the capacity of the present exhaust system. Assuming uniform conditions over the cross-section of the enclosure, these exhaust flows imply coflow velocities of roughly 6, 10 and 24 mm/s at the plane of the source exit, which are less than 1.3 percent of the source velocity.

Table 11. Summary of Self-Preserving Turbulent Plume Constants[a]

Source	Present Study	Papanicolaou and List (1987, 1988)	Shabbir and George(1992)	George et al. (1977)	Ogino et al. (1980)	Nakagome and Hirata (1977)
Medium	gas	liquid	gas	gas	liquid	gas
$(x-x_0)/d$	87-151	12-62	10-25	8-16	6-36	5-13
$(x-x_0)/\ell_M$	12-43	5-62	6-15	6-12	5-15	∞
k_f^2	125	80	68	65	---	---
$\ell_f/(x-x_0)$	0.09	0.11	0.12	0.12	---	---
F(0)	12.6	11.1-14.3	9.4	9.1	---	---
$(\bar{f}'/\bar{f})_c$	0.45	0.40	0.40	0.40	---	---
k_u^2	92	90	58	55	51	48
$\ell_u/(x-x_0)$	0.10	0.11	0.13	0.14	0.14	0.14
U(0)	4.3	3.9	3.4	3.4	3.4	3.9
$(\bar{u}/\bar{u})_c$	0.22	0.25	0.32	0.28	---	0.25
E_0	0.086	0.088	0.109	0.112	0.117	0.120

[a]Round turbulent plumes in still, unstratified environments. Range of streamwise distances are for conditions where quoted self-preserving properties were found from measurements over the cross section of the plumes. Entries are ordered in terms of decreasing k_u.

The new measurements at the nominal exhaust flow rate agreed with our earlier results within experimental uncertainties; therefore, these results will be represented by their earlier correlations. Present measurements of mean mixture fractions and streamwise velocities in the self-preserving region of buoyant turbulent plumes are illustrated in Fig. 17 for the various exhaust flow ratios. The values of $\bar{f}$ and $\bar{u}$ are plotted as a function of η according to the self-preserving scaling parameters of Eqs. (30) and (31). The present measurements were limited to $(x-x_o)/d=151$ because this was the most critical condition with respect to potential coflow effects.

As can be seen from the results illustrated in Fig. 17, the effect of varying plume exhaust rates, and thus coflow velocities, is negligible over the present range. In fact, the profiles of $\bar{f}$ and $\bar{u}$ for all coflow rates agree within experimental uncertainties. Thus, including the new measurements with the earlier results of Dai et al. (1994a, 1995a) yields the same universal fitting parameters as before (listed in Table 11): $F(0)=12.6$ and $k_f^2=125$, $U(0)=4.3$ and $k_u^2=93$. The main effect of increased coflow velocities was evidence of a slight increase of streamwise velocity near the edge of the plume, which can be seen most clearly at the outmost points of $\bar{u}$ for an exhaust flow rate of $0.22 m^3/s$.

Radial profiles of r.m.s. fluctuating mixture fractions and streamwise velocities are illustrated in Fig. 18 for the various exhaust flow rates. The values of $\bar{f}'$ and $\bar{u}'$ are normalized by $\bar{f}_c$ and $\bar{u}_c$ and plotted as a function of η, which corresponds to the self-preserving scaling observed by Dai et al. (1994a, 1995a). The test conditions for these fluctuating properties are the same as for the mean properties in Fig 17.

Similar to the results for mean properties in Fig. 17, the fluctuating properties illustrated in Fig. 18 exhibit variations with exhaust rate within experimental uncertainties. Thus, present estimates of mixture fraction and streamwise velocity intensities at the axis are not changed significantly from the findings of Dai et al. (1994fa, 1995a) as summarized in Table 11: $(\bar{f}'/\bar{f})_c=0.45$ and $(\bar{u}'/\bar{u})_c=0.22$.

3.5 Modeling Implications

Evaluation Methodology. Two general types of models have been evaluated using present measurements for round buoyant turbulent plumes; namely, the simple k-ε-g approach that is widely used in field models of buoyant turbulent flows in flame environments, e.g., Gore and Faeth (1986, 1988), Jeng et al. (1984), Kounalakis et al. (1991) and Tamanini (1977, 1978) and references cited therein; and higher-order closures, or Reynolds stress models, due to Hanjalac and Launder (1972) and Daly and Harlow (1970). Calculations required to evaluate these models were limited to the self-preserving region which removes uncertainties about initial conditions and improves computational accuracy, see Pivovarov et al. (1992) for a discussion of this issue.

The formulation of the turbulence model calculations for the self-preserving region varies with the type of turbulence model considered. Since present evaluations of existing turbulence models were not very encouraging, it does not seem worthwhile to reproduce these rather extensive formulations here; instead, Dai (1995) and Pivovarov et al. (1992) can be consulted for the details.

The computation domain and the numbers of grid cells were determined from numerical experiments such that further increasing the outer edge of the computational

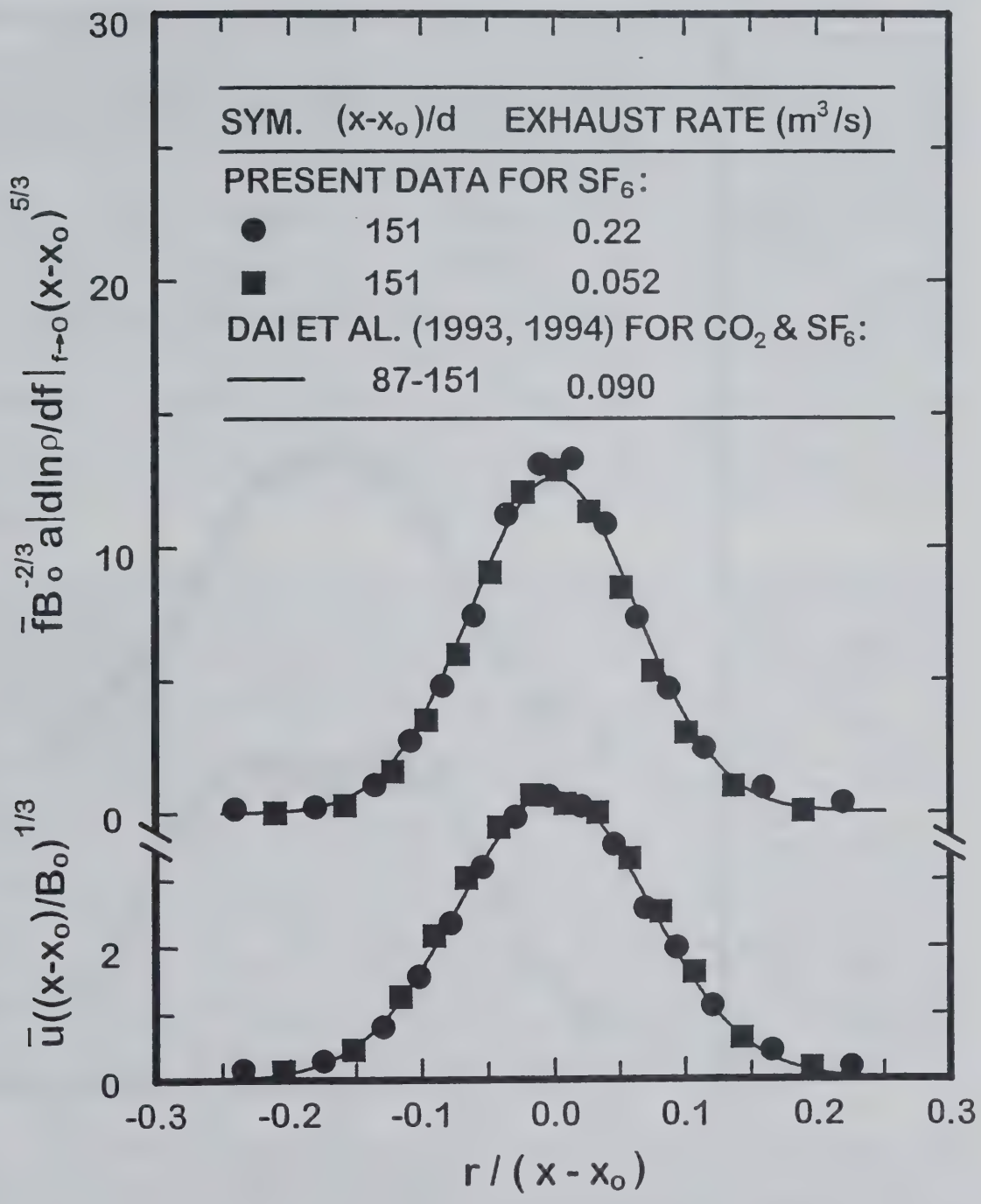

Figure 17. Radial profiles of mean mixture fractions and streamwise velocities in round buoyant turbulent plumes at various coflow rates.

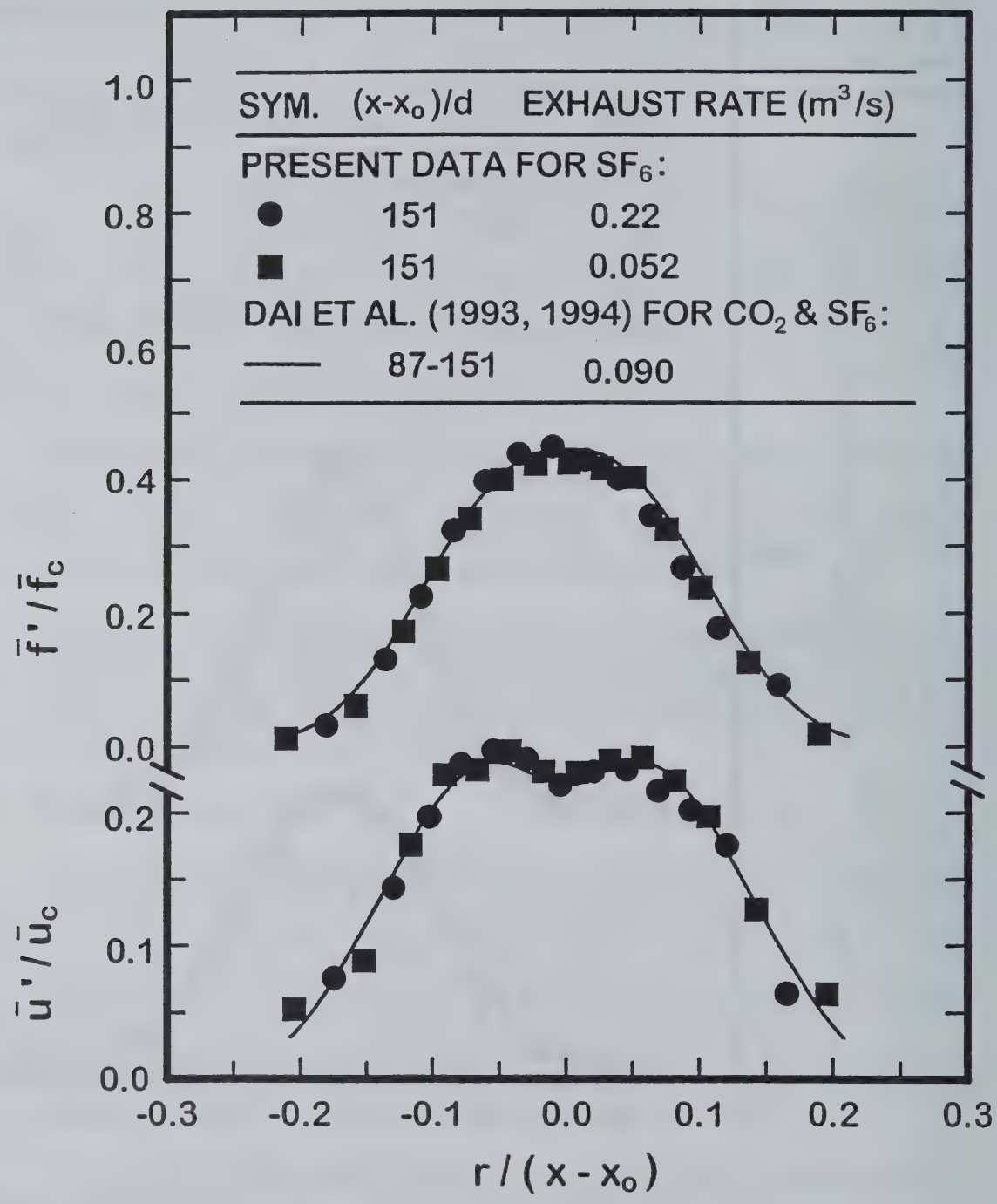

Figure 18. Radial profiles of r.m.s. mixture fraction and streamwise velocity fluctuations for round self-preserving buoyant turbulent plumes at various coflow rates.

domain, and increasing the number of grid cells, only affected computed results less than 1%. Results reported here are at this limit where the outer edge of the computational domain is at η=0.4, with 1200 grid cells employed in the calculation.

Evaluation of Simple Models. Predicted mean mixture fraction and streamwise velocity distributions for the k-ε–g and Reynolds stress (RS) models are compared with present measurements for self-preserving round buoyant turbulent plumes in Fig. 19. The performance of the Reynolds stress models will be discussed later, comments for the present will be confined to the k-ε–g model. The k-ε–g model using standard model constants, see Lockwood and Naguib (1975) and Gore and Faeth (1986, 1988), is seen to provide a fair representation of the measurements except for overestimating the width of the F distribution somewhat. This might be encouraging except that similar behavior can be obtained using even simpler models (eddy viscosity or mixing length) for the present simple boundary layer flow. In addition, many details about the turbulence properties are not predicted very well by the k-ε–g approach, raising questions about the reliability of these methods for more complex flows. Three examples of problems with k-ε–g calculations are illustrated in Figs. 20 and 21; namely, the turbulent Prandtl/Schmidt number and the turbulence model "constants" C_μ and C_{g2}. While all three of these parameters are treated as constants in k-ε–g turbulence models, it is evident that they actually vary substantially across the width of the present flow even for self-preserving conditions.

Other difficulties with simple k-ε–g model are encountered when turbulent transport properties such as turbulent mass fluxes and Reynolds stresses are considered. Present measurements of turbulent mass fluxes for the self-preserving region of the two plumes are illustrated in Fig. 22. The tangential turbulent mass flux, $\overline{f'w'}$=0, for an axisymetric flow, which is seen to be adequately represented by the measurements illustrated in Fig. 22. The radial turbulent mass flux, $\overline{f'u'}$=0 at the axis due to symmetry, and then increases to a maximum near η = 0.06 (in the absolute sense), before decreasing to zero once again at large r. The consistency of this parameter with other measurements was found by integrating the mean scalar transport equation; the results illustrated in Fig. 22 show good agreement with measured values of radial mass fluxes, both ignoring and considering turbulent mass fluxes. Finally, $\overline{f'u'}$ exhibits rather large values in the present flows; in fact the correlation coefficient for this parameter reaches values of roughly 0.7 near the axis, which is unusually large. This behavior is caused by the intrinsic instability of plumes where large values of f provide corresponding potential to generate large values of u through effects of buoyancy (George et al., 1977). Another aspect of the large values of $\overline{f'u'}$ is that the turbulent mass flux contribution to the total buoyancy flux of the plume is roughly 15 percent, which is appreciable and must be considered in conservation checks and other computations of plume properties.

The gradient diffusion approximation is normally used for treating transport with simple k-ε–g models, while it has just been seen that buoyant turbulent plumes require consideration of turbulent transport in both the cross stream and streamwise directories. Adopting the gradient diffusion approximation for radial and streamwise turbulent mass fluxes then implies:

$$\overline{f'v'}=-(\nu_T/\sigma_T)\partial \bar{f}/\partial r,\ \overline{f'u'}=-(\nu_T/\sigma_T)\partial \bar{f}/\partial x \qquad (37)$$

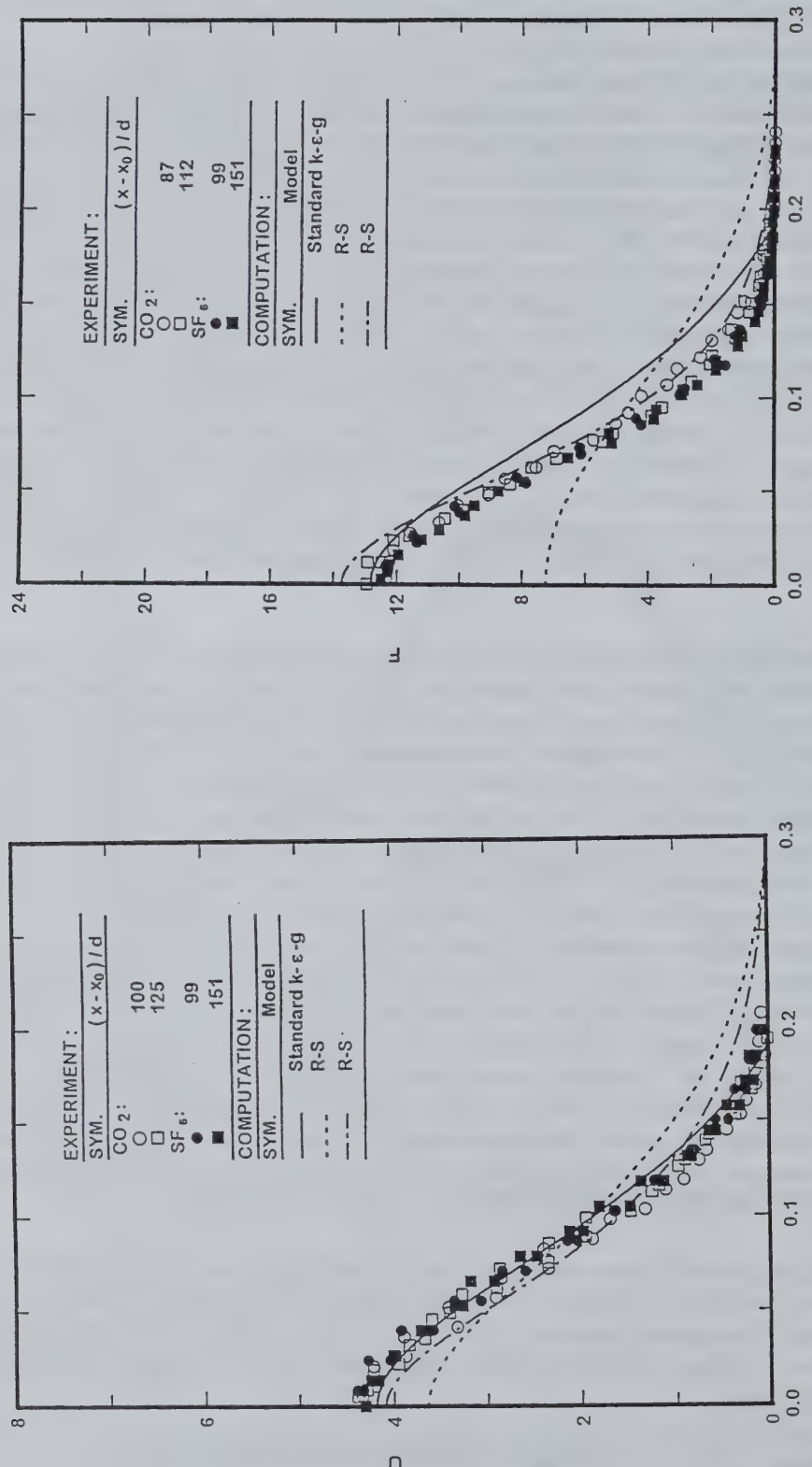

Figure 19. Measured and predicted mean streamwise velocity and mixture fraction distributions.

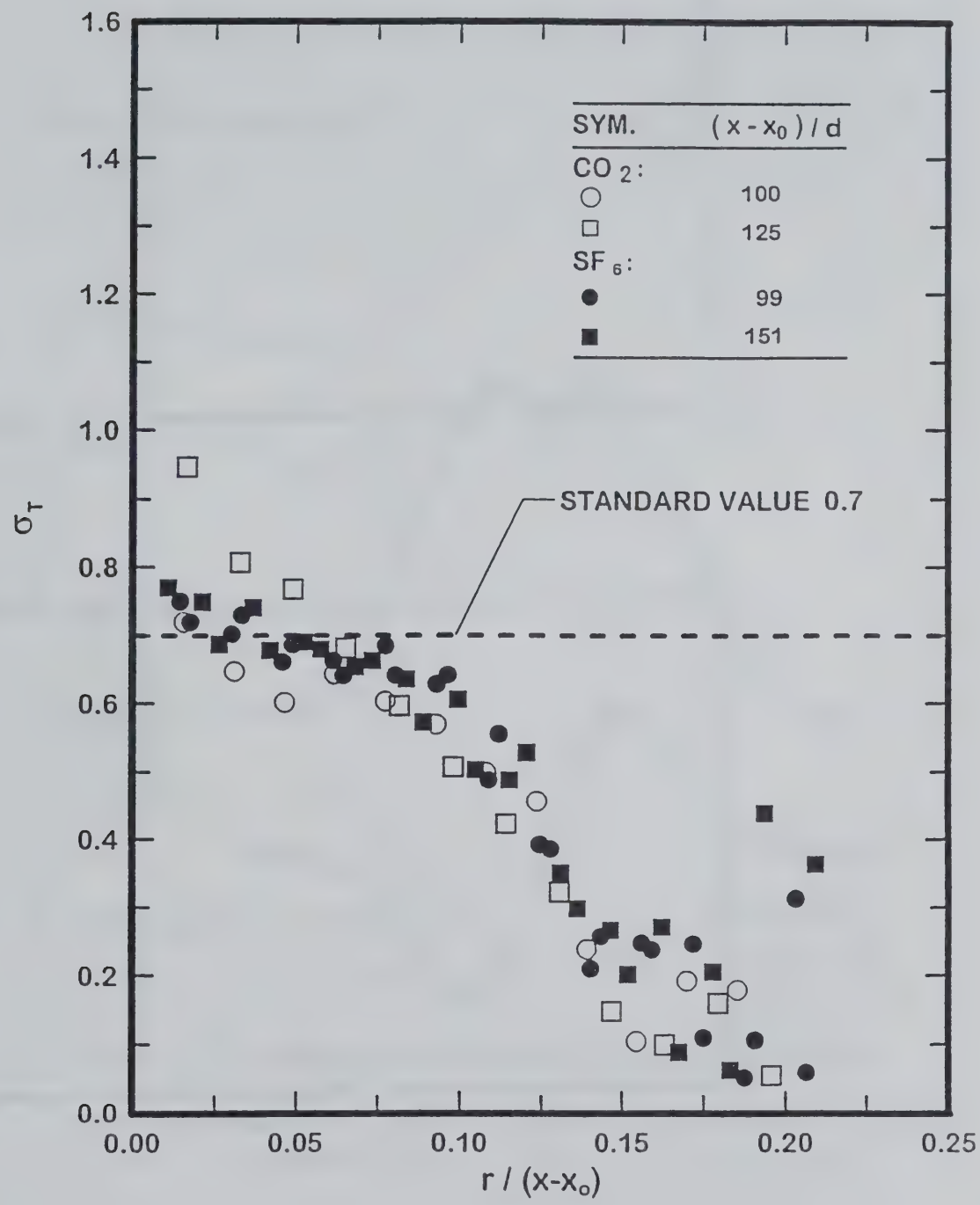

Figure 20. Measured and predicted turbulence Prandtl/Schmidt numbers.

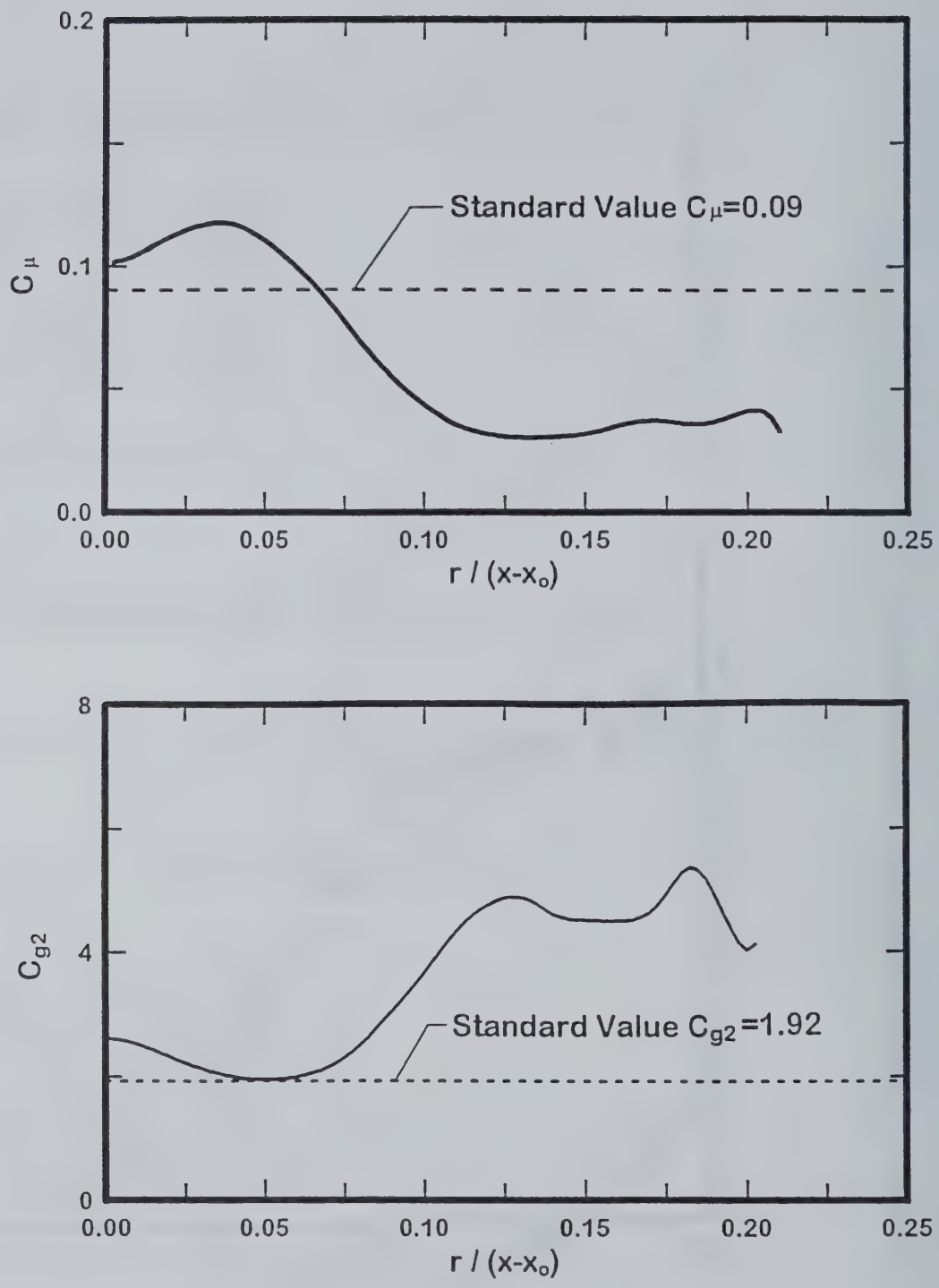

Figure 21. Distributions of the mechanical/scalar time scale ratios, C_μ and C_{g2}.

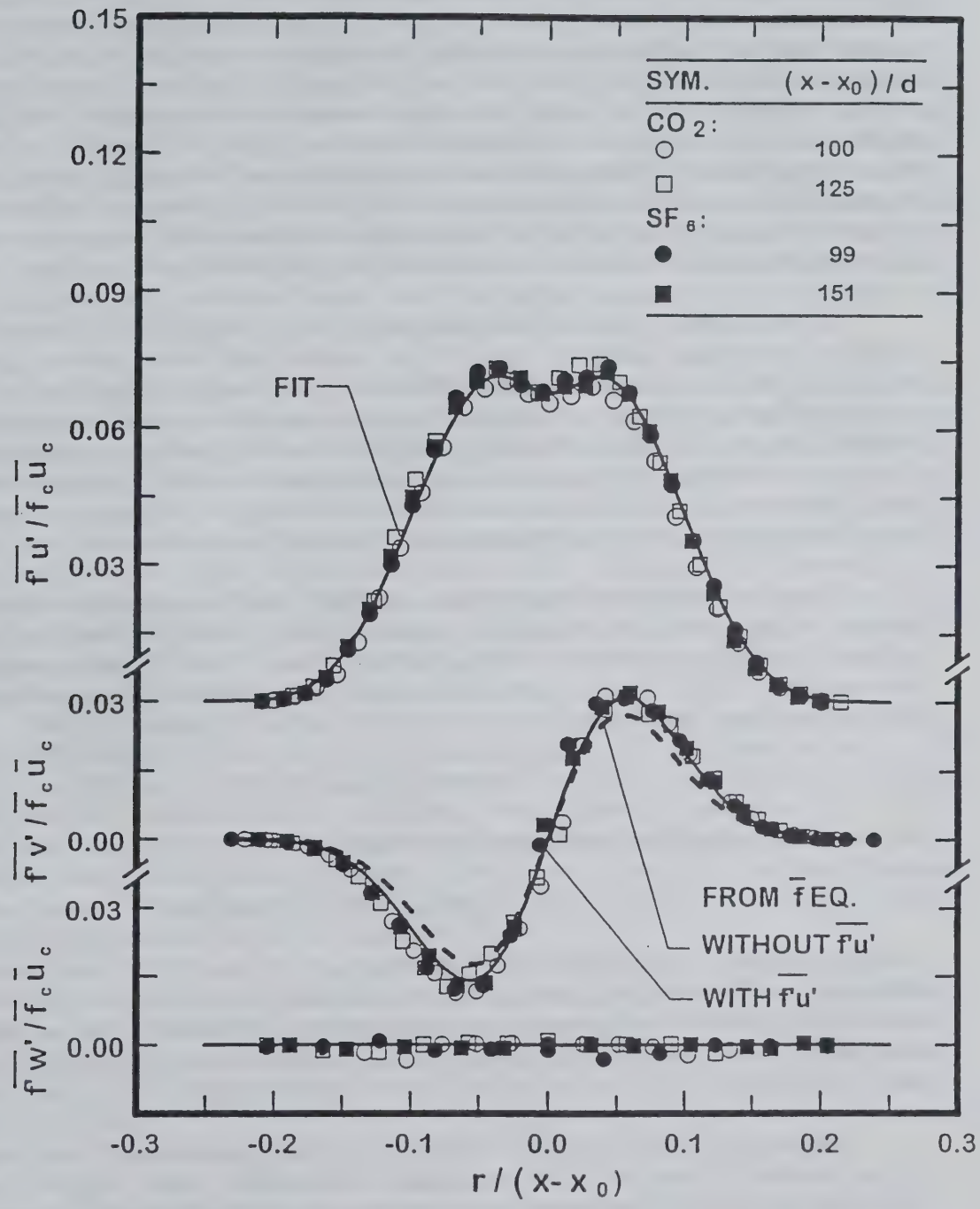

Figure 22. Radial profiles of turbulent mass fluxes in round buoyant turbulent plumes.

This approach is generally acceptable in the radial direction, based on the present measurements of $\overline{f'v'}$ illustrated in Fig. 22 and the correlation of $\bar{f}$ illustrated for the self-preserving region in Fig. 13. Unfortunately, this approach yields estimates of countergradient diffusion in the streamwise direction, e.g., $\overline{f'u'} > 0$ from Fig. 22 but $\partial \bar{f}/\partial x \geq 0$ when $r/(x-x_o) \geq (5/6)^{1/2}/k_f = 0.082$, which implies an unphysical negative value of ν_T near the edge of the flow as well as a clear absence of the isotropy implied by Eq. (37). Analagous considerations of turbulent stresses similarly indicate acceptable gradient diffusion behavior in the radial direction, however, countergradient diffusion is encountered for the streamwise direction when $r/(x-x_o) \geq (1/6)^{1/2}/k_u = 0.042$. Naturally, these countergradient diffusion effects are not very important for boundary layer flows like the present plumes, when streamwise transport is ignored in any event; nevertheless, these deficiencies raise concerns about the use of simple gradient diffusion hypotheses for the more complex buoyant turbulent flows of interest for practical fire environments.

Taken together, present findings highlight several serious deficiencies of simple models of turbulence along the lines of the widely used k-ε–g models: substantial variations of model "constants" across the flow width, the presence of significant effects of gradient diffusion, and lack of transport isotropy implied by simplified treatment of turbulent transport. Thus, the reasonably good predictions of mean quantities seen in Figs. 13 and 14 are not very definitive and there are serious problems about important features of k-ε–g type models, raising questions about their value for treating the complex buoyant/turbulent flows typically encountered in practical fire environments.

The more complex Reynolds stress models avoid assumptions of gradient-diffusion, isotropy and constant transport parameters like C_μ and C_{g2}. Thus, they have the potential for effective treatment of complex turbulent flows. Two Reynolds stress models are considered in Fig. 19: one (dashed line) treating pressure/mixture-fraction-fluctuation-gradient correlations as follows:

$$S_{fi2} = -C_{2f}\overline{f'u'_j}\partial \bar{u}_i/\partial x_i \tag{38}$$

and the other (chained line) finding this term as follows:

$$S_{fi2} = -C_{2f}\overline{f'u'_j}(\partial \bar{u}_i/\partial x_j + \partial \bar{u}_j/\partial x_i) \tag{39}$$

The first approach, due to Launder (1990) and Malin and Younis (1990), clearly is not very satisfactory, while the second approach, due to Launder (1990), retrieves performance of mean property predictions comparable to the k-ε–g model. Nevertheless, the predictions of the Reynolds stress models still are not very reliable for turbulence properties as discussed next.

Similar to the earlier evaluation of the k-ε–g model, predictions of mean quantities do not provide a very definitive evaluation of Reynolds stress models; therefore, predictions of third and fourth moments will be considered in the following. Several third-moment models were evaluated, finding that the complex approach of Lumley (1978) was only slightly better than the simple gradient diffusion model of Daly and Harlow (1970) (D-H model) and the isotropization of production model of Hanjalic and Launder (1972) (H-L model), see Dai (1995). Therefore, only the D-H and H-L models will be considered here.

The third velocity moment measurements and predictions of the D-H and H-L models for self-preserving round buoyant turbulent plumes are illustrated in Figs. 23 and 24. The corresponding measurements and predictions of combined third moments are illustrated in Figs. 24 and 26. It is seen that both the D-H and H-L models provide very good predictions of third moments involving radial velocity fluctuations, such as $\overline{v'^3}$, $\overline{u'w'^2}$ and $\overline{f'u'v'}$, with the H-L model yielding slightly better results than the D-H model. On the other hand, however, the predictions of both models for moments involving streamwise and tangential velocity fluctuations, such as $\overline{u'^3}$, $\overline{u'w'^2}$, $\overline{f'u'^2}$ and $\overline{f'w'^2}$, are generally much smaller than the measurements. Similar to counter-gradient diffusion effects, these deficiencies are not very important for modeling a boundary layer flow, similar to the present round buoyant turbulent plumes. Nevertheless, such deficiencies are a concern because these terms become important for the complex buoyant turbulent flows of practical fire environments. Dai (1995) considers a variety of turbulence properties and existing higher order turbulence models with the similar outcome that existing models are not very satisfactory for complex buoyant turbulent flows.

The fourth moments of velocity fluctuations considered during the present investigation, along with corresponding quasi-Gaussian approximations based on the measurements of second moments of velocity fluctuations due to Dai et al. (1995a), are illustrated in Fig. 27. A variety of single correlations are considered along with one correlation sum whose components could not be separated using the present experimental arrangement and methods. Typical of other properties, these correlations exhibit self-preserving behavior within experimental uncertainties. Similar to the observations of Panchepakesan and Lumley (1993) for nonbuoyant round turbulent jets, the quasi-Gaussian approximation is reasonable even though present flows exhibit significant intermittency for $\eta > 0.1$.

Fourth moments involving combined mixture fraction and velocity fluctuations, along with estimates based on the quasi-Gaussian approximation, are illustrated in Figs. 27 and 28. In this case, second moments of combined velocity/mixture-fraction correlations needed for the quasi-Gaussian approximation were obtained from Dai et al. (1995b). These results also indicate reasonably good self-preserving behavior for combined fourth moments as well as reasonable predictions of these correlations using the quasi-Gaussian approximation. This behavior should be helpful for estimating and modeling rates of transport of higher-order turbulence quantities.

On the surface, the results illustrated in Figs. 19-26 are discouraging with no existing model yielding reliable predictions of both mean and turbulent properties for round buoyant turbulent plumes in the self-preserving region. Hopefully, the availability of new measurements of various properties for these flows will assist the development of more effective methods.

3.6 Conclusions

Mixture fraction, velocity and combined mixture-fraction/velocity statistics were measured in round buoyant turbulent plumes in still air; and the new measurements were used to evaluate several contemporary models of buoyant turbulent flows. The test conditions involved buoyant jet sources of carbon dioxide and sulfur hexafluoride with (x-

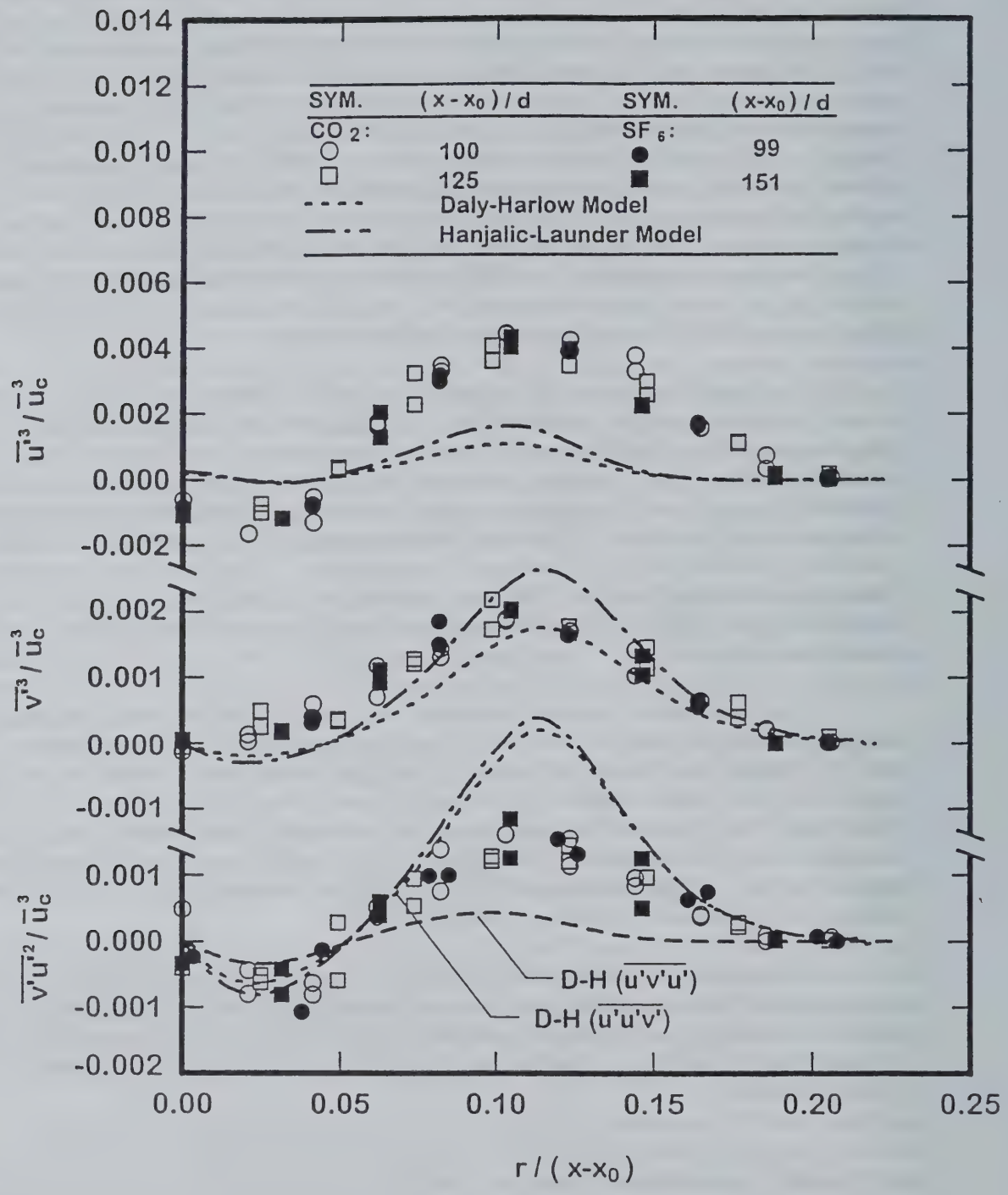

Figure 23. Measured and predicted third velocity moments in round buoyant turbulent plumes.

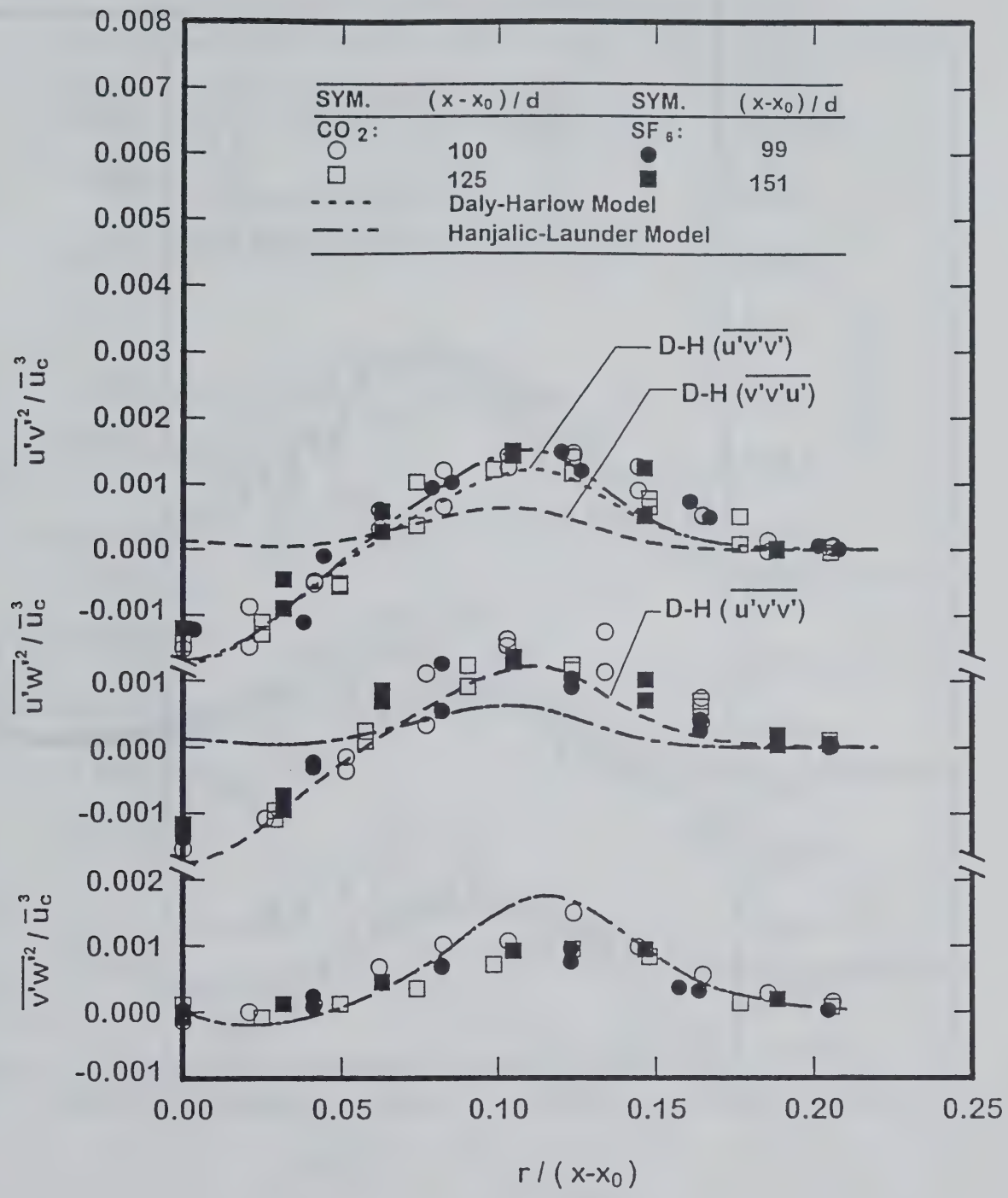

Figure 24. Measured and predicted third velocity moments in round buoyant turbulent plumes.

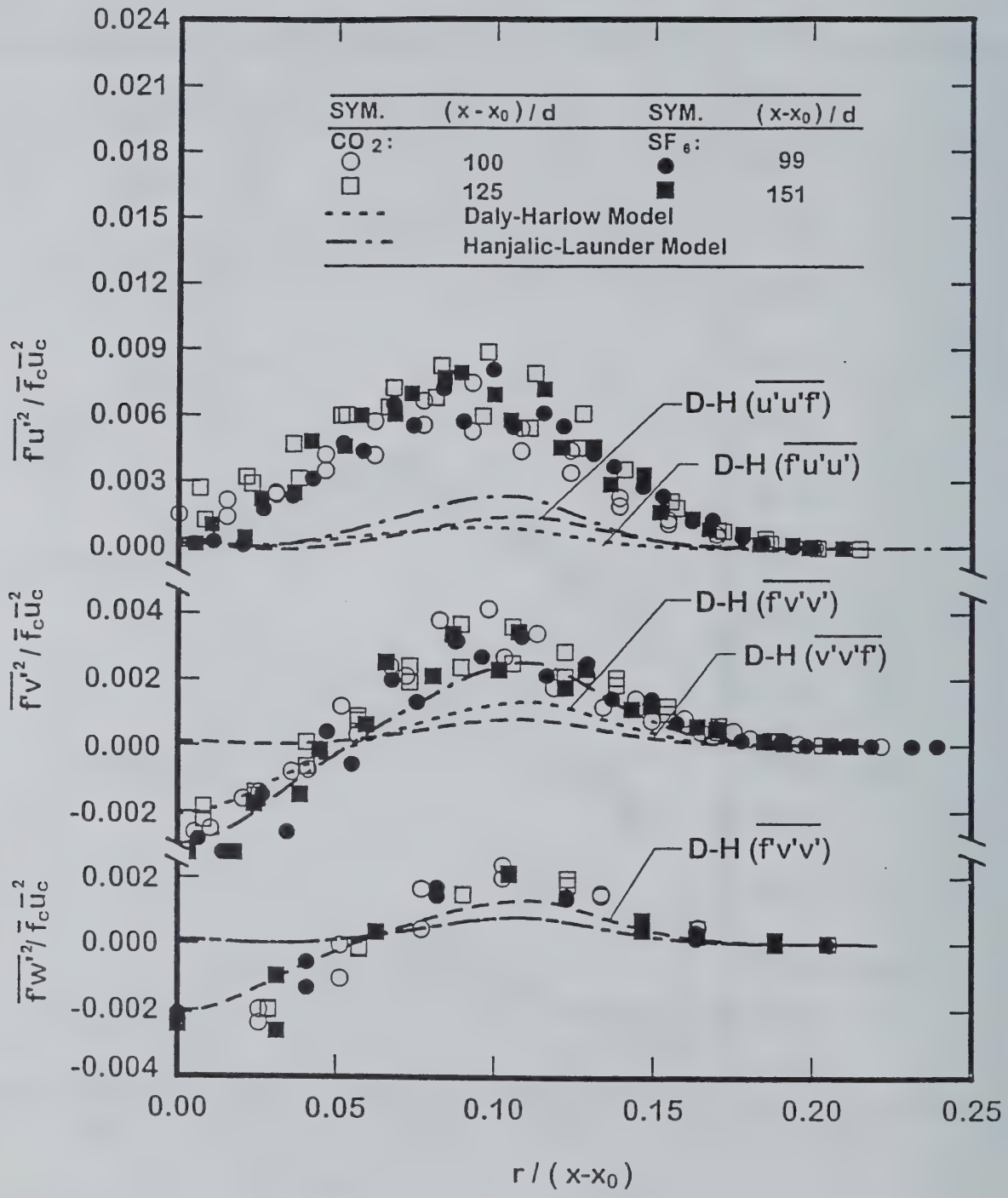

Figure 25. Measured and predicted combined third velocity moments in round buoyant turbulent plumes.

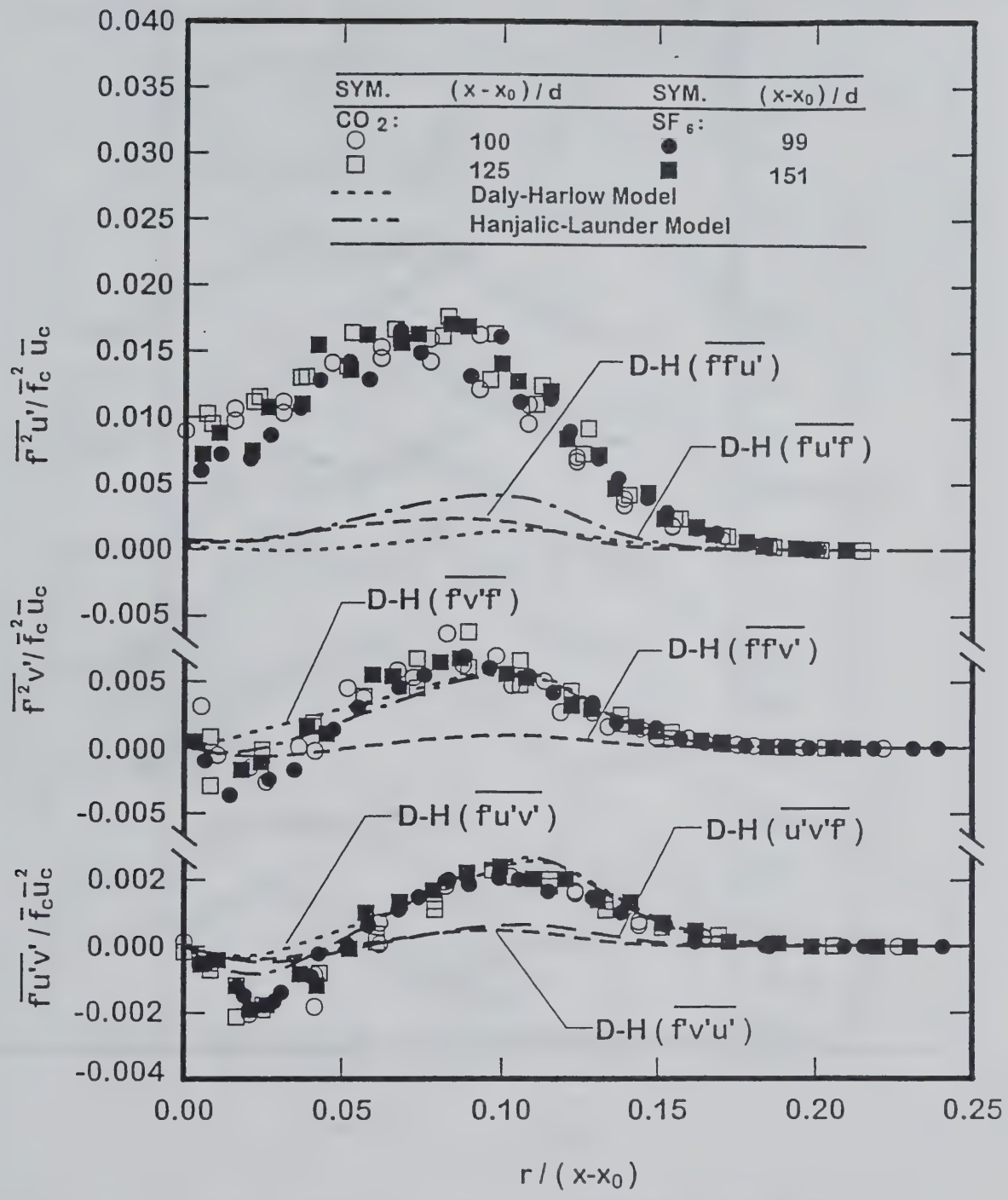

Figure 26. Measured and predicted combined third velocity moments in round buoyant turbulent plumes.

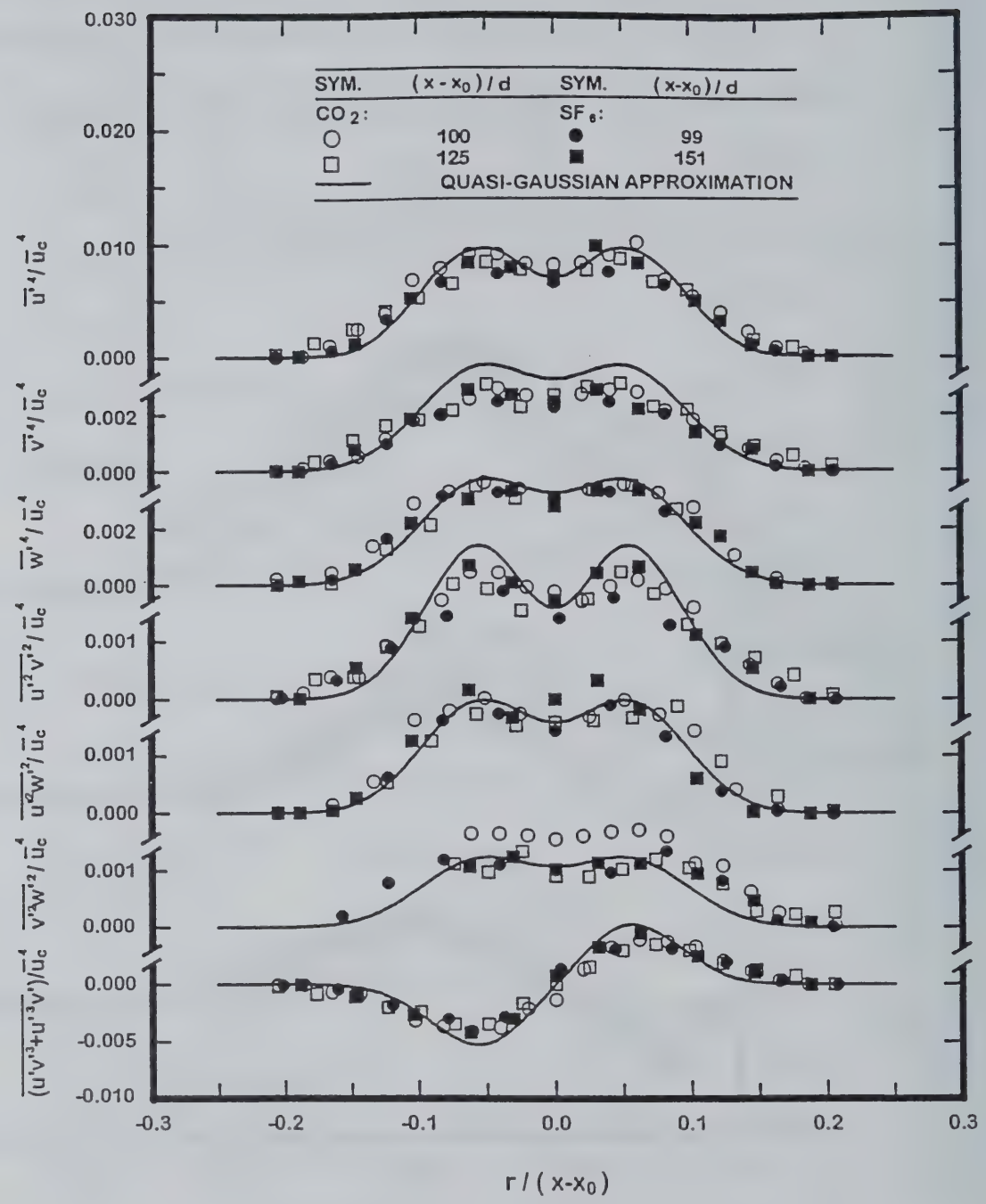

Figure 27. Radial distributions of fourth moments of velocity fluctuations in round buoyant turbulent plumes.

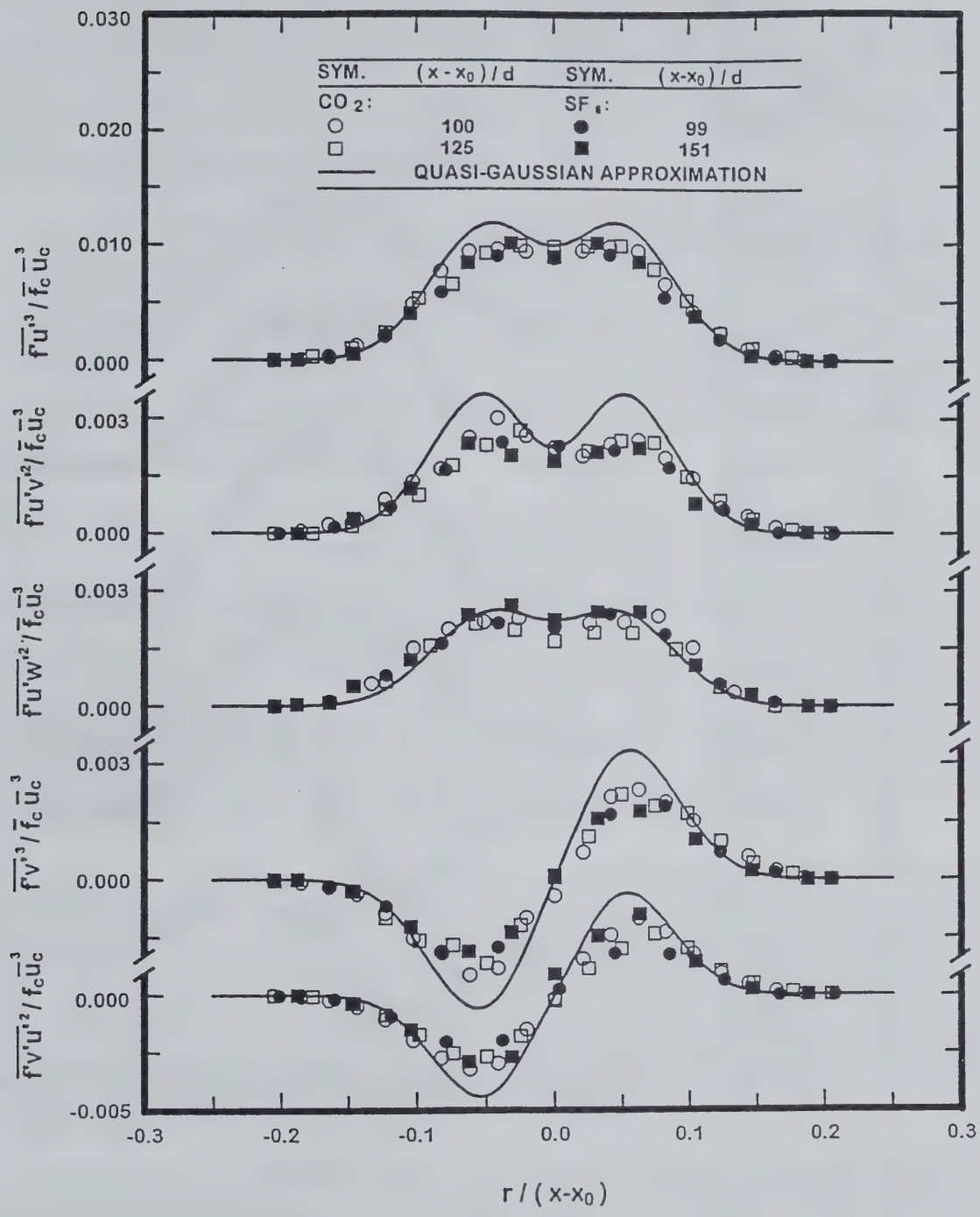

Figure 28. Radial distributions of fourth moments of velocity/mixture fraction fluctuations involving first moments of mixture fraction fluctuations in round buoyant turbulent plumes.

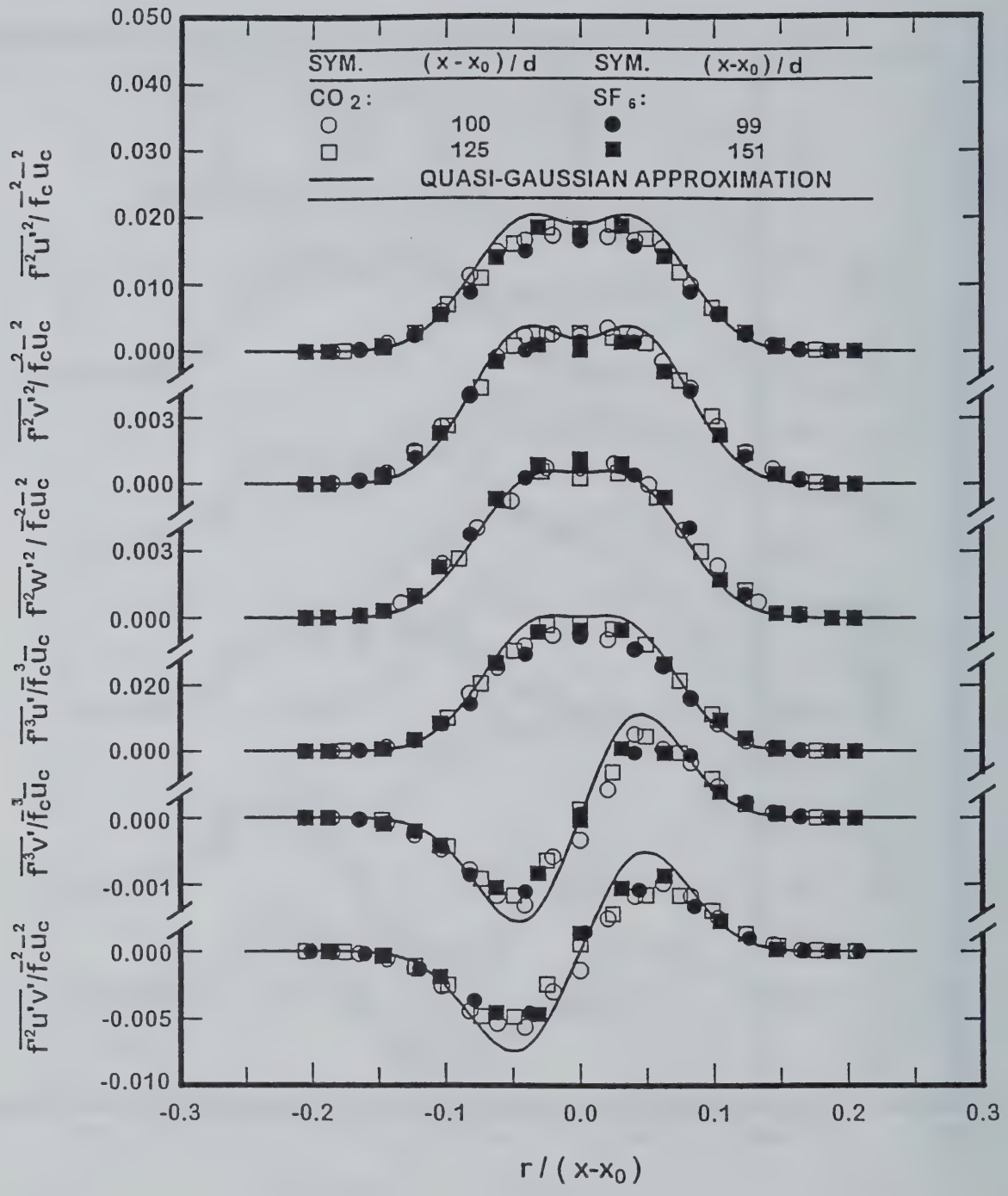

Figure 29. Radial distributions of fourth moments of velocity/mixture fraction fluctuations involving higher moments of mixture fraction fluctuations in round buoyant turbulent plumes.

x_o)/d in the range 0-151 and $(x-x_o)/\ell_m$ in the range 0-43. The major conclusions of the study are as follows:

1. Direct measurements for various co-flow conditions have established that the earlier measurements of Dai et al. (1994a, 1995a,b) were not affected by confinement within experimental uncertainties; therefore, these measurements correctly indicate that self-preserving round buoyant turbulent plumes are narrower, with larger scaled mean values at the axis, than previously thought.

2. The present measurements indicate that predictions of mean properties in the self-preserving region are reasonably good using a k-ε–g model with "standard constants" prescribed by Lockwood and Naguib (1975) and used by others for a variety of combusting buoyant turbulent flows with some success, see Gore and Faeth (1986, 1988) and references cited therein. Thus, the earlier conclusion by Pirovarov et al. (1992) that k-ε–g constants must be varied for successful predictions of buoyant turbulent flows is not correct because the data they used to evaluate their predictions were still in the developing portion of the flow as opposed to the self-preserving conditions that they assumed.

3. In spite of the promising predictions of mean properties using a simplified k-ε–g model that were just discussed, however, such models have several significant deficiencies that raise questions about their potential effectiveness for the complex buoyant turbulent flows of interest for practical fire environments. These difficulties can be summarized as follows: while the radial turbulent transport of mass and momentum properly satisfy gradient diffusion approximations used in simple models, streamwise turbulent transport does not near the edge of the flow; these effects of countergradient diffusion clearly invalidate approximations of transport coefficient isotropy that are widely used in simplified models; and even dominant transport rates are not properly represented by existing simple models because parameters assumed to be constant, e.g., σ_T, C_μ and C_{g2}, vary widely even in simple turbulent boundary layer flows.

4. Higher-order turbulence models offer one approach for correcting the problems of simple models that were just discussed, however, current high-order models are not very developed and are deficient in many respects. The gradient-diffusion models of Daly and Harlow and the isotropization production models of Hanjalic and Launder for third moments generally were satisfactory for the present flows although both methods were not effective for treating third moments that have strong streamwise and tangential velocity fluctuations. As a result, the predictions of basic Reynolds stress models of Launder (1990) and Malin and Younis (1990) were not in good agreement with present measurements.

5. Fourth moments of velocity and velocity/mixture fraction fluctuations generally satisfied the quasi-Gaussian approximation across the flow width, although effects of intermittancy, including departure of the probability density functions from Gaussian behavior, near the edge of the flow must still be resolved.

Thus, in spite of some promising predictions for existing methods for treating buoyant turbulent flows, there are significant concerns about applying these methods to the complex buoyant turbulent flows that are encountered in practical fire environments, where rates of development of the flow in all directions often are comparable. It is hoped

that the extensive data base for self-preserving round buoyant turbulent plumes available from the present investigation, see Dai (1995), Dai and Faeth (1995) and Dai et al. (1994a, 1995a,b) and references cited therein, will prove helpful for developing more effective methods of predicting buoyant turbulent flows.

REFERENCES

Abraham, G., 1960, "Jet Diffusion in Liquid of Greater Density," ASCE J. Hyd. Dev., Vol. 86, pp. 1-13.

Anselmet, F., and Antonia, R.N. (1985) Joint Statistics Between Temperature and its Dissipation in a Turbulent Jet. Phys. Fluids, Vol. 28, pp. 1048-1054.

Batten, C.E. (1985) Spectral Optical Constants of Soots from Polarized Angular Reflectance Measurements. Appl. Optics 24, 1193-1199.

Becker, H.A., Hottel, H.C., and Williams, G.C. (1967) "The Nozzle-Fluid Concentration Field of the Round, Turbulent, Free Jet." J. Fluid Mech. Vol. 30, pp. 285-303.

Berry, M. V., and Percival, I. C., 1986, "Optics of Fractal Clusters Such as Smoke," Optica Acta Vol. 33, pp. 577-591.

Bilger, R.W. (1976) "Turbulent Jet Diffusion Flames," Prog. Energy Combust. Sci. Vol. 1, pp. 87-109.

Bohren, C.F., and Huffman, D.R.,1983, *Absorption and Scattering of Light by Small Particles*, Wiley and Sons, New York, pp.477-482.

Boyer, L., and Queiroz, M. (1991) Temperature Dissipation Measurements in a Lifted Turbulent Diffusion Flame. Combust Sci. Tech., Vol. 79, pp. 1-34.

Cai, J., Lu, N., and Sorensen, C.M. (1993) Comparison of size and morphology of soot aggregates as determined by light scattering and electron microscope analysis. Langmuir 9:2861-2867.

Chang, H.Y., and Charalampopoulos, T. T. (1990) "Determination of the Wavelength Dependence of Refractive Indices of Flame Soot," Proc. R. Soc. London A, Vol. 430, pp. 577-591.

Charalampopoulis, T.T., 1992, "Morphology and Dynamics of Agglomerated Particulates in Combustion Systems Using Light Scattering Techniques," Prog. Energy Combust. Sci. Vol. 18, pp. 13-45.

Chen, C. J., and Chen, C.H. (1979) On Prediction and Unified Correlation for Decay of Vertical Buoyant Jets. J. Heat Trans., Vol. 101, pp. 532-537.

Chen, C.J. and Rodi, W. (1980) *Vertical Turbulent Buoyant Jets: A Review of Experimental Data,* Pergamon Press, Oxford, p. 16.

Choi, M.Y., Hamins, A., Mulholland, G.W., and Kashiwagi, T. (1994) Simultaneous Optical Measurement of Soot Volume Fraction and Temperature. Combust. Flame, Vol. 99, pp. 174-186.

Choi, M.Y., Hamins, A., Mulholland, G.W., and Kashiwagi, T. (1995) Comparisons of the Soot Volume Fraction using Gravimetric and Light Extinction Techniques.. Combust. Flame, Vol. 102, pp. 161-169

Crawford, N.L., Liew, S.K. and Moss, J.B. (1985) Experimental and Numerical Simulation of a Buoyant Fire. Combust. Flame, Vol. 61, pp. 63-77.

Dahm, W.J.A., Southerland, K.B., and Buch, K.A. (1991) Direct, High Resolution, Four-Dimensional Measurements of the Fine Scale Structure of Sc >> 1 Molecular Mixing in Turbulent Flows. Phys. Fluids, Vol. A3, pp. 1115-1127.

Dai, Z. (1995) "Structure of Self-Preserving Round Buoyant Turbulent Plumes," Ph.D. Thesis, The University of Michigan, Ann Arbor, Michigan.

Dai, Z. and Faeth, G.M., (1995)"Measurements of the Sturcture of Self-Preserving Round Buoyant Turbulent Plumes," J.Heat Trans., submitted.

Dai, Z., L.-K. Tseng and G.M. Faeth, "Mixture Fraction and Velocity Statistics in Fully-Developed Turbulent Plumes." Fall Technical Meeting, Eastern Section of the Combustion Institute, Pittsburgh, PA, pp. 173-176, 1993.

Dai, Z., Tseng, L.-K., and Faeth, G.M., "Structure of Round, Fully-Developed, Buoyant Turbulent Plumes," J. Heat Trans., Vol. 116, No. 2, pp. 409-417, 1994.

Dai, Z., Tseng, L.-K., Köylü, Ü.Ö. and Faeth, G.M., "Mixing and Radiation Properties of Buoyant Turbulent Diffusion Flames," Report No. GDL/GMF-94-01, The University of Michigan, Ann Arbor, MI, October 1994.

Dai, Z., Tseng, L.-K., and Faeth, G.M., "Buoyant Turbulent Plumes Revisited." Heat and Mass Transfer 94 (A.R. Balakrishnan and S.S. Murthy, ed.), Tata McGraw-Hill Publishing Co., Lmtd., New Delhi, pp. 59-66, 1994.

Dai, Z., Tseng, L.-K. and Faeth, G.M., "Velocity Statistics of Round, Fully-Developed Buoyant Turbulent Plumes," J. Heat Transfer, Vol. 117, No. 1, pp. 138-145, 1995.

Dai, Z., L.-K. Tseng and G.M. Faeth, "Velocity/Mixture-Fraction Statistics of Round, Self-Preserving Buoyant Turbulent Plumes," J. Heat Trans., submitted

Dalzell, W.H., and Sarofim, A.F., "Optical Constants of Soot and Their Application to Heat Flux Calculations," J. Heat Trans. Vol. 91, No. 1, 1969, pp. 100-104.

Dalzell, W.H., Williams, G.C., and Hottel, H.C., (1970), "A Light Scattering Method for Soot Concentration Measurements," Combust. Flame, Vol. 14, pp. 161-170.

Dekeyer, I., and Launder, B.E. (1985) A Comparison of Triple-Moment Temperature-Velocity Correlations in the Asymmetric Heated Jet With Alternative Closure Models. Turbulent Shear Flows 4 (L.J.S. Bradbury et al., eds.), Springer-Verlag, New York City, pp. 102-117.

Dibble, R.W., Kollmann, W., and Schefer,R.W. (1984) Measurements and Predictions of Scalar Dissipation in Turbulent Jet Flames. Twentieth Symposium (International) on Combustion, The Combustion Institute, Pittsburgh, pp. 345-352.

Dobbins, R.A., and Megaridis, C.M. "Morphology of Flame-Generated Soot as Determined by Thermophoretic Sampling," Langmuir Vol. 3, 1987, pp. 254-259.

Dobbins, R.A., and Megaridis, C.M., 1991, "Absorption and Scattering of Light by Polydisperse Aggregates," Appl. Optics, Vol. 30, pp. 4747-4754.

Dobbins, R.A., Mulholland, G.W. and Bryner, N.P. (1993) Comparison of a Fractal Smoke Optics Model with Light Extinction Measurements. Atmospheric Environment, in press.

Durão, D.F.G, Pereira, J.C.F., and Rocha, J.M.P. (1989) Evaluation of a k-ε Turbulence Model for Predicting Buoyant Free Round Jets. Heat Transfer in Convective Flows, HTD-Vol. 107, ASME, New York, pp. 99-107.

Dyer, T.M. (1979) Rayleigh Scattering Measurements of Time-Resolved Concentration in a Turbulent Propane Jet. AIAAJ., Vol. 17, pp. 912-914

Effelsberg, E., and Peters,N. (1988) Scalar Dissipation Rates in Turbulent Jets and Jet Diffusion Flames. Twenty-Second Symposium (Internationsl) on Combustion, the Combustion Institute, Pittsburgh, pp. 693-700.

Erickson, W.D., Williams, G.C., and Hottel, H.C., 1964, "Light Scattering Measurements on Soot in a Benzene-Air Flame," Combust. Flame, Vol. 8, pp. 127-132.

Everest, D., Driscoll, J.F., Dahm, W.J.A., and Feikema, D. (1995) Images of the 2-D Temperature Field and Temperature Gradients to Quantify Mixing Rates Within a Non-Premixed Turbulent Jet Flame. Combust. Flame, Vol. 101, pp. 58-58.

Faeth, G. M. and Köylü, Ü.Ö., "Soot Morphology and Optical Properties in Nonpremixed Turbulent Flame Environments," *Proceedings of the Spring Technical Meeting*, Canadian Section of the Combustion Institute, Kingston, Ontario pp. 2-1 to 2-5.

Faeth, G.M. (1995) Optical and Radiative Properties of Soot in Flame Environments. Prog. Energy Combust. Sci., invited.

Faeth, G.M., and Köylü, Ü.Ö., 1993, "Soot Morphology and Optical Properties in Nonpremixed Turbulent Flame Environments," Combust.Sci. Tech., Vol. 108, pp. 207-229.

Faeth, G.M., Gore, J.P., and Sivathanu, Y.R. (1987). Radiation from Soot-Containing Flames. *Combustion and Fuels in Gas Turbine Engines*, AGARD Conference Proceedings No. 422, NATO, Paris, 17-1 — 17-12.

Faeth, G.M., Gore, J.P., Chuech, S.G., and Jeng, S.-M. (1989). Radiation from Turbulent Diffusion Flames. *Annual Review of Numerical Fluid Mechanics and Heat Transfer*, Vol. 2, Hemisphere Publishing Corp., Washington, 1-38.

Faeth, G.M., Kounalakis, M.E., and Sivathanu, Y.R. (1990) Stochastic Aspects of Turbulent Combustion Processes. Chemometrics and Intelligent Laboratory Systems, 10, 199-210.

Farias, T., Carvalho, M.G., Köylü, Ü.Ö. and Faeth, G.M. "A Computational Study of the Absorption and Scattering Properties of Soot," Fall Technical Meeting, Eastern States Section of the Combustion Institute, Princeton, New Jersey, U.S.A., October 1993, pp. 394-397.

Farias, T., Carvalho, M.G., Köylü, Ü.Ö. and Faeth, G.M., "Computational Evaluation of Approximate Rayleigh-Debye-Gans/Fractal-Aggregate Theory for the Absorption and Scattering of Light by Aggregated Small Particles. " J. Heat Trans., submitted.

Farias, T.L., Carvalho, M.G., Köylü, Ü.Ö. and Faeth, G.M. (1995b) "Absorption and Scattering from Soot Aggregates with Radially Inhomogeneous Primary Particles," Int. J. Heat and Technology, submitted.

Felske, J.D., and Ku, J.C. (1992). A technique for determining the spectral refractive indices, size, and number density of soot particles from light scattering and spectral extinction measurements in flames." Combust. Flame, Vol. 91, pp. 1-20.

Felske, J.D., Charalampopoulos, T.T. and Hura, H. (1984). Determination of the refractive indices of soot particles from the reflectivities of compressed soot pellets. Combust. Sci. Tech. 37, 263.

Foster, P.M. and Howarth, C.R. (1963) Optical Constants of Carbons and Coals in the Infrared. Carbon, Vol. 6, pp. 719-729.

Gandopadhyay, S., Elmenyawi, I., and Sorensen, C.I. (1991) Optical Structure Factor Measurements of Soot Particles in a Premixed Flame. Applied Optics, Vol. 30, pp. 4859-4864.

George, W.K., Jr., Alpert, R.L., and Tamanini, F., 1977, "Turbulence Measurements in an Axisymmetric Buoyant Plume," Int. J. Heat Mass Trans., Vol. 20, pp. 1145-1154.

Gibson, M.M., and Launder, B.E. (1976) On the Calculation of Horizontal Non-Equilibrium Turbulent Shear Flows Under Gravitational Influence. J. Heat Trans., Vol. 98, pp. 81-87.

Gore, J.P., and Faeth, G.M., "Structure and Spectral Radiation Properties of Turbulent Ethylene/Air Diffusion Flames," *Twenty-First Symposium (International) on Combustion*, The Combustion Institute, Pittsburgh, 1986, pp. 1521-1531.

Gore, J.P., and Faeth, G.M., "Structure and Radiation Properties of Luminous Turbulent Acetylene/Air Diffusion Flames," J. Heat Trans.. Vol. 110, No. 1, 1988, pp. 173-181.

Hinze, J. O., 1975, *Turbulence*, 2nd ed., McGraw-Hill, New York, pp. 175-319.

Hossain, M.S., and Rodi, U. (1982) A Turbulence Model for Buoyant Flows and its Application to Buoyant Jets. Turbulent Buoyant Jets and Plumes (W. Rodi, ed.), Pergamon, New York City, pp. 121-178.

Iskander, M.F., Chen, H.Y., and Penner, J.E., 1989, "Optical Scattering and Absorption by Branched Chains of Aerosols," Appl. Optics, Vol. 28, pp. 3083-3091.

Jeng, S.-M., Lai, M.-C., and Faeth, G. M., (1984) Nonluminous Flame Radiation in Turbulent Buoyant Axisymmetric Flames. Combust. Sci. Tech., 40, 41-52.

Jullien, R., and Botet, R. (1987) *Aggregation and Fractal Aggregates*, World Scientific Publishing Co., Singapore, pp. 45-60.

Kerker, M. (1969) *The Scattering of Light,* Academic Press, New York, pp. 414-486.

Kotsovinos, N.E. (1985) "Temperature Measurements in a Turbulent Round Plume," Int. J. Heat Mass Trans., Vol. 28, pp. 771-777.

Kotsovinos, N.E., and List, E.J. (1977) "Turbulent Buoyant Jets. Part 1. Integral Properties," J. Fluid Mech., Vol. 81, pp. 25-44.

Kounalakis, M.E., Sivathanu, Y.R., and Faeth, G.M., 1991, "Infrared Radiation Statistics of Nonluminous Turbulent Diffusion Flames," J. Heat Trans., Vol. 113, pp. 437-445.

Köylü, Ü.Ö. (1992), "Emission, Structure and Optical Properties of Overfire Soot from Buoyant Turbulent Diffusion Flames," Ph.D. Thesis, The University of Michigan, Ann Arbor, Michigan.

Köylü, Ü.Ö., and Faeth, G.M. (1991) Properties of Carbon Monoxide and Soot Emissions from Buoyant Turbulent Diffusion Flames. Final Report, Grant No. 60NANB8D0833, University of Michigan, Ann Arbor. Köylü, Ü.Ö., and Faeth, G.M., (1991) "Carbon Monoxide and Soot Emissions from Liquid-Fueled Buoyant Turbulent Diffusion Flames," Combust. Flame, Vol. 87, No. 1, pp. 61-76.

Köylü, Ü.Ö., and Faeth, G.M., (1992) "Structure of Overfire Soot in Buoyant Turbulent Diffusion Flames at Long Residence Times," Combust. Flame, Vol. 89, No. 2, pp. 140-156.

Köylü, Ü.Ö., and Faeth, G.M. (1993) Radiative Properties of Flame-Generated Soot. J. Heat Trans., Vol. 115, No. 2, pp. 409-417.

Köylü, Ü. Ö., and Faeth, G.M. (1993) "Soot Scattering Properties at Fuel-Rich Conditions in Buoyant Laminar Diffusion Flames." Proceedings of the Eastern and Central States Sections Technical Meeting, The Combustion Institute, Pittsburgh, pp. 547-551, March 1993.

Köylü, Ü.Ö., and Faeth, G.M., "Optical Properties of Overfire Soot in Buoyant Turbulent Diffusion Flames at Long Residence Times," J. Heat Trans. Vol. 116, No. 1, pp. 152-159 (1994).

Köylü, Ü.Ö., and Faeth, G.M., "Optical Properties of Soot in Buoyant Laminar Diffusion Flames," J. Heat Trans., 116:971-979 (1994).

Köylü, Ü.Ö., and Faeth, G.M., "Spectral Extinction Coefficients of Soot Aggregates from Turbulent Diffusion Flames," J. Heat Trans., in press.

Köylü, Ü.Ö., Sivathanu, Y., and Faeth, G.M. (1991) Carbon Monoxide Emissions from Buoyant Turbulent Diffusion Flames. *Third International Symposium on Fire Safety Science*, Elsevier, London, 625-634.

Köylü, Ü.Ö., Dai, Z., Tseng, L.-K., and Faeth, G.M., (1992) "Radiation and Mixing Properties of Buoyant Turbulent Diffusion Flames." Report No. GDL/GMF-92-03, The University of Michigan, Ann Arbor, Michigan.

Köylü¸ Ü.Ö., Dai, Z., Tseng, L.-K., and Faeth, G.M., "Radiation and Mixing Properties of Buoyant Turbulent Diffusion Flames," Report No. GDL/GMF-93-01, Annual Report, NIST Grant No. 60NANB1D1175, 71 p., October 1993.

Köylü, Ü.Ö., Faeth, G.M., Farias, T.L. and Carvalho, M.G., "Fractal and Projected Structure Properties of Soot Aggregates." Combust. Flame, Vol. 100, No. 4, pp. 621-633, 1995.

Ku, J.C., and Felski, J.D. (1986) Determination of Refractive Indices of Mie Scatterers from Kramers-Kronig analysis of Spectral Extinction Data. J. Opt. Soc. Am., Vol. 3, pp. 617-623.

Ku, J.C., and Shim, K.-H., 1992b, "A Comparison of Solutions for Light Scattering and Absorption by Agglomerated or Arbitrarily-Shaped Particles, J. Quant. Spect. and Rad. Trans., 47, 201-220.

Kwon, S., Wu, M.-S., Driscoll, J. F., and Faeth, G. M. (1992) Flame Surface Properties of Premixed Flames in Isotropic Turbulence: Measurements and Numerical Simulations. Combust. Flame, Vol. 88, pp. 221-238.

Lai, M.-C., and Faeth, G.M. (1987) "Turbulence Structure of Vertical Adiabatic Wall Plumes," J. Heat Trans., Vol. 109, pp. 663-670.

Lai, M.-C., and Faeth, G.M., 1987, "A Combined Laser-Doppler Anemometer/Laser-Induced Fluorescence System for Turbulent Transport Measurements," J. Heat Trans. Vol. 109, pp. 254-256.

Lai, M.-C., Jeng, S.-M., and Faeth, G.M. (1986) Structure of Turbulent Adiabatic Wall Plumes. J. Heat Trans. 108, 827-834.

Launder, B.E. (1975) On the Effects of a Gravitational Field on the Turbulent Transport of Heat and Momentum. J. Fluid Mech., Vol. 67, pp. 569-590.

Launder, B.E. (1978) Heat and Mass Transport. Topics in Physics, Vol. 12: Turbulence, Springer-Verlag, New York City, pp. 231-287.

Launder, B.E. (1990) Phenomenological Modelling: Present ... and Future. Whither Turbulence? (J.L. Lumley, ed.), Springer-Verlag, Berlin, pp. 439-485.

Lee, S.C., and Tien, C.L. (1980) Optical Constants of Soot in Hydrocarbon Flames. *Eighteenth Symposium (International) on Combustion,* The Combustion Institute, Pittsburgh, pp. 1159-1166.

Lee, S.C., and Tien, C.L. (1983) Effect of Soot Shape on Soot Radiation. J. Quant. Spectrosc. Radiat. Transfer 29, 259-265.

List, E.J., 1982, "Turbulent Jets and Plumes," Ann. Rev. Fluid Mech. Vol. 14, pp. 189-212.

Lockwood, F.C., and Naguib, A.S., 1975, "The Prediction of Fluctuations in the Properties of Free, Round-Jet Turbulent Diffusion Flames," Combust. Flame, Vol. 24, pp. 109-124.

Lou, W. and Charalampopoulos, T.T. (1994) On the Electromagnetic Scattering and Absorption of Agglomerated Small Spherical Particles. J. Phys. D: Appl. Phys., Vol. 27, pp. 2258-2270.

Lou, W. and Charalampopoulos, T.T. (1995) A New Approach for In-Situ Determination of the Optical Properties and Morphology of Agglomerated Particles. *Proceedings of the Central States Section Meeting,* The Combustion Institute, Pittsburgh, pp. 110-114

Ludwig, C. B., Malkmus, W., Reardon, J. E., and Thomson, J. A. (1973) *Handbook of Infrared Radiation from Combustion Gases*. NASA SP-3080, 1988.

Lumley, J.L. (1978) Computational Modeling of Turbulent Flows. Adv. Appl. Mech., Vol. 18, pp. 123-176.

Lumley, J.L. (1980) Second-Order Modeling of Turbulent Flows. *Prediction Methods for Turbulent Flows* (W. Kollman, ed.), Hemisphere Publishing Co., New York, pp. 1-31.

Magnussen, B.F., 1974, "An Investigation into the Behavior of Soot in a Turbulent Free Jet C_2-H_2-Flame," *Fifteenth Symposium (International) on Combustion*, The Combustion Institute, Pittsburgh, pp. 1415-1425.

Malin, M.R., and Younis, B.A. (1990) Calculation of Turbulent Buoyant Plumes with a Reynolds Stress and Heat Flux Transport Closure. Int. J. Heat Mass Trans., Vol. 33, pp. 2247-2264.

Martin, J.E., and Hurd, A.J. (1987) "Scattering from Fractals," J. Appl. Cryst., Vol. 20, pp. 61-78.

Medalia, A.I. and Heckman, F.A. (1969) "Morphology of Aggregates — II. Size and Shape Factors of Carbon Black Aggregates from Electron Microscopy," Carbon 7, 567-582.

Megaridis, C.M., and Dobbins, R.A., "Comparison of Soot Growth and Oxidation in Smoking and Nonsmoking Ethylene Diffusion Flames," Combust. Sci. Tech. Vol. 66, No. 1, 1989, pp. 1-16.

Megaridis, C.M., and Dobbins, R.A. (1990) "Morphological Description of Flame-Generated Materials," Combust. Sci. Tech., Vol. 71, pp. 95-109.

Mizukami, M., Parthasarathy, R.N., and Faeth, G.M., (1992) "Particle-Generated Turbulence in Homogeneous Dilute Dispersed Flows," Int. J. Multiphase Flow, Vol. 18, No. 2, pp. 397-412.

Mizushima, T., Ogino, F., Veda, H., and Komori, S. (1979) "Application of Laser-Doppler Velocimetry to Turbulence Measurements in Non-Isothermal Flow," Proc. Roy. Soc. London, Vol. A366, pp. 63-79.

Morton, B.R., 1959, "Forced Plumes," J. Fluid Mech., Vol. 5, pp. 151-163.

Morton, B.R., Taylor, G.I., and Turner, J.S., 1956, "Turbulent Gravitational Convection from Maintained and Instantaneous Sources," Proc. Roy. Soc. London, Vol. A234, pp. 1-23.

Mountain, R.D., and Mulholland, G.W. (1988) "Light Scattering from Simulated Smoke Agglomerates," Langmuir Vol. 4, pp. 1321-1326.

Mulholland, G.W., Samson, R.J., Mountain, R.D., and Ernst, M.H. (1988) "Cluster Size Distribution for Free Molecular Aggregation," J. Energy Fuels, Vol. 2, pp. 481-486.

Nakagome, H., and Hirata, M. (1977), "The Structure of Turbulent Diffusion in an Axi-Symmetrical Thermal Plume," *Heat Transfer and Turbulent Buoyant Convection* (D.B. Spalding and N. Afgan, eds.), McGraw-Hill, New York, pp. 367-372.

Namazian, M., Schefer, R.W., and Kelly, J. (1988) Scalar Dissipation Measurements in the Developing Region of a Jet. Combust. Flame, Vol. 74, pp. 147-160.

Nelson, J., 1989a, "Test of a Mean Field Theory for the Optics of Fractal Clusters," J. Modern Optics, Vol. 36, pp. 1031-1057.

Nelson, J., 1989b, "Fracticality of Sooty Smoke: Implications for the Severity of Nuclear Winter," Nature, Vol. 339, pp. 611-613.

Ogino, F., Takeuchi, H., Kudo, I., and Mizushima, T. (1980) "Heated Jet Discharged Vertically in Ambients of Uniform and Linear Temperature Profiles," Int. J. Heat Mass Trans., Vol. 23, pp. 1581-1588.

Panchapakesan, N.R., and Lumley, J.L. (1993b) "Turbulence Measurements in Axisymmetric Jets of Air and Helium. Part 2. Helium Jet," J. Fluid Mech., Vol. 246, pp. 225-247.

Papanicolaou, P.N., and List, E.J., 1987, "Statistical and Spectral Properties of Tracer Concentration in Round Buoyant Jets," Int. J. Heat Mass Trans., Vol. 30, pp. 2059-2071.

Papanicolaou, P.N., and List, E.J., 1988, "Investigation of Round Vertical Turbulent Buoyant Jets," J. Fluid Mech., Vol. 195, pp. 341-391.

Papantoniou, D., and List, E.J. (1989) "Large Scale Structure in the Far Field of Buoyant Jets," J. Fluid Mech., Vol. 209, pp. 151-190.

Peterson, J., and Bayazitoglu, Y., 1992, "Measurements of Velocity and Turbulence in Vertical Axisymmetric Isothermal and Buoyant Plumes," J. Heat Trans., Vol. 114, pp. 135-142.

Pitts, W.M., and Kashiwagi, T. (1984) The Application of Laser-Induced Rayleigh Light Scattering to the Study of Turbulent Mixing. J. Fluid Mech. 141, 391-429.

Pivovarov, M.A., Zhang, H., Ramaker, D.E., Tatem, P.A., and Williams, F.W., 1992, "Similarity Solutions in Buoyancy-Controlled Diffusion Flame Modelling," Combust. Flame, Vol. 92, pp. 308-319.

Pope, S.B. (1990) Computations of turbulent combustion: progress and challenges. *Twenty-third Symposium (International) on Combustion*, The Combustion Institute, Pittsburgh, pp. 591-612.

Puri, R., Richardson, T.F., Santoro, R.J., and Dobbins, R.A. (1993) "Aerosol Dynamic Processes of Soot Aggregates in a Laminar Ethene Diffusion Flame," Combust. Flame, Vol. 92, pp. 320-333.

Ramaprian, B.R., and Chandrasekhara, M.S. (1985) LDA Measurements in Plane Turbulent Jets. J. Fluids Engry., vol. 107, pp. 264-271.

Ramaprian, B.R., and Chandrasekhara, M.S. (1989) Measurements in Vertical Plane Turbulent Plumes. J. Fluids Engry, Vol. 111, pp. 69-77.

Rosner, D.E., Mackowski, D.W., and Garcia-Ybarra, P. "Size- and Structure-Insensitivity of the Thermophoretic Transport of Aggregated 'Soot' Particles in Gases," Combust. Sci. Tech. Vol. 80, No. 1, pp. 87-101 (1991) .

Rouse, H., Yih, C.S., and Humphreys, H.W., 1952, "Gravitational Convection from a Boundary Source," Tellus, Vol. 4, pp. 201-210.

Rudder, R.R., and Bach, D. R., 1968, "Rayleigh Scattering of Ruby-Laser Light by Neutral Gases," J. Opt. Soc. Amer., Vol. 58, pp. 1260-1266.

Samson, R. J., Mulholland, G. W.. and Gentry, J. W. (1987) Structural Analysis of Soot Agglomerates. Langmuir 3, 272-281.

Seban, R.A., and Behnia, M.M. (1976), "Turbulent Buoyant Jets in Unstratified Surroundings," Int. J. Heat Mass Trans., Vol. 19, pp. 1197-1204.

Shabbir, A. (1987) An experimental study of an axisymmetric turbulent buoyant plume and evaluation of closure hypotheses. Ph.D. Thesis, SUNY-Buffalo.

Shabbir, A., and George, W.K. (1992) Experiments on a Round Turbulent Buoyant Plume. NASA Technical Memorandum 105955.

Shabbir, A., and Taulbee, D.B. (1990) Evaluation of Turbulence Models for Predicting Buoyant Flows. J. Heat Trans., Vol. 112, pp. 945-951.

Shih, T.-H., Lumley, J.L., and Janicka, J. (1987) Second-Order Modeling of a Variable-Density Mixing Layer. J. Fluid Mech., vol. 180, pp. 93-116.

Sivathanu, Y.R., and Faeth, G.M., "Soot Volume Fractions in the Overfire Region of Turbulent Diffusion Flames," Combust. Flame , Vol. 81, No. 2, 1990, pp. 133-149.

Sorensen, C.M., Cai, J., and Lu, N., 1992, "Test of Static Structure Factors for Describing Light Scattering from Fractal Soot Aggregates," Langmuir, Vol. 8, pp. 2064-2069.

Sorensen, C.M., Cai, J., and Lu, N. (1992) "Light-Scattering Measurements of Monomer Size, Monomers per Aggregate, and Fractal Dimension for Soot Aggregates in Flames," Applied Optics, Vol. 31, pp. 6547-6557.

Speziale, C.G. (1990) Turbulence Modeling: Present and Future. Wither Turbulence? (J.L. Lumley, ed.),Springer Verlag, Berlin, pp. 490-512.

Stagg, B.J. and Charalampopoulos, T.T. (1990) Method to Minimize the Effects of Polarizer Leakage on Reflectivity Measurements. Appl. Optics, Vol. 29, pp. 4638-4645.

Stagg, B.J. and Charalampopoulos, T.T. (1991) Surface-Roughness Effects on the Determination of Optical Properties of Materials by the Reflection Method. Appl. Optics, Vol. 30, pp. 113-4118.

Stagg, B.J. and Charalampopoulos, T.T. (1993) Refractive Indices of Pyrolytic Graphite, Amorphous Carbon, and Flame Soot in the Temperature Range 25° to 600° C. Combust. Flame, Vol. 94, pp. 381-396.

Stårner, S. H., and Bilger, R W. (1983) "Differential Diffusion Effects on Measurements in Turbulent Diffusion Flames by the Mie Scattering Technique," Prog. Astro. and Aero., AIAA, Washington, DC, Vol. 88, pp. 81-104.

Sugiyama, G., "Nonluminous Diffusion Flame of Diluted Acetylene in Oxygen Enriched Air," *Twenty-fifth Symposium (International) on Combustion*, The Combustion Institute, Pittsburgh, 1994, pp. 601-608.

Sunderland, P.B., Köylü, Ü.Ö., and Faeth, G.M., "Soot Formation in Weakly Buoyant Acetylene-Fueled Laminar Jet Diffusion Flames Burning in Air," Combust. Flame Vol. 100, Nos. 1/2, pp. 310-322, 1995.

Szekely, G.A., Jr. and Faeth, G.M. (1982) Reaction of Carbon Black Slurry Agglomerates in Combustion Gases. *Nineteenth Symposium (International) on Combustion*, The Combustion Institute, Pittsburgh, pp. 1077-1085 or 1495-1502.

Tamanini, F. (1977) "Reaction Rates, Air Entrainment and Radiation in Turbulent Fire Plumes," Combust. Flame, Vol. 30, pp. 85-101.

Tamanini, F. (1978) The Effect of Buoyancy on the Turbulence Structure of Vertical Round Jets. J. Heat Trans., Vol. 100, pp. 659-664.

Taulbee, D.B. (1992) An improved algebraic Reynolds stress model and corresponding nonlinear stress model. Phys. Fluids A 4:2555-2561.

Tence, M., Chevalier, J.P., and Jullien, R. (1986) On the measurement of the fractal dimension of aggregated particles by electron microscopy: experimental method, corrections and comparison with numerical models. J. Physique (Paris) 47:1989-1998.

Tennekes, H., and Lumley, J.L., (1972) *A First Course in Turbulence*, MIT Press, Cambridge, Massachusetts, 1972, pp. 113-124.

Tien, C. L., and Lee, S. C. (1982) "Flame Radiation," Prog. Energy Combust. Sci., Vol. 8, pp. 41-59.

Vaglieco, B.M., Beretta, F., and D'Alessio, A. (1990) In Situ Evaluation of the Soot Refractive Index in the uv-Visible from the Measurements of Scattering and Extinction Coefficients in Rich Flames. Combust. Flame 79, 259-271.

van de Hulst, H.C. (1957) *Light Scattering by Small Particles*, Dover Publications, New York.

Viskanta, R., and Mengüc, M.P., 1987, "Radiation Heat Transfer in Combustion Systems," Prog. Energy Combust. Sci., Vol. 13, pp. 97-160.

Wersborg, B.L., Howard, J.B., and Williams, G.C. (1972) "Physical Mechanisms in Carbon Formation in Flames," *Fourteenth Symposium (International) on Combustion*, The Combustion Institute, Pittsburgh, pp. 929-940.

Zeman, O., and Lumley, J.L. (1976) Modeling Buoyancy Driven Mixed Layers. J. Atm. Sci., Vol. 33, pp. 1988.

Zhang, H.X., Sorensen, C.M., Ramer, E.R., Olivier, B.J., and Merklin, J.F. (1988) In Situ Optical Structure Factor Measurements of an Aggregating Soot Aerosol. Langmiur, Vol. 4, pp. 867-871.

Zhou, Z. and Choi, M.Y. (1995) Measurements of Dimensionless Extinction Constant of Soot Generated using Various Fuels. *Proceedings of the Central States Section Meeting*, The Combustion Institute, Pittsburgh, pp. 87-91.

Zimin, V.D., and Frik, P.G. 1977, "Averaged Temperature Fields in Asymmetrical Turbulent Streams over Localized Heat Sources," Izv. Akad. Nauk. SSSR, Mekhanika Zhidkosti Gaza, Vol. 2, pp. 199-203.

NIST-114
(REV. 6-93)
ADMAN 4.09

U.S. DEPARTMENT OF COMMERCE
NATIONAL INSTITUTE OF STANDARDS AND TECHNOLOGY

MANUSCRIPT REVIEW AND APPROVAL

(ERB USE ONLY)
ERB CONTROL NUMBER | DIVISION
PUBLICATION REPORT NUMBER: NIST-GCR-96-691 | CATEGORY CODE
PUBLICATION DATE: June 1996 | NUMBER PRINTED PAGES

INSTRUCTIONS: ATTACH ORIGINAL OF THIS FORM TO ONE (1) COPY OF MANUSCRIPT AND SEND TO THE SECRETARY, APPROPRIATE EDITORIAL REVIEW BOARD

TITLE AND SUBTITLE (CITE IN FULL)

Mixing and Radiation Properties of Buoyant Luminous Flame Environments

CONTRACT OR GRANT NUMBER: Grant No. 60NANB4D1696
TYPE OF REPORT AND/OR PERIOD COVERED: October 1995

AUTHOR(S) (LAST NAME, FIRST INITIAL, SECOND INITIAL)
Dai, Z., Krishnan, S.K., Sangras, R., Wu, J.S., and Gaeth, G.M.
Department of Aerospace Engineering
The University of Michigan, Ann Arbor, MI 48109-2118

PERFORMING ORGANIZATION (CHECK (X) ONE BOX)
[ ] NIST/GAITHERSBURG
[ ] NIST/BOULDER
[ ] JILA/BOULDER

LABORATORY AND DIVISION NAMES (FIRST NIST AUTHOR ONLY)

SPONSORING ORGANIZATION NAME AND COMPLETE ADDRESS (STREET, CITY, STATE, ZIP)
U.S. Department of Commerce
National Institute of Standards and Technology
Gaithersburg, MD 20899

PROPOSED FOR NIST PUBLICATION

[ ] JOURNAL OF RESEARCH (NIST JRES)	[ ] MONOGRAPH (NIST MN)	[ ] LETTER CIRCULAR
[ ] J. PHYS. & CHEM. REF. DATA (JPCRD)	[ ] NATL. STD. REF. DATA SERIES (NIST NSRDS)	[ ] BUILDING SCIENCE SERIES
[ ] HANDBOOK (NIST HB)	[ ] FEDERAL INF. PROCESS. STDS. (NIST FIPS)	[ ] PRODUCT STANDARDS
[ ] SPECIAL PUBLICATION (NIST SP)	[ ] LIST OF PUBLICATIONS (NIST LP)	[X] OTHER NIST-GCR
[ ] TECHNICAL NOTE (NIST TN)	[ ] NIST INTERAGENCY/INTERNAL REPORT (NISTIR)	

PROPOSED FOR NON-NIST PUBLICATION (CITE FULLY) [ ] U.S. [ ] FOREIGN

PUBLISHING MEDIUM
[X] PAPER [ ] CD-ROM
[ ] DISKETTE (SPECIFY)
[ ] OTHER (SPECIFY)

SUPPLEMENTARY NOTES

ABSTRACT (A 2000-CHARACTER OR LESS FACTUAL SUMMARY OF MOST SIGNIFICANT INFORMATION. IF DOCUMENT INCLUDES A SIGNIFICANT BIBLIOGRAPHY OR LITERATURE SURVEY, CITE IT HERE. SPELL OUT ACRONYMS ON FIRST REFERENCE.) (CONTINUE ON SEPARATE PAGE, IF NECESSARY.)

An investigation of the radiation and mixing properties of buoyant turbulent diffusion flames is described. The study was divided into two phases: (1) the optical and radiative properties of soot, which must be understood in order to develop non-intrusive methods for measuring soot properties and to estimate the continuum radiation properties of soot in flame environments, and (2) the structure and mixing properties of buoyant turbulent plumes, which must be understood in order to resolve effects of turbulence/radiation interactions and to benchmark computationally tractable models of buoyant turbulent flows.

Consideration of the optical and radiative properties of soot involved evaluation of the Rayleigh-Debye-Gans (RDG) scattering approximation for soot aggregates and the use of this theory to measure the refractive indices in the visible region (350-800 nm). In addition, dimensionaless extinction coefficients and the soot fractal dimensions were measured. The structure and mixing properties of buoyant turbulent plumes were investigated by examination of the effects of coflow on earlier measurements and by evaluating various modeling approximations, with an emphasis on self-preserving round buoyant turbulent plumes.

KEY WORDS (MAXIMUM OF 9; 28 CHARACTERS AND SPACES EACH; SEPARATE WITH SEMICOLONS; ALPHABETIC ORDER; CAPITALIZE ONLY PROPER NAMES)
diffusion flames; fire research; optical properties; soot; turbulent flames

AVAILABILITY
[X] UNLIMITED [ ] FOR OFFICIAL DISTRIBUTION - DO NOT RELEASE TO NTIS
[ ] ORDER FROM SUPERINTENDENT OF DOCUMENTS, U.S. GPO, WASHINGTON, DC 20402
[X] ORDER FROM NTIS, SPRINGFIELD, VA 22161

NOTE TO AUTHOR(S): IF YOU DO NOT WISH THIS MANUSCRIPT ANNOUNCED BEFORE PUBLICATION, PLEASE CHECK HERE. [ ]

WORDPERFECT